

Power Conversion Circuitry for Electrostatic Energy Harvester

BUSKERUD AND VESTFOLD UNIVERSITY COLLEGE



Son Hoai Nguyen

Supervisor: Professor Einar Halvorsen

Department of Micro and Nano Systems Technology

May 27, 2014

Power Conversion Circuitry for Electrostatic Energy Harvester

By

SON HOAI NGUYEN

B.S. (Ho Chi Minh City University of Technology) 2006

DISSERTATION

Submitted in partial satisfaction of the requirements for the degree of

MASTER OF SCIENCE

in

Micro and Nano Systems Technology

in the

Department of Micro and Nano Systems Technology

of the

BUSKERUD AND VESTFOLD UNIVERSITY COLLEGE

Approved:

Committee in Charge

2014

Abstract

Energy harvesting is a potential approach to power autonomous wireless sensor systems and electronic circuits. It can potentially replace batteries, reduce the required size of batteries or even make sensors possible where batteries cannot be used. One among several possibilities is to harvesting energy from ambient vibrations. This project focuses on designing a power circuit for electrostatic energy harvesters which is based on the doubler of charge. The advantages of the circuit are very low power loss thanks to a simple structure, achieving high power by maintaining high bias voltage, able to recharge a storage capacitor without using additional circuits. The efficiency of the circuit remarkably depends on the displacement of a proof mass. The thesis carries out the analyses and comparisons between the doubler operation in asymmetrical energy harvesters and that in symmetrical ones to propose many advantages of asymmetrical structures in terms of higher output power and smaller minimum required mass displacement. Furthermore, buck converters with an autonomous MEMS switch or a controlled electronic switch are utilized in order to transfer the energy in the storage capacitor into a load and keep the output power maximal. LTSPICE simulations and experiments show intriguing results of the doubler circuit in symmetrical and asymmetrical energy harvesting systems.

Acknowledgments

First and foremost, I would like to express sincere gratitude to my supervisor, Professor Einar Halvorsen, for his intellectual support and enthusiasm guidance in this project. He has provided enormous meaningful knowledge in energy harvesting and many useful research skills. I wish the best for him in research projects. I also would like to thank all members of Energy Harvesting Group and engineering staffs of the Department of Micro and Nano Systems Technology for their help and suggestions on experiments in the lab.

Secondly, I want to show my grateful thanks to Buskerud and Vestfold University College for providing a supportive environment for me to study and conduct researches during my master program in Norway. I also wish to thank to all professors for their inspiration and interesting lectures during the course of my study. I have made many friends at Buskerud and Vestfold University College. Ridiculous conversations with them help me release stress and make my master study enjoyable.

Last but not least, I would like to express my sincere thankfulness to my girl friend and my parents. Their love, encouragement and continuous support have always accompanied with every achievement in my life.

List of Figures

1.1	Four popular topologies of electrostatic energy harvesting.	3
1.2	The operation of the doubler of charge.	4
2.1	The in-plane overlap harvester with linear spring.	7
2.2	In-plane overlap harvesters modesl a) without and b) with resistive load [1].	8
2.3	Equivalent circuit of the linear harvesting system with resistive load.	9
2.4	Output power peak versus normalized angular frequency under optimal load resistance condition.	10
2.5	Relationship between optimal normalized load resistance and angular frequency.	11
2.6	Output power performance versus angular frequency and load resistance with different normalized vibration frequency.	12
2.7	Mass displacement versus bias voltage V_e with different acceleration values.	13
2.8	Curved-spring harvester.	14
2.9	Angled-spring harvester.	15
2.10	The equivalent circuit using lumped element modeling for nonlinear spring harvesters.	16
2.11	Output voltage in down/up sweep of energy harvester with a) angled spring or b) curved spring.	16
3.1	(a) Simple passive power converter with diode bridge and (b) optimal output voltage at U_{Cb} [2].	18
3.2	Different active power converters [2].	19
3.3	Different types of SSHI converter [3], [4].	20

3.4	Harvested powers of different power converters as a function of the electromechanical figure of merit [2].	21
3.5	a) Charge-constrained conversion cycle and b) voltage-constrained conversion cycle.	22
3.6	Two types of switched electrostatic harvesting system.	23
3.7	An example of combined voltage- and charge-constrained converters [5]. . .	24
3.8	The doubler of charge topologies.	26
3.9	Voltage, charge and displacement waveforms on harvesting capacitors in doubler operation.	27
3.10	Voltage and charge diagram of harvesting capacitors with linear spring. . .	29
3.11	The minimum required displacement as a function of A and B.	32
3.12	Q and V diagram of harvesting capacitors with nonlinear spring.	33
3.13	The doubler of charge with a buck converter.	35
4.1	Output voltage and mass displacement of a linear-spring harvester with 0.1 g acceleration when $V_e = 10, 20$ and 30 V.	39
4.2	Output voltage and mass displacement of a linear-spring harvester with $V_e = 5$ V when acceleration changes from 0.1 to 0.3 g	39
4.3	Output voltage and mass displacement of a angled-spring harvester with $V_e = 30$ V when $a = 0.11$ and 0.2 g	41
4.4	Output voltage and mass displacement of a angled-spring harvester with 0.2 g acceleration when $V_e = 10, 30$ and 60 V.	41
4.5	Output voltage and mass displacement of a $40\mu\text{m}$ -curved-spring harvester with $V_e = 20$ V in frequency down sweep when $a = 0.1$ and 0.3 g	44
4.6	Output voltage and mass displacement of a $40\mu\text{m}$ -curved-spring harvester with 0.3 g acceleration in frequency down sweep when $V_e = 10, 20$ and 30 V.	44
4.7	Output voltage and mass displacement of a $50\mu\text{m}$ -curved-spring harvester with $V_e = 20$ V in frequency down sweep when $a = 0.1$ and 0.2 g	45
4.8	Output voltage and mass displacement of a $50\mu\text{m}$ -curved-spring harvester with 0.2 g acceleration in frequency down sweep when $V_e = 10, 20$ and 30 V.	45

4.9	Output power and mass displacement as functions of bias voltage V_e	46
4.10	Symmetrical and asymmetrical prototypes of the doubler circuits	46
4.11	A comparison in harvested power of linear-spring doubler between two different asymmetrical structures	48
4.12	A comparison in harvested power of angled-spring doubler between two different asymmetrical structures	48
4.13	Voltage on C_{store} and mass displacement of linear-spring doubler with different values of storage capacitor C_{store}	49
4.14	Q-V plane contours of two harvesting capacitors of linear-spring doubler .	49
4.15	A comparison in voltage on C_{store} and mass displacement of two angled-spring prototypes with $C_{store} = 90$ pF	50
4.16	Voltage at nodes 1,2 and 3 of the doubler with $40 \mu\text{m}$ curved spring.	51
4.17	Voltage at nodes 1,2 and 3 of the doubler with $50 \mu\text{m}$ curved spring.	51
4.18	The equivalent circuit of diode for transient analysis.	52
4.19	A comparison in harvested power and mass displacement of linear-spring doubler with two different diodes at $V_e = 60$ V, $a = 0.38 g$	54
4.20	A comparison in harvested power and mass displacement of angled-spring doubler with two different diodes at $V_e = 30\text{V}$, $a = 0.25 g$	55
4.21	Voltage on C_{store} , output power and mass displacement of linear-spring doubler with $C_{store} = 90$ pF and diode BAS716	55
4.22	Voltage on C_{store} and mass displacement of angled-spring doubler with $C_{store} = 90$ pF and diode BAS716.	56
4.23	The linear-spring doubler circuit connected to a buck converter with controlled electronic switch	56
4.24	Load Current, Voltage on C_{store} and mass displacement of linear-spring doubler connected to a buck converter with controlled electronic switch, diode BAS716 and 0.25 acceleration) during transient state a) or during steady state b)	57
4.25	The angled-spring doubler circuit connected to a buck converter with controlled electronic switch	58

4.26	Load Current, Voltage on C_{store} and mass displacement angled-spring doubler connected to a buck converter with controlled electronic switch during transient state a) or during steady state b).	59
4.27	The linear-spring doubler circuit connected to a buck converter with MEMS switch	60
4.28	Load Current, Voltage on C_{store} and mass displacement of linear-spring doubler connected to a buck converter with MEMS switch and diode BAS716 during transient state a) or during steady state b).	61
4.29	The angled-spring doubler circuit connected to a buck converter with MEMS switch	62
4.30	I_{load} , V_{Cstore} and x_{mass} of angled-spring doubler connected to a buck converter with MEMS switch and diode BAS716 during transient state a) or steady state b).	63
5.1	Curved-spring harvester fabricated by Son Duy Nguyen [1].	65
5.2	The spring, endstop, and fingers of the curved-spring harvester with $40\mu\text{m}$ tip displacement.	65
5.3	The spring, endstop, and fingers of the curved-spring harvester with $50\mu\text{m}$ tip displacement.	66
5.4	The PCBs with doubler circuits and curved-spring harvesters	66
5.5	The measurement system for conducting all experiments	67
5.6	The output voltage of $40\mu\text{m}$ curved-spring harvesters with different accelerations a) and bias voltages V_e b).	68
5.7	The output voltage of $40\mu\text{m}$ curved-spring harvesters with different accelerations a) and bias voltages V_e b).	69
5.8	The 9328 Ceramic Trimmer Capacitor produced by Johanson Manufacturing.	69
5.9	The output voltage of the $40\mu\text{m}$ - and $50\mu\text{m}$ -curved-spring harvesters with vibration frequency sweep.	70
5.10	The voltage at nodes 1, 2 and 3 of the doubler circuit with $40\mu\text{m}$ - and $50\mu\text{m}$ -curved-spring harvester.	71

5.11 Parasitic capacitance measuring instrument and its designed circuit.	71
5.12 Output and input voltage of the measurement circuit when measuring the 50 μ m-curved-spring doublers.	72
5.13 Output and input voltage of the measurement circuit when measuring the 50 μ m-curved-spring doubler.	73

List of Tables

2.1	Model parameters for electrostatic energy harvesting device.	8
3.1	Voltage and charge on capacitors C_a and C_b with linear-spring harvesters. .	26
3.2	Capacitance value of C_a and C_b at X and Y points.	33
3.3	Voltage and charge on C_a and C_b with nonlinear spring harvesters.	34
4.1	Model parameters for linear-spring harvesting device [6].	38
4.2	Model parameters for angled-spring harvesting device [7].	40
4.3	Model parameters for $40\mu\text{m}$ -curved-spring harvesting device [8].	42
4.4	Model parameters for $50\mu\text{m}$ -curved-spring harvesting device [8]	43
4.5	Harvested powers of the doubler circuit with different mass displacements and theoretical required mass displacements in three prototypes (where $A =$ $\frac{C_{oa}+C_{pa}}{C_{oa}}x_{oa}$ and $B = \frac{C_{ob}+C_{pb}}{C_{ob}}x_{ob}$).	47
4.6	Harvested powers of the doubler circuit with different diode forward voltages V_f	52
4.7	Harvested powers of the doubler circuit with different diode leakage currents at $V_f = 1\text{ V}$ and $C_{diode} = 1\text{ pF}$	53
4.8	Harvested powers of the doubler circuit with different junction capacitance values at $V_f = 1\text{ V}$	53
4.9	Harvested powers of the doubler circuit with different diodes.	54
5.1	Testing results of the capacitance measuring instrument with different fixed capacitors	72

Contents

Abstract	ii
Acknowledgments	iii
List of Figures	viii
List of Tables	ix
1 Introduction	1
1.1 Background	1
1.2 Contributions of the Thesis	4
1.3 Organization of the Thesis	5
2 Electrostatic Energy Harvesters	6
2.1 Linear-spring Harvesters	7
2.1.1 Power Optimization	8
2.1.2 Proof Mass Displacement	13
2.2 Nonlinear-Spring Harvesters	14
3 Power Conversion Circuit	17
3.1 Conventional Circuits	17
3.1.1 Continuous Electrostatic Harvesting Systems	18
3.1.2 Switched Electrostatic Harvesting Systems	22
3.2 The Doubler of Charge	25
3.2.1 Symmetrical Harvesting Systems	25

3.2.2	Asymmetrical Harvesting Systems	30
3.3	The Doubler of Charge with Buck Converter	34
4	Simulation Results	37
4.1	Symmetrical and Asymmetrical Energy Harvesters	37
4.1.1	Linear-spring Harvester	38
4.1.2	Angled-spring Harvester	40
4.1.3	Curved-spring Harvesters	42
4.2	The Doubler of Charge	44
4.2.1	The Doubler Circuit with Bias Battery	45
4.2.2	The Doubler Circuit with Storage Capacitor	50
4.3	The Doubler of Charge with Non-ideal Diodes	53
4.4	The Doubler of Charge with Buck Converter	59
4.4.1	Controlled Electronic Switch	59
4.4.2	Autonomous MEMS Switch	61
5	Circuit Design and Experimental Results	64
5.1	Curved-spring Energy Harvesters	64
5.2	Circuit Design and Experimental Results	68
5.3	Parasitic Capacitance Measurement	70
6	Conclusions and Future Work	74
6.1	Conclusions	74
6.2	Future Work	75
	Bibliography	79

Chapter 1

Introduction

1.1 Background

Nowadays, along with the spread of low-power devices (including sensor, pacemaker, radio transmitter, hearing aid, and so on), energy harvesting has recently attracted enormous attention from different research groups. The development of energy harvesting systems enables the breakthrough of wireless devices thanks to increasing their lifetime, reducing maintenance and cost, and avoiding the environmental problems compared to using batteries. Energy harvesting, broadly speaking, is the process of two steps, conversion and storage. While the conversion, which captures ambient energy and turns it into electricity, is mainly related to transducer technologies, the latter considers output power electronic designs such as conditioning and storage circuits which transfer unsuitable energies into usable forms to power autonomous devices.

Among an abundance of potential ambient energies (e.g. chemical, thermal, or radiation power), vibration, sunlight and temperature differences [9] are the most appropriate sources for energy harvesting. The paper [9] characterized each kind of energy harvesting, presented the comparison of those three popular and concluded that the wide range of power level is available and proportional to device volume. Specifically, there are three prevalent conversion mechanisms of vibration energy harvesting, i.e. electromagnetic, piezoelectric and electrostatic, which are classified based on how mechanical kinetic energy is converted into electricity. Electromagnetic systems function thanks to the relative movement between a

magnet and a coil creating an electromotive force which stimulates a one-direction flow of charge or a current in the coil. The electromagnetic conversion is inferior to the two others in terms of compact design but able to generate very high power. Piezoelectric generators have piezoelectric films, for example, attached on a cantilever beam which absorbs strain energy once the beam is deformed. The piezoelectric conversion obtains high harvesting efficiency with simple design structures and requires less complicated power electronics; however, piezoelectric materials (such as PZT and AlN) are costly and highly dependent on environmental factors, especially temperature. Furthermore, the fabrication process with piezoelectric materials is dusty and therefore triggers the negative issues for integrated circuit designs later on. Electrostatic devices have varying capacitive structures with movable electrode plates or fingers. The electrostatic conversion mechanism somewhat resembles to piezoelectric ones; the charge flow is obtained due to the relative motion of capacitive plates. Electrostatic devices which are of MEMS capacitive structures can be fabricated in a very small scale, less sensitive to surroundings, and compatible to ASIC technology; as a result, electrostatic energy harvesting has recently inspired numerous concentrations from different researchers. The thesis focuses on the electrostatic vibration-to-electric energy harvesting only.

Electrostatic energy harvesters have been structured in four dominant prototypes: in-plane overlap varying, in-plane gap closing, out-of-plane gap closing and in-plane overlap plate harvesters shown in Figure 1.1, which are categorized based on structural shapes and the relative motion between capacitive plates. Roundy *et al.* [10] calculated the mechanical damping, capacitance values and electrostatic forces of the first three types and made comparisons between those models. They demonstrated that the in-plane gap closing produces the highest power density and represents a preferable design; the in-plane overlap and out-of-plane gap closing converters, however, cause the potential instability and two-plate stiction respectively. The gap closing transducers also have instabilities: pull-in phenomenon. The in-plane overlap plate converter has recently researched by Cuong Le and Einar Halvorsen [11] and Boisseau *et al.* [12].

In terms of electrostatic conversion principles, Mitcheson [13] divided the electrostatic harvesters into two categories, switched and continuous systems, which are taken into con-

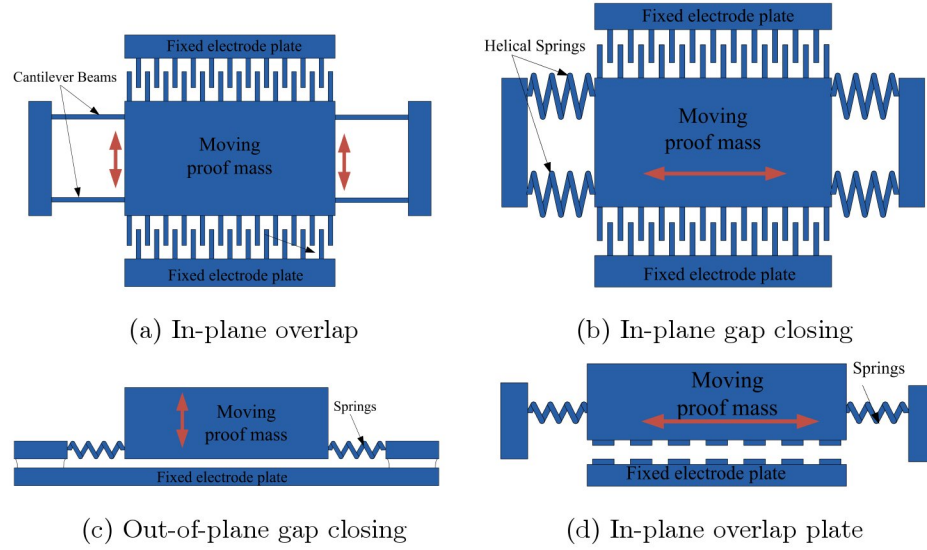


Figure 1.1: Four popular topologies of electrostatic energy harvesting.

sideration of the combination of transducer structures and output power circuits. For instance, in the switched systems, vibrating passive capacitive harvesters generate energy conversion cycles (including charge-constrained, voltage-constrained, or combined charge- and voltage-constrained cycles) using complex embedded micropower electronic circuits. The continuous systems have their transducers continuously transfer electrical energy to loads. The typical examples of this type are electrostatic converters with permanent bias voltage and electret layers. The detailed overview of switched and continuous harvesting systems and their power electronic designs will be mentioned in Chapter 3.

In 1787, one novel charge doubler system named "the doubler of electricity" or known as "Bennet's doubler" was invented by Abraham Bennet. The doubler includes the configuration of three plates, in which the movement of one plate and the interconnection between the plates and ground create the flow of charge into a storage capacitor and thus lead to charge doubling. The operation of the charge doubler is shown in Figure 1.2. At first, plate a , connected to plate c , contains an initial constant charge of $+Q$. When plates a and b overlap each other, because of electrostatic attraction, there exists a flow of charge from ground to b which generate the charge of $-Q$ in plate b . In the second stage, the interconnection between plates a and c is removed; simultaneously, plate b disconnects to ground and moves toward plate c . Once plate c connects to ground, the flow of positive

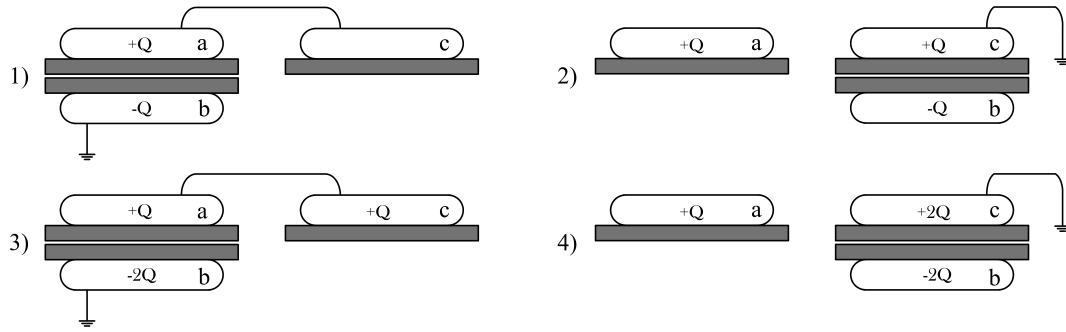


Figure 1.2: The operation of the doubler of charge.

particles or holes from ground into plate *c* due to electrostatic induction creates a charge of $+Q$ to plate *c*. In the next stage, plate *b* returns to plate *a* and is grounded; the interconnection between plates *a* and *c* generates further attraction of negative particles or electrons from ground to plate *b*. Plate *b* is obtained a double charge $-2Q$. The last stage of doubling operation is the same as the previous second stage in which plate *b* move toward plate *c* and the charge in plate *c* is doubled. With the periodical movement of plate *b*, the charge in each plate gradually increases from very low initial energy. Recently, the doubler circuit has been applied for electrostatic energy harvesting by the Queiroz's group [14], [15], [16]. Their researches showed that the harvesting efficiency of doubler circuits remarkably depends on a harvester maximum to minimum capacitance ratio and the doubler of charge avoids high power loss compared to other circuits due to asynchronous and uncomplicated design. From enormous potential advantages from the circuit, this thesis mainly concentrates on the analysis of the charge doubler circuit employed in vibration-to-electric variable capacitor energy harvesters.

1.2 Contributions of the Thesis

The previous researches have focused on the doubler of charge in vibration energy harvesters with symmetrical structures. There is no paper exploring the operation of the doubler in asymmetrical harvesters. Therefore, this thesis will investigate a novel theory in the combination of the doubler of charge and asymmetrical in-plane overlap electrostatic energy harvesters with nonlinear spring stiffness. The structural asymmetry of harvesters brings

forth the reduction in high proof mass displacement which is an indispensable factor in the doubler operation and therefore increases harvested output power for the doubler circuit. Furthermore, the charge doubling system independent of output load enables the nonlinear-spring harvester to scavenge vibration energy in wider bandwidths. In this thesis, a buck converter with an autonomous MEMS switch or a controlled switch is utilized to deliver stored energy from a reservoir into a battery. In addition, the thesis, different from the previous papers which ignored the impact of bias voltage on mass displacement, presents the relations between mechanical and electrical parts of the harvesting system with doubler circuit using simulation results. Finally, the experiment is an attempt to employ the doubler of charge in tiny curved-spring harvesters which was previously fabricated by Son [1].

1.3 Organization of the Thesis

This chapter has just discussed the backgrounds of energy harvesting, its classifications, the general introduction of the doubler of charge and the thesis contribution. The next chapter comprises the analyses of MEMS vibration electrostatic energy harvesters with linear and nonlinear spring stiffness including their lumped modeling, equivalent circuits, output harvesting power and proof mass displacement. The optimizations in harvesting power is also derived in Chapter 2 so as to pave the way for the utilization of the doubler of charge integrated in a harvesting system. Chapter 3 deeply investigates the fundamental operations of the doubler circuit in linear-spring-stiffness harvesters first and explores the superior advantages of the utilization of the circuit in nonlinear-spring-stiffness harvesters. Also, a DC to DC buck converter is used to deliver stored energy in a storage capacitor to a purely resistive load. In Chapter 4, LTSPICE simulation is employed to demonstrate the proposed advantages of the doubler of charge; nonlinear-spring harvester behaviors are also considered in the simulation designs. Furthermore, the effects and power losses of non-ideal devices in the electronic circuit such as diodes, MEMS switches, op-amp buffers and capacitors are also mentioned. Chapter 5 presents the experimental results of the doubler with curved-spring harvesters which are then compared with computer simulations. The final chapter summarizes the key results of the thesis and future work.

Chapter 2

Electrostatic Energy Harvesters

The main goal of the thesis is to research the doubler of charge applied for energy harvesting transducers. As presented in the above chapter, the operation of the charge doubling system is based on Bennet's doubler principles, in which a capacitive harvester driven by vibration force works as a charge pump sustaining a closed-loop charge flow in the system started up from a low bias voltage level. Among different vibration-to-electric energy conversion structures, MEMS capacitive comb-drive transducers are potential solutions for the Bennet's doubler design. After taken into several comparisons, the in-plane overlap harvester is the best candidate deserving interesting research for the doubler of electricity. At first glance, that the proof mass of those harvesters periodically moves between plates due to vibration energy brings forth the charge delivery relatively resembling that in the Bennet's doubler. Furthermore, the in-plane harvesters possess a comb-drive design which provides a high capacitance value. Finally, compared to in-plane gap closing or out-of-plane gap closing shapes, the in-plane overlap varying converters are, according to Roundy [10], able to offer a large proof mass displacement in design and as a consequence create an sufficient maximum to minimum capacitance ratio essential for the doubler operation. From those reasons, the thesis chooses the in-plane overlap devices for research in the doubler of charge only.

This chapter concentrates on analyzing electromechanical features of the selected harvesters. The first section considers the characteristics of simple linear-spring harvesters such as mechanical differential equations, lumped element modeling and equivalent circuits and then derives analytical calculations in output power and mass displacement. With the same

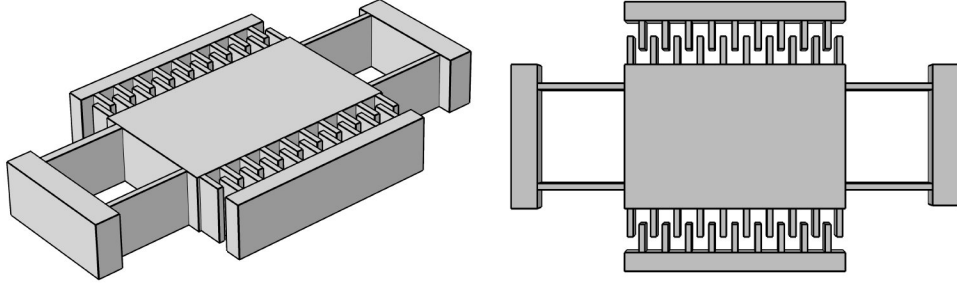


Figure 2.1: The in-plane overlap harvester with linear spring.

procedure, the second section examines the nonlinear-spring-stiffness harvesters including angle-beam and curve-beam harvester and estimates the output power and displacement using harmonic balance methods thanks to Cuong's research [8].

2.1 Linear-spring Harvesters

The symmetric comb-drive harvester, which is used for characterizing, has shown in Figure 2.1. The parameters of this device are listed in Table 2.1. The harvester consists of a movable mass suspended by four linear-spring-stiffness cantilever beams which are all connected to two fixed electrode supports. Driven by surrounding kinetic energy, the mass vibrates between two plates horizontally with the displacement x . Based on [17], [1], the schematic diagram of the symmetric harvester can be presented as an ideal mass-spring-damper system in Figure 2.2. At the first attempt of analysis, two transducer capacitors are connected to purely resistive loads and a bias voltage source in series; therefore, the harvesting system operates in continuous mode in which the transducers are polarized thanks to the bias voltage source and the vibration energy with acceleration a is converted to an electrical charge flow continuously supplying the loads. The energy harvester herein contains two physical systems, i.e. mechanical system (including a mass m , a spring with stiffness k_m and a damper with damping factor b) and electrical system (including resistors R and a voltage source V_e). In order to research doubler systems, it is necessary to firstly understand the operation of linear spring stiffness harvesters and the influences of parameters (e.x. bias voltages, output resistance, or frequency) on their output power and proof mass motion. Therefore, next sections will investigate those characteristics of linear-spring harvester.

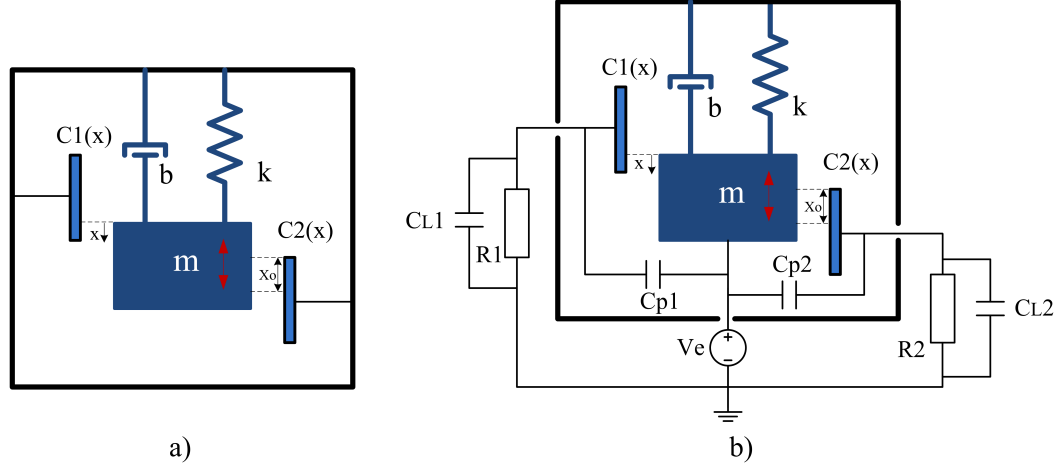


Figure 2.2: In-plane overlap harvesters models a) without and b) with resistive load [1].

Table 2.1: Model parameters for electrostatic energy harvesting device.

Parameters	Value	Unit
Proof mass, m	1.2	mg
Spring stiffness, k_m	21.1	Nm^{-1}
Damping constant, b	2.5e-5	Nsm^{-1}
Initial capacitance, C_o	1.3	pF
Parasitic capacitance, C_p	7.5	pF
Load resistance, R_L	15.2	$M\Omega$
Load capacitance, C_L	5.0	pF

2.1.1 Power Optimization

To analytically calculating this system, a lumped element modeling method is applied to represent mechanical systems in electrical domain. The differential equations of the systems can be expressed as

$$\begin{aligned}
 m\ddot{x} + b\dot{x} + kx + \frac{\Gamma}{C}q &= ma \\
 \dot{q}R + \frac{q}{C} &= -\frac{\Gamma}{C}x
 \end{aligned}
 \tag{2.1}$$

where $k = k_m + k_e = k_m + \frac{\Gamma^2}{C}$ is the total mechanical and electrical stiffness constant (k_m and k_e); C is the half of the sum of initial, parasitic and load capacitance (denoted C_o , C_p ,

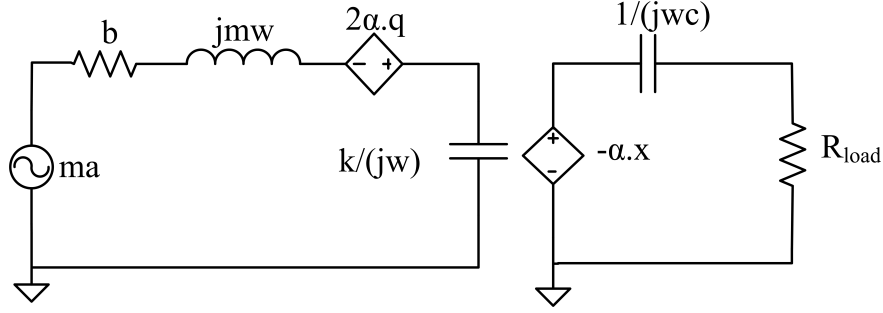


Figure 2.3: Equivalent circuit of the linear harvesting system with resistive load.

and C_L respectively); q is a half of charge difference between two harvesting capacitors. While the first equation of displacement describes the behavior of mechanical part, the second expresses the output electrical performance on the resistor R . The electromechanical coupling factor $a = \frac{\Gamma}{C} = -Ve \frac{C_o}{x_o C}$ shows the relationship between mechanical and electrical systems of the harvester. From (2.1), the equivalent circuit using lumped element modeling of the harvesting system in Figure 2.3 is built for simulation purposes and electrically examined the system behaviors. Using the equivalent circuit in Figure 2.3, the peak value of harvesting power dissipated on resistive load R is

$$P = \frac{a^2 k_m \kappa^2 \omega_c^2 r / \omega_o^3}{[1 - \omega_c^2 (1 + 2\xi r)]^2 + [2\xi \omega_c + \omega_c r (1 + \kappa^2 - \omega_c^2)]^2} \quad (2.2)$$

where $\xi = \frac{b}{2m\omega_o}$ is damping ratio; $\omega_c = \frac{\omega}{\omega_o}$ and $r = \omega_o C R$ are normalized frequency and resistive load respectively. Squared coupling coefficient $\kappa^2 = \frac{k_e}{k_m}$ is defined as the ratio of electrical and mechanical couplings.

It can be seen that the output power depends on angular frequency ω_c , load resistance r and coupling coefficient κ . This section in turns analyzes the maximum points of dissipated power as a function of those variables. Williams and Yates [17] shows that the limited average power of generator is

$$P_{lim} = \frac{m Y_o^2 \omega_o^3}{4\xi} = \frac{m^2 a^2}{2b} \quad (2.3)$$

since the harvester is open-circuit. With a certain value of load resistance, Renno J. M. *et al.* [18] had researched optimal conditions for maximum harvesting power. Their paper showed exact solutions for optimal angular frequency obtained using a trial and error process.

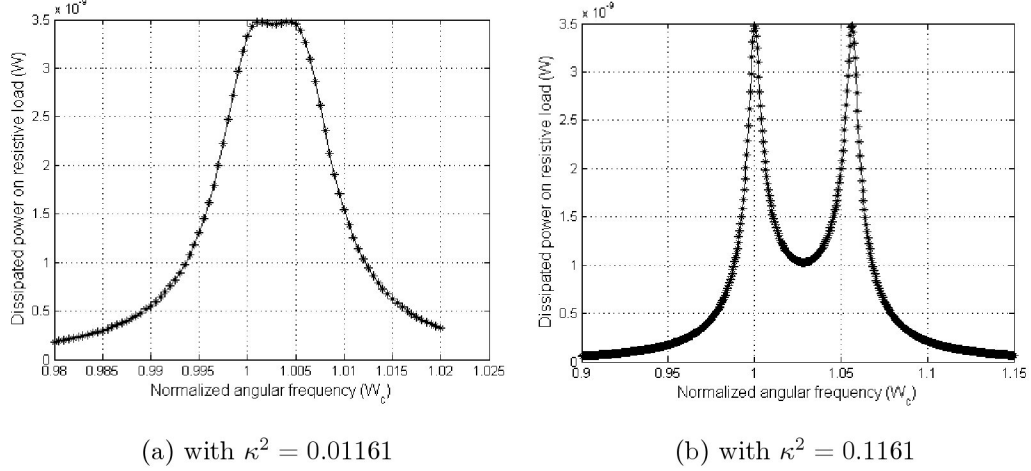


Figure 2.4: Output power peak versus normalized angular frequency under optimal load resistance condition.

$$\omega_r = \frac{\sqrt{2 - 4\xi^2 + \kappa^2 - \sqrt{16\xi^4 - 16\xi^2 - 8\xi^2\kappa^2 + \kappa^4}}}{\sqrt{2}} \quad (2.4)$$

$$\omega_{ar} = \frac{\sqrt{2 - 4\xi^2 + \kappa^2 + \sqrt{16\xi^4 - 16\xi^2 - 8\xi^2\kappa^2 + \kappa^4}}}{\sqrt{2}}. \quad (2.5)$$

The resonant and antiresonant frequencies of electromechanical system are respectively denoted ω_r and ω_{ar} . With the assumption of very small damping,

$$\omega_r = 1 \quad (2.6)$$

$$\omega_{ar} = \sqrt{1 + \kappa^2}. \quad (2.7)$$

From the above equation, it can be seen that the coupling coefficient does not influence the optimized output power when the harvesting system operates at resonant angular frequency $\omega_c = 1$. In the regions of vibration frequency higher than resonant frequency, the squared coupling coefficient κ^2 can be used to conditionally optimize the output power tracking the “new” resonant frequency. Nevertheless, changing the coupling coefficient or frequency value is not enough to make the output power reaching maximum; the output resistive load plays a significant role in obtaining maximal power and therefore must also be optimized.

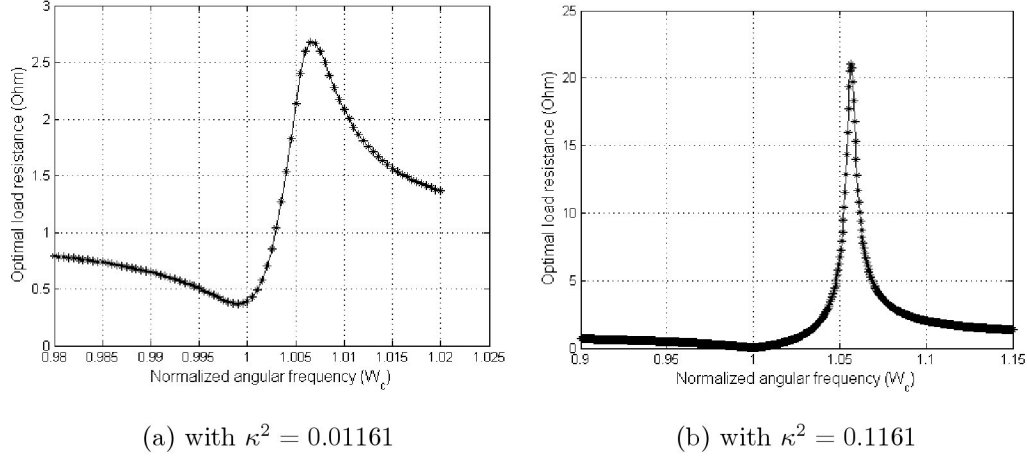


Figure 2.5: Relationship between optimal normalized load resistance and angular frequency.

When the derivative of output power versus load resistance is equal to zero, the squared optimal load resistance value r_{opt}^2 is determined as

$$r_{opt}^2 = \frac{[1 - \omega_c^2]^2 + 4\xi^2\omega_c^2}{4\xi^2\omega_c^4 + \omega_c^2(1 + \kappa^2 - \omega_c^2)^2}. \quad (2.8)$$

With the squared coupling coefficient κ^2 of 0.01161 or 0.1161, Figure 2.4 shows the relationship between maximal output power and normalized angular frequency under the condition of optimizing the output resistance load and Figure 2.5 expresses the optimal normalized load resistance value versus normalized angular frequency. It appears more understandably with the three dimension picture in Figure 2.6 showing output power peak with different fixed values of vibration normalized frequency when squared coupling coefficient and load resistance vary.

One may question the likelihood of coupling coefficient optimization for accomplishing highest power. Let's take the derivative of output power versus κ^2 equal to zero; the result can be obtained that

$$\kappa_{opt}^2 = \frac{1}{r\omega_c} \sqrt{[1 - \omega_c^2(1 + 2\xi_o r)]^2 + [2\xi_o\omega_c + r(\omega_c - \omega_c^3)]^2}. \quad (2.9)$$

With the assumption of very small damping and output resistive loads optimized, the optimal coupling is given as

$$\kappa_{opt}^2 = |1 - \omega_c^2| \sqrt{1 + \left(\frac{1 + \kappa_{opt}^2 - \omega_c^2}{1 - \omega_c^2}\right)^2}. \quad (2.10)$$

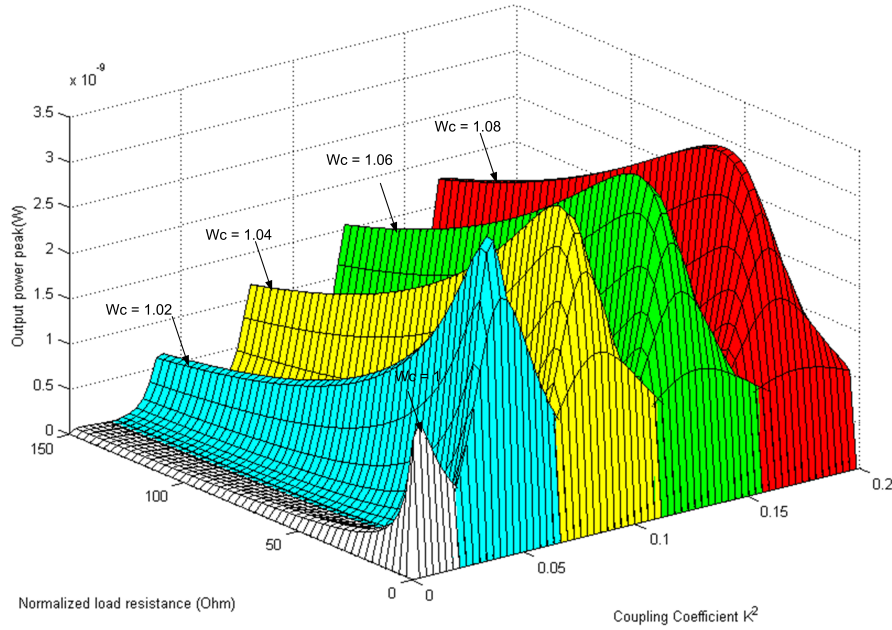


Figure 2.6: Output power performance versus angular frequency and load resistance with different normalized vibration frequency.

Equation (2.10) has two solutions which are $\omega_c = 1$ and $\kappa_{opt}^2 = \omega_c^2 - 1$. It can be concluded that the power optimization conditions for frequency and coupling coefficient are the same; in other words, all stationary points of maximal power position are at resonant frequency $\omega_r = 1$ as well as lie on the curve $\omega_{ar} = \sqrt{1 + \kappa^2}$ and satisfy the optimal resistance condition (2.6).

Through calculation and drawn figures, the harvesting system is highly sensitive to resonant frequency and harvesting output power value, at resonant frequency, considerably depends to output resistance. One proposed solution is offered to reduced this problem by driving the harvester in antiresonant frequency regions; the bias voltage V_e is used to adjust the coupling coefficient which changes the antiresonant points of the system matched with the vibration frequency. Figure 2.6 demonstrates that, at antiresonant frequencies $w_c > 1$, energy harvesters accomplish high output power in wide range of resistive load.

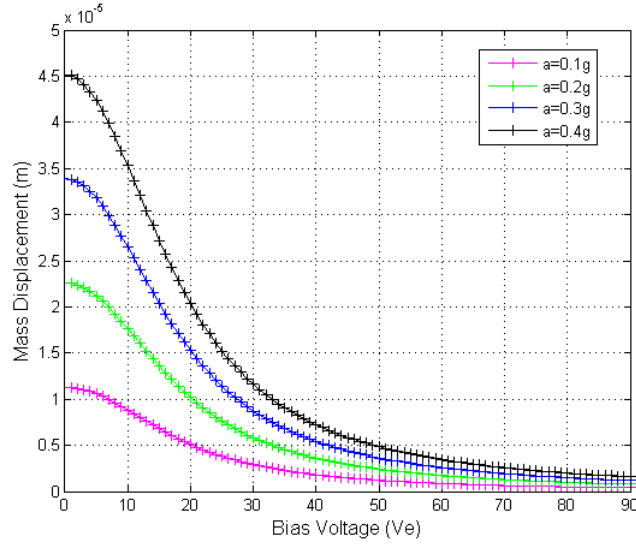


Figure 2.7: Mass displacement versus bias voltage V_e with different acceleration values.

2.1.2 Proof Mass Displacement

As mentioned in Chapter 1, the maximum to minimum capacitance ratio of harvester greatly affects the power of doubler systems; as a result, the displacement of the proof mass m and parasitic capacitance of harvesters require much attention. Without resistive load, the displacement limit at resonant frequency, which the harvester proof mass motion can reach, is

$$X_{lim} = \frac{a}{2\xi\omega_o^2}. \quad (2.11)$$

The symmetric structure of the harvester with linear spring stiffness brings about the equal initial overlaps and maximum or minimum displacement amplitude for both two harvesting capacitors. Therefore, based on (2.1), the general relative displacement peak depending on frequency between the mass and fixed plates can be given as

$$X_o = \frac{a\sqrt{1 + \omega_c^2 r^2 / \omega_o^2}}{\sqrt{[1 - \omega_c^2 (1 + 2\xi r)]^2 + [2\xi\omega_c + \omega_c r (1 + \kappa^2 - \omega_c^2)]^2}} \quad (2.12)$$

The denominator of squared proof mass displacement is the same as that of dissipated power; as a result, mass displacement optimal points are derived with the same results as ones in the previous section. More importantly, when the bias voltage V_e or coupling coefficient increases, the mass displacement, from the equation (2.12), reduces remarkably.

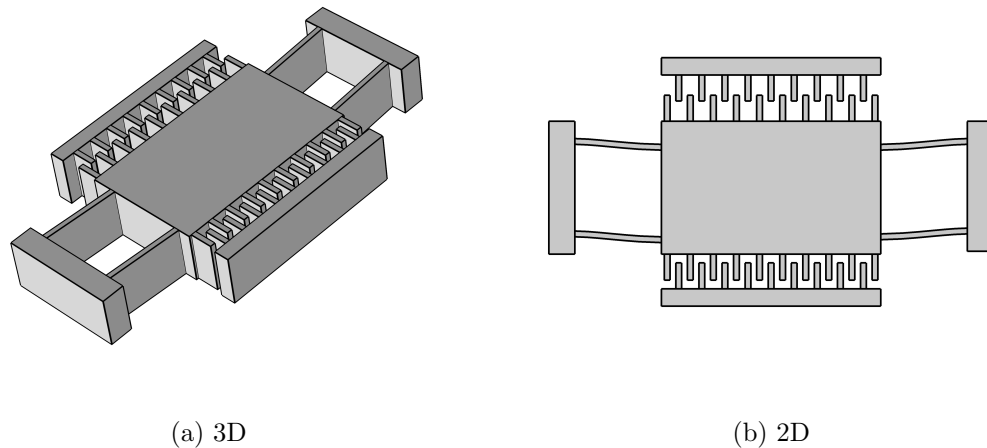


Figure 2.8: Curved-spring harvester.

In Chapter 4, the LTSPICE simulation also illustrates the influence of the bias voltage in doubler circuit on the mechanical mass displacement.

2.2 Nonlinear-Spring Harvesters

This section discusses two types of nonlinear spring harvesters with angled springs and curved springs shown in Figure 2.9 and 2.8. In [1], Son D. Nguyen presented the analysis and calculation of those harvesters using the finite element method (FEM), fabrication process as well as experimental results on asymmetric MEMS energy harvesters with angled and curved springs. [1] first made a comparison between hardening springs and softening springs which demonstrated that the harvesters with softening springs perform higher output power and offer greater potentials for broadening the harvesting bandwidth under white noise vibrations. In order to create softening behaviors, Son proposed inclined springs with two-segment beams, i.e. angled springs, and curved springs, which was originated from MEMS electrostatic actuators and maintain asymmetric bistable characteristic. Both angled-spring and curved-spring harvesters are experimentally proved to bring forth larger bandwidths and mass displacement under frequency down-sweep and white noise vibration than the linear-spring ones.

Equation (2.13) [1] generally describes the nonlinear electromechanical behavior of harvesters with angled springs and curved springs.

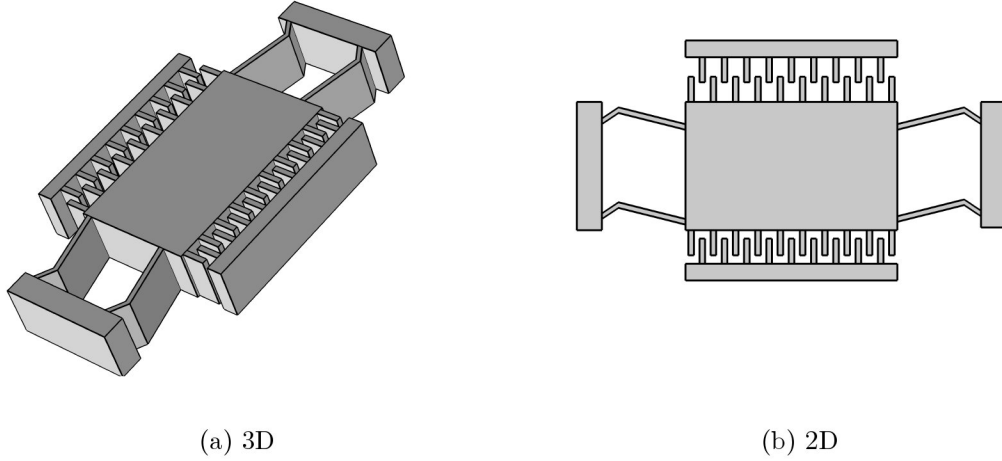


Figure 2.9: Angled-spring harvester.

$$\ddot{x} + b\dot{x} + F_e + F_r + F_s = ma \quad (2.13)$$

$$V_{1/2} = \frac{Q_{1/2}}{C_{1/2}(x)} + V_e \quad (2.14)$$

where F_e is the electrical force calculated as

$$F_e = \frac{1}{2}Q_1^2 \frac{d}{dx} \frac{1}{C_1(x)} + \frac{1}{2}Q_2^2 \frac{d}{dx} \frac{1}{C_2(x)}; \quad (2.15)$$

F_r is the restoring force as

$$F_r = K_1x + K_2x^2 + K_3x^3 + K_4x^4 + K_5x^5 + K_6x^6 + K_7x^7 \quad (2.16)$$

and F_s shows the influences of endstops.

In his thesis, Son D. Nguyen provided an equivalent circuit in Figure 2.10 using lumped element modeling for angled-spring harvesters which was then built in LTSPICE simulations. The parameters of damping b , mass m , the coefficient of nonlinear spring stiffness (K_1 - K_7) and so on were valued thanks to fitting process between simulation and experimental results. The parameters in simulation circuits for curved-spring harvesters in this thesis was also fitted from Cuong H. Nguen's research [8].

In [1], the output voltage for frequency up- and down-sweep from energy harvesters with angled and curved springs are displaced in Figure 2.11. It can be seen that the frequency down sweep mode offers very large power as well as displacement and therefore is

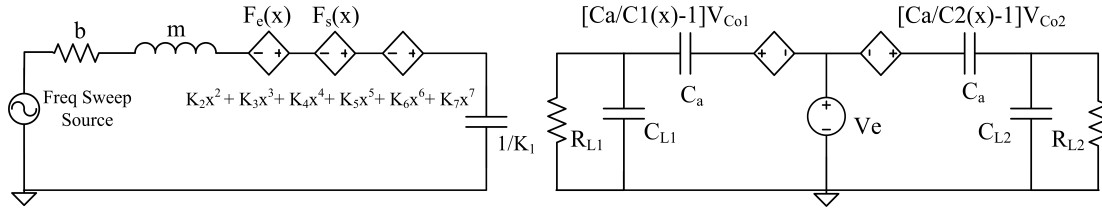


Figure 2.10: The equivalent circuit using lumped element modeling for nonlinear spring harvesters.

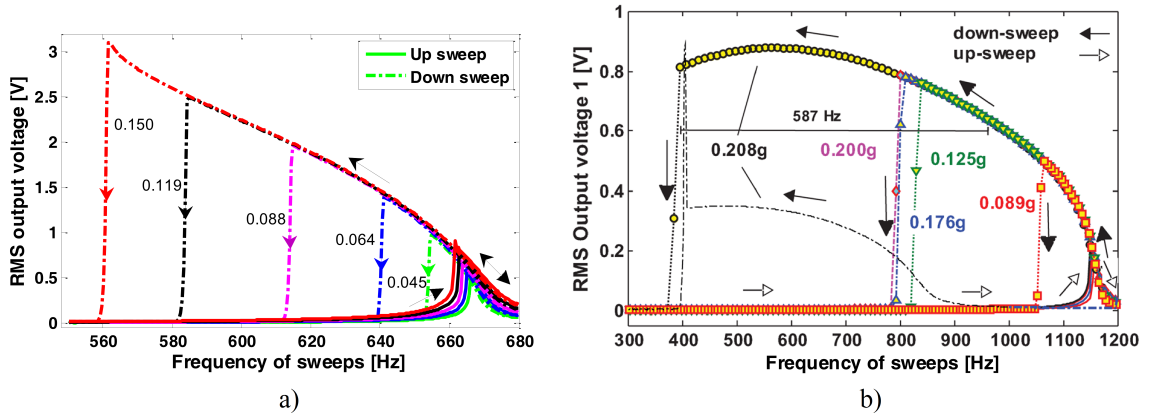


Figure 2.11: Output voltage in down/up sweep of energy harvester with a) angled spring or b) curved spring.

preferable in the operation of charge doubler. One more important factor which supports the suitable combination between the doubler of charge and nonlinear-spring harvester is that the doubler, different from continuous energy converters which harvesting power is tremendously reduced unless output load resistance reaches optimal value, is independent from the output resistance value; therefore, the circuit appropriately functions in wider bandwidth where frequency change varies the output impedance value.

Because of the essential requirement of proof mass displacement in doubler circuit operation, its advantageous features and availabilities for research, the curved harvester designed with the doubler of charge is utilized to conduct experiments in this project. Chapter 3 will investigate the operation and characteristic of the doubler of charge in linear-spring and demonstrate the crucial benefits of the combination nonlinear-spring harvesters with the doubler circuit. This is also the new ideas of the thesis.

Chapter 3

Power Conversion Circuit

Now that the power and mass displacement consideration of linear and nonlinear electrostatic generators with purely resistive load has studied and analyzed, this chapter first summarizes some techniques of designing an energy harvesting circuit and then mainly focuses on a novel power conversion circuitry, the doubler of charge. The doubler circuit is initially employed in linear-spring symmetric harvesting structures; afterwards, the advantageous features of the utilization of doubler circuit in asymmetric harvesters are demonstrated thanks to broadening harvesting bandwidth, decreasing the required minimum displacement and providing higher output power for doubler systems. In the last sections, the usage of a buck converter and the effects of non-ideal devices are presented to show realistic applicability of the doubler of charge in practice.

3.1 Conventional Circuits

Distinct electronic interfaces are designed based on the requirements of two different types of harvesting systems: continuous and switched electrostatic harvesting systems. The former consists of electret layers keeping permanent charge or a bias voltage source to polarize the harvesting capacitors. The design of conversion circuits for this structure is concentrating on resistive load optimization or electromechanical coupling factor improvement. The later is operated using an initial temporary bias voltage and therefore requires more complex power circuits able to pump the harvested energy back to the stored reservoir as well as

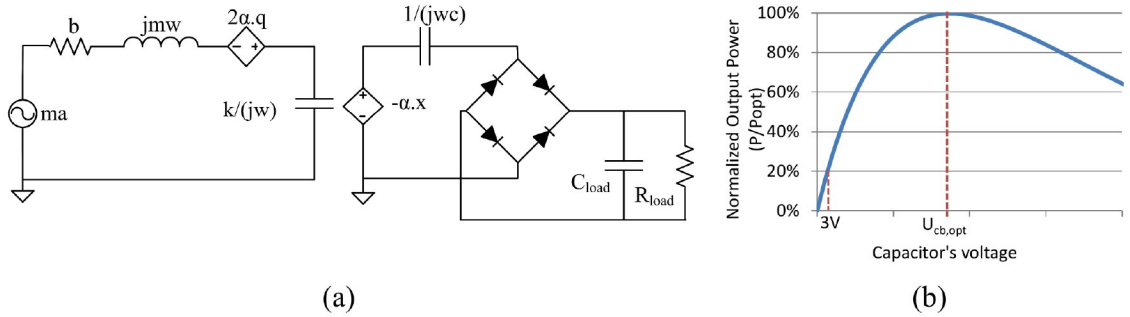


Figure 3.1: (a) Simple passive power converter with diode bridge and (b) optimal output voltage at U_{Cb} [2].

charge and discharge the harvester capacitors. This section will review some popular power conversion circuits for different harvesters.

3.1.1 Continuous Electrostatic Harvesting Systems

In this type of systems, harvested vibration energy is continuously delivered into the load. Due to the assumption of harvesting energy from periodic vibrating sources, the output of electrostatic generator is of near sinusoidal waveform; therefore, harvesting systems needs AC/DC converter to convert the AC output voltage from the generator into DC form as sensors or storing batteries must be charged by DC power. Diode bridge rectifier is a simple standard interface circuit for such converter, which is popular and less costly. However, very low power conversion efficiency and power loss on diodes are the main disadvantages of this standard circuit. In order to increase the efficiency, Lefeuvre *et al.* [19] and D'Hulst *et al.* [20] developed buck boost converters which comprise of a twofold goal: tracking the generators optimal working point through tuning active resistive loads and generating a proper DC voltage for output sensors no matter how low or high the output voltage from transducers is. Guyomar and Liang *et al.* proposed synchronized switch harvesting on inductor (SSHI) technique [3] and modified SSHI technique [4] to reduce power loss as well as obtain higher efficiency. In general, SSHI circuits are utilized to increase coupling efficiency by switching a MOSFET series with an inductor to increase the generator voltage and put this voltage in phase with the vibration velocity. Following sections will mention these approaches for continuous electrostatic harvesting systems

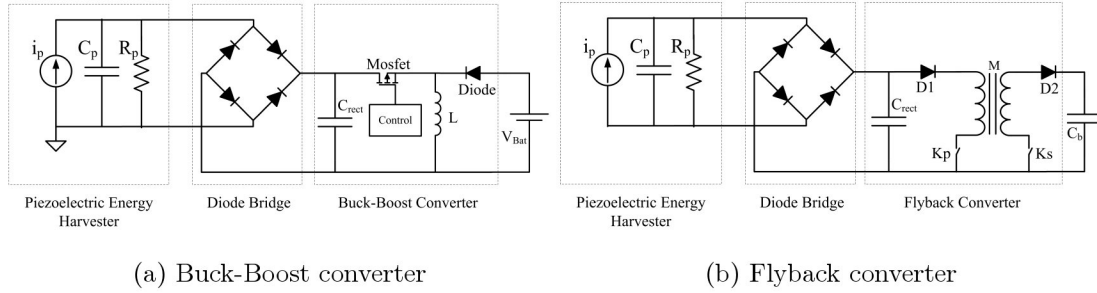


Figure 3.2: Different active power converters [2].

Standard Interface Circuit

Standard interface circuit in Figure 3.1 includes a diode bridge rectifier, a filtering capacitor, and a load. This power circuit maintains two drawbacks. First, in [21], Shu and Lien showed the calculation of AC-DC power output for a rectified piezoelectric¹ device and indicated optimal load resistance values for uncoupled, in-phase, and analytic calculation of harvesting systems. Nevertheless, the passive power converter is not able to change the load resistance needed for tracking optimal power points. Second, the optimized power of the vibration harvester, from Figure 3.1, is obtained at a high value of capacitor's voltage U_{Cload} which is much higher than the proper voltage supplying for sensors. If harvesting system works at low rectified voltage, e.g. 3V DC, the efficiency will be dropped down remarkably. To solve these issues, some active power converters such as the buck boost converter, the flyback converter or SSHI converters are proposed.

Buck Boost Converters

D'hulst and Lefevre *et al.* showed an active power converter in Figure 3.2a, i.e. buck boost converter, used to track the optimal working points of the generators. The circuit input, when the power circuit works in discontinuous current mode, can be equivalent to a changeable resistive load independent on the sensor or battery output voltage and current,

$$R_{in} = \frac{2Lf_s}{D^2} \quad (3.1)$$

¹It is shown that the piezoelectric and electrostatic harvesters have the same equivalent electromechanical circuits, so their power converter analysis are compatible for each other.

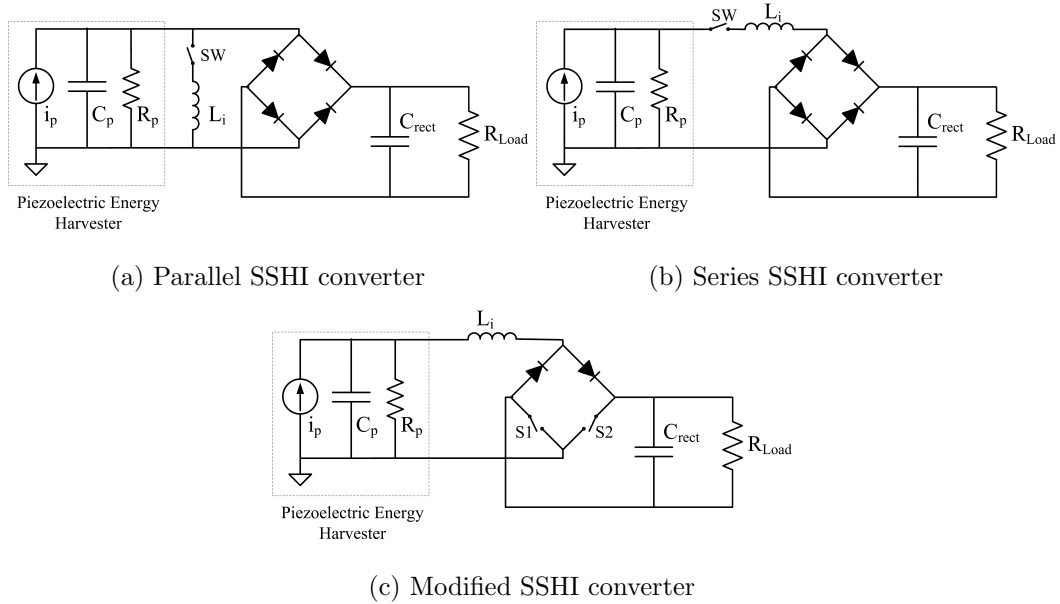


Figure 3.3: Different types of SSHI converter [3], [4].

In the Chapter 2, the optimal load resistance values and generator power output function were brought forth for a purely scavenging system with a resistive load only. In [22], the power output of harvesters followed with a diode bridge rectifier, a voltage smoothing capacitor and a load is taken into account. This calculation (which is similar to the in-phase analysis from Shu and Lien [21]) assumed that the driving force F and the relative velocity of the mass \dot{x} are in phase. The maximal power can be achieved since the active input average resistance of the DC-DC converter is perfectly matched with the optimal points. Another benefit of this power circuit is offering a compatible output voltage for sensors or batteries in any case of high or low input rectified voltage. Further loss power measurements of whole system can be found in [20].

Flyback Converter

The flyback converter shown in Figure 3.2b also has the same potentials of tracking optimal points. This type of circuit gives more flexibility to control winding ratio which affects the output voltage amplitude. Further study on this circuit is presented in [2] (which does not mention how to calculate the active resistance). Another similar circuit of this type is synchronized electric charge extraction (SECE) circuit [22].

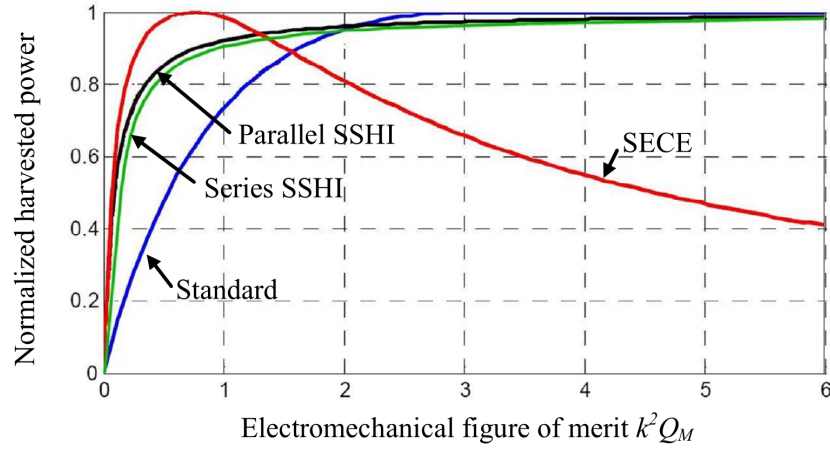


Figure 3.4: Harvested powers of different power converters as a function of the electromechanical figure of merit [2].

SSHI Converters

Guyomar et al. [3] applied the synchronized switch harvesting on inductor (SSHI) technique using the circuit in Figure 3.3a for weakly electromechanically coupled harvesters in which an inductor and a MOSFET switch are in series and all inserted between the harvester and the diode bridge. The switch is opened almost of time of harvesting cycles and briefly closed when the displacement extremum occurs. This results in piezoelectric generator voltage inversed and having the same sign as the mass velocity. That the output voltage of generator increases leads to the output power optimization. [3] also calculated the output power and optimal load resistance in case of weak coupling factor for the whole harvesting systems. The effectiveness of SSHI technique, according to this paper, is highly significant and increase the power up to 900% compared to the standard circuit as it is employed for the weakly coupling structures or the harvesters not working at their resonance. For the harvesters working at resonance, the technique is beneficial at low coupling coefficient.

The method proposed by Guyomar is also called Parallel SSHI technique. The Series SSHI circuit [22] in Figure 3.3b has the same functions but is created by connecting a conductor and switch in series with the harvester and diode bridge. In this case, the harvester is always in open-circuit configuration. The active SSHI power circuit controls the switch synchronously. From the original SSHI techniques, its modified circuits (in Figure

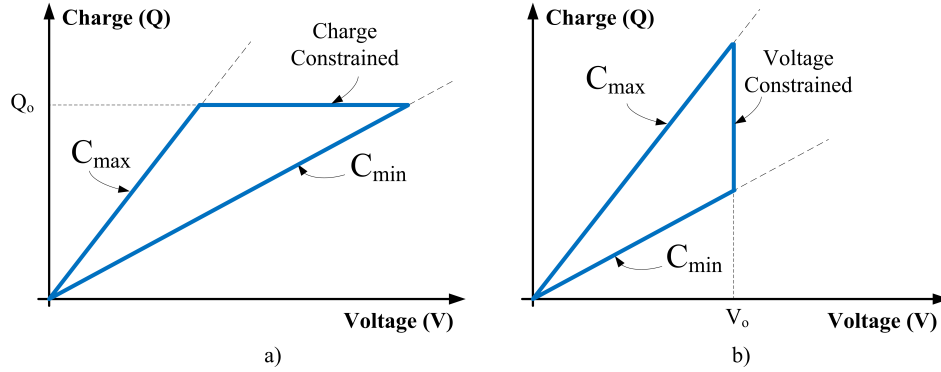


Figure 3.5: a) Charge-constrained conversion cycle and b) voltage-constrained conversion cycle.

3.3c) discussed in [4] can decrease loss power on diodes in the previous circuits thanks to replacing two diodes of the rectifier by two MOSFETs. The comparison of these techniques [2] is shown in Figure 3.4.

3.1.2 Switched Electrostatic Harvesting Systems

A large number of researches have focused on continuous electrostatic harvesters thanks to their circuitry simplification and therefore less power loss. Another reason is due to the development of microfabrication techniques to create the electret layers. However, the less availability and high cost are main downsides of the electret fabricating techniques, so it is worth to further research in circuits for switched-mode electrostatic harvesters. The main challenge of this type of vibration-to-electric converter is to create a conversion cycle through charging and discharging the harvester capacitor. There are three types of conversion cycle including charge-constrained, voltage-constrained and combined voltage- and charge-constrained cycles, which are straightforwardly described through Q-V diagrams in Figure 3.5. Those conversion cycles will be described in the following section.

Charge-constrained Converters

A typical example of the charge-constrained circuit [23] is shown in Figure 3.6a. The harvester starts a harvesting cycle at maximum values of capacitor $C_{var} = C_{max}$. The reservoir capacitor is charged with an initial voltage. The MOSFET M2 opens and the M1 closes.

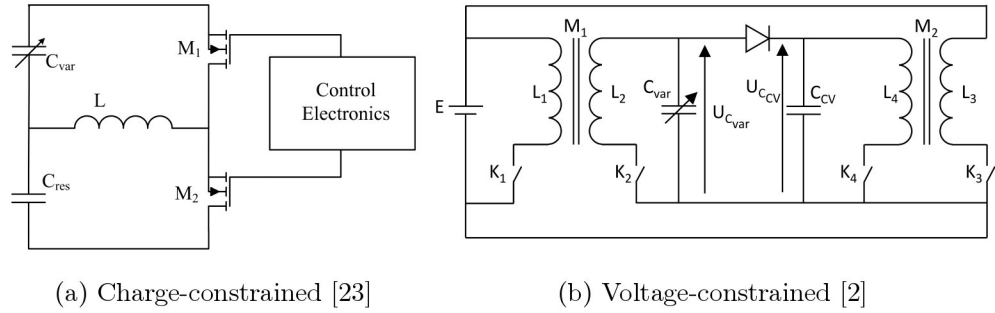


Figure 3.6: Two types of switched electrostatic harvesting system.

The charge is transferred from the reservoir to an inductor L and leads to the increase of energy in inductor L . After a certain moment, the switch $M1$ turns off, and $M2$ turns on simultaneously. All energy in the inductor is pumped into harvesting capacitor C_{var} . Until the current I_L is zero, the switch $M2$ is off and the charge step finishes. The discharge step starts when the harvesting capacitor C_{var} reduces to minimum C_{min} . $M1$ turns on and a reverse inductor current ramps up until all charge from the harvesting capacitor is delivered to C_{res} . Then, $M1$ is off and $M2$ is on till all the energy in the inductor is transferred into the storage capacitor. From that, the conversion cycle repeats. The advantage of this charge-constrained circuit is the simplicity of the designed system. However, there exist several disadvantages such as utilizing bidirectional switches, requiring a synchronous control system and having high power loss.

Voltage-constrained Converters

There is no specific example of this converter which is rarely used in designing an energy harvesting conversion. However, an example of a voltage-constrained converter in Figure 3.6b is mentioned in [2]. The operation difference between a voltage-constrained converter and a charge-constrained converter illustrated in Figure 3.5 and 3.6 is when the harvester capacitance drops from C_{max} to C_{min} . While the voltage-constrained power circuit disconnects the transducer from the bias voltage so that its charge keeps constant and its voltage increases, the transducer in charge-constrained conversion is connected to a fixed voltage source V_o ; the reduction in harvester capacitance leads to the decrease of charge ΔQ . The conversion cycle is created with the harvested energy equal to $\Delta E = \frac{1}{2}\Delta Q V_o$.

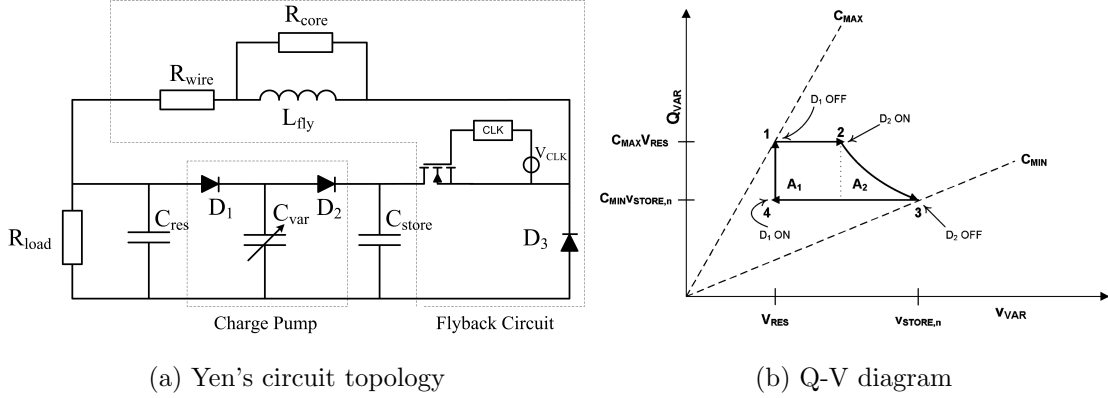


Figure 3.7: An example of combined voltage- and charge-constrained converters [5].

Combined voltage- and charge-constrained converters.

Yen's circuit shown in Figure 3.7 [5] is a kind of combined voltage- and charge-constrained converter in which the harvesting capacitor works as a pump to transfer charge from reservoir capacitor into a storage capacitor. Two diode D_1 and D_2 work as asynchronous switches opening and closing based on the voltage difference between three capacitors - C_{res} , C_{var} , C_{store} . Yen proved that the power flow have a limitation when the voltage on storage capacitor reaches the saturated value as

$$V_{store_maximum} = \frac{C_{max}}{C_{min}} V_{reservoir} \quad (3.2)$$

In order to reduce the saturation of pumped energy in storage capacitor and recharge the reservoir capacitor for next power conversion cycles, a flyback circuitry is designed as feedback circuit to get out the energy in the storage capacitor to supply resistive load and recharge C_{res} . The paper also discussed that the source-referenced clock minimizes the energy injection more than the ground-referenced clock. The harvesting energy efficiency, according to the paper, is about 19.1%.

Next section will focus on a new combined voltage- and charge-constrained converter named the doubler of charge, which is appropriately designed for the in-plane comb-drive structures with two opposite variable capacitors. By using only diodes, the converter can work in asynchronous mode like the Yen's circuit but has a simpler design which consumes less power.

3.2 The Doubler of Charge

With the harvesters generating very low power of few micro watts, the requirement of power conversion design is low power loss. The first circuit designing attempt is to reduce as many number of switch components as possible to minimize the energy needed for switching synchronous controls and switching loss. Furthermore, the number of passive devices such as diodes, capacitors needs to be decreased in low power circuits. Another consideration in power conversion circuits for electrostatic harvester is their ability to recharge harvesting capacitors. Some researches in Yen's paper using flyback circuit or in Mitcheson's buck-boost circuits with bidirectional switches offered several solutions in harvester recharging. However, the tradeoff between power loss and harvesting efficiency occurs in these proposed circuits. This chapter proposes a design of power circuit which applies the theory of the doubler of charge. The simple structure of the doubler brings forth several advantages such as achieving very low power loss thanks to using only passive devices with asynchronous controls, obtaining high power in high bias voltage, and recharging a storage capacitor without using additional circuits. The doubler circuit with a bias battery is firstly used to straightforwardly investigate the operation of the doubler and several influences of bias voltage, asymmetrical structures and real diodes on the doubler performance. After that, a storage capacitor replaces the battery to store harvested energy in the circuit. In the following sections, the doubler of charge with symmetrical and asymmetrical harvesting systems will be analyzed in details.

3.2.1 Symmetrical Harvesting Systems

The charge doubling circuit can be used to directly charge for a battery or build up the energy in a storage capacitor as in Figure 3.8. In order to analyze the doubler operation straightforwardly, it is assumed that the displacement of the proof mass is independent of the change in bias voltage on each harvesting capacitor. Another assumption of ideal lossless diode in the doubling circuit is to ignore the influence of leakage current, diode capacitance and forward bias voltage. The harvesters with linear springs are utilized to explore the doubler operation. This is because the linear-spring harvesting systems normally

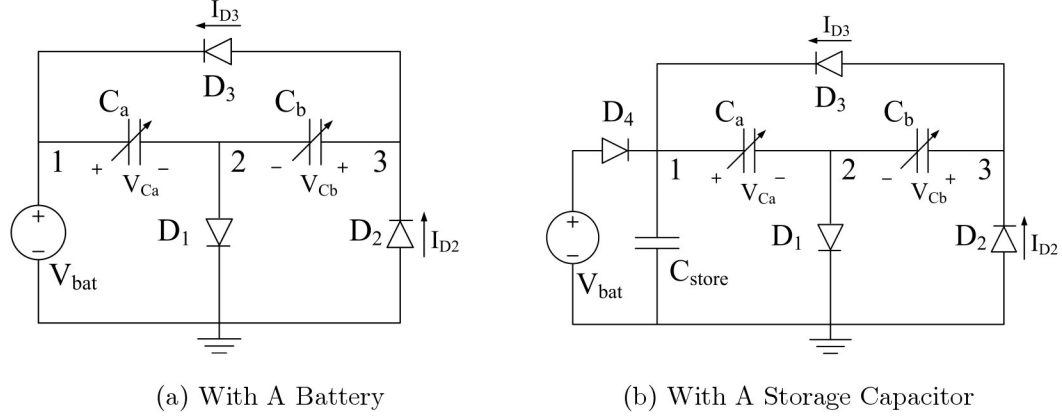


Figure 3.8: The doubler of charge topologies.

Table 3.1: Voltage and charge on capacitors C_a and C_b with linear-spring harvesters.

Value of C_a ; C_b	V_{Ca}	V_{Cb}	Q_{Ca}	Q_{Cb}
$C_{max}; C_{min}$	V_{bat}	V_{bat}	$V_{bat}C_{max}$	$V_{bat}C_{min}$
$C_{max} - \Delta C_x; C_{min} + \Delta C_x$	$V_{bat} \frac{x}{x+1-\sqrt{x+1}}$	$V_{bat} \sqrt{\frac{1}{x+1}}$	$V_{bat}C_{max}$	$V_{bat}C_{min}$
$C_{min}; C_{max}$	$V_{bat} \frac{2x+1}{x+1}$	$V_{bat} \frac{x}{x+1}$	$V_{bat} \frac{2x+1}{x+1} C_{min}$	$V_{bat} \frac{x}{x+1} C_{max}$
$C_{min} + \Delta C_y; C_{max} - \Delta C_y$	V_{bat}	V_{bat}	$V_{bat} \frac{2x+1}{x+1} C_{min}$	$V_{bat} \frac{x}{x+1} C_{max}$

Note: x is the ratio between C_{max} and C_{min} .

have perfectly symmetric structures in which two harvester capacitors have the same initial overlap x_o , parasitic capacitor C_p and the displacement is considered to oscillate about the time axis with the amplitude x_m . Therefore, harvester capacitors C_b and C_a maintain the equal maximum C_{max} and minimum C_{min} . The relationships between voltage, current and displacement on harvester capacitors C_b and C_a are shown in Figure 3.9 and the value of harvester capacitance, charge and voltage in four stages of doubler circuit operation are also expressed in Table 3.1.

Initially, in Figure 3.9, the battery charges C_a until $V_{Ca} = V_{bat}$. After a few transient vibration cycles, the voltage and charge on each capacitor are changed periodically. In the first stage, when $C_a = C_{max}$ and $C_b = C_{min}$ the voltage of those capacitors are approxi-

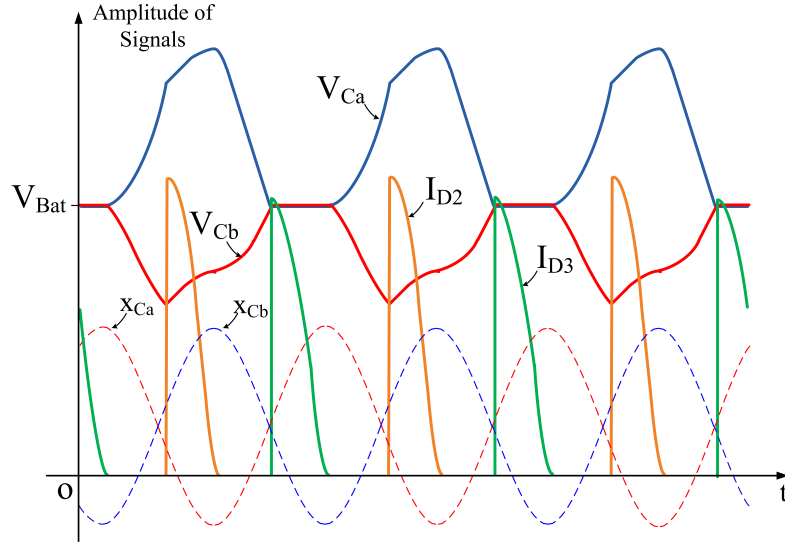


Figure 3.9: Voltage, charge and displacement waveforms on harvesting capacitors in doubler operation.

mately equal to V_{bat} due to the charge pumped from C_b to C_a in the previous cycle. Due to vibration energy, the proof mass m displaces Δx ; C_a decreases while C_b increases with the same amount of ΔC_x . However, there is no flow of charge on diodes D1, D2 and D3 because the condition (3.3) is satisfied.

$$V_{Cb} < V_{bat} < V_{Ca} < V_{Cb} + V_{bat}. \quad (3.3)$$

With the constant charge $Q_{Cax} = Q_{oCa} = V_{bat}C_{max}$ and $Q_{Cbx} = Q_{oCb} = V_{bat}C_{min}$, the voltage in capacitor C_a increases to satisfy the relationship $Q = V.C$ and the voltage in capacitor C_b decreases simultaneously. Until the condition (3.4) occurs, the capacitor C_a and C_b change to the value of C_{ax} and C_{bx} respectively; the diode D2 starts to conduct. The values of ΔC_x can be determined based on following equations (3.4)-(3.6)

$$V_{Cax} = V_{Cbx} + V_{bat} \quad (3.4)$$

$$\frac{V_{bat}C_{max}}{C_{max} - \Delta C_x} = \frac{V_{bat}C_{min}}{C_{min} + \Delta C_x} + V_{bat} \quad (3.5)$$

$$\Delta C_x = \sqrt{(C_{max} + C_{min})C_{min}} - C_{min}. \quad (3.6)$$

From the derived capacitor ΔC_x , the voltage and capacitance on C_a and C_b are calculated in Table 3.1. In the second stage, because $V_{Cax} \geq V_{Cbx} + V_{bat}$, the capacitor C_a pumps

amount of charge ΔQ_x into C_b . In order to achieve positive charge ΔQ_x , there are two requirements which are the low leakage currents on diodes D1, D2, D3 so that the charge stored in each capacitor is not depleted and the value of Δx smaller than twice maximum proof mass displacement amplitude x_m or the pumped charge ΔQ_x generated before the proof mass displacement reaches maximum. With no leak power loss, the latter is satisfied since the mass displacement amplitude x_m of a harvester is larger than x_{req} which is

$$x_m > x_{req} = M(\sqrt{5} - 2) \quad (3.7)$$

where $M = \frac{C_p + C_o}{C_o} x_o$. The paper [15] presents that the requirement of achieving positive energy is the ratio of C_{max} and C_{min} is larger than the golden ratio. Actually, further calculation demonstrates that two conditions are equivalent; however, the minimum required displacement shows an essential factor in designing the harvesters working in doubler circuits and the condition of the limited displacement is preferably employed to analyze the nonlinear-spring harvester in next section.

In the next stage, the capacitor C_a continues pumping out the charge until reaching C_{min} . With the relation $V_{Ca} \geq V_{Cb} + V_{bat}$, C_b obtains more charge and the voltage V_{Cb} goes up. Once the value of the capacitor C_a is C_{min} , the diode D2 stops conducting; V_{Ca} is still V_{bat} larger than V_{Cb} . The total charge transferring from C_a to C_b can be calculated as

$$\Delta Q_x = V_{bat} \frac{\frac{C_{max}}{C_{min}} - \frac{C_{min}}{C_{max}} - 1}{\frac{1}{C_{max}} + \frac{1}{C_{min}}}. \quad (3.8)$$

Afterwards, the condition (3.3) reoccurs; the diodes D1, D2, and D3 are reverse-biased. Due to the charge of each capacitor keeping constant, when C_a increases to C_{ay} and C_b drops to C_{by} , the voltage V_{Ca} starts plummeting whereas the voltage V_{Cb} starts sloping up. Because connected to the bias voltage of battery V_{bat} , the voltage of C_a cannot be smaller than V_{bat} . At a certain capacitance change of ΔC_y in C_a or C_b , the voltage on C_b begins to be equal and then slightly larger than the voltage on C_a ; it is the time when the conduction of diode D3 takes place. The value of ΔC_y is calculated as

$$\Delta C_y = \frac{C_{max} C_{min}}{C_{max} + C_{min}}. \quad (3.9)$$

In the same manner, the condition to obtain positive charge ΔQ_y , which is pumped from C_b to C_a , is taken into consideration. The proof mass displaces amount of Δy . From

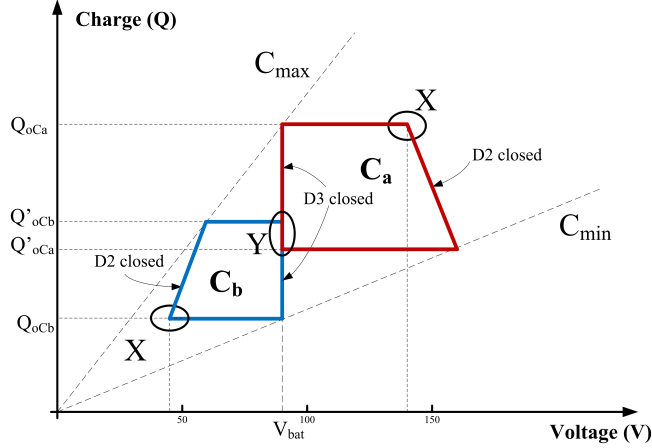


Figure 3.10: Voltage and charge diagram of harvesting capacitors with linear spring.

the equation of $\Delta y < 2x_m$, the mass displacement amplitude x_m must be again larger than $x_{req} = M(\sqrt{5} - 2)$.

In the final stage, the charge from C_b is transferred into C_a until C_b reaches C_{max} and $C_a = C_{min}$. Because of the requirement of constant voltage of V_{Ca} , V_{Cb} and V_{Ca} are equal to V_{bat} ; therefore, the flowing charge ΔQ_y can be derived as

$$\Delta Q_y = V_{bat} \frac{\frac{C_{max}}{C_{min}} - \frac{C_{min}}{C_{max}} - 1}{\frac{1}{C_{max}} + \frac{1}{C_{min}}} = \Delta Q_x. \quad (3.10)$$

With the pumped charge of ΔQ_y , the capacitors C_a and C_b again have the same initial charge of $V_{bat} \cdot C_{max}$ and $V_{bat} \cdot C_{min}$ respectively. The new cycle of energy transfer, which is the same as vibration cycle, repeats. Notably, without considering the loss on diode or capacitor, the energy is conserved in a doubler conversion cycle.

From these calculation results shown in Table 3.1, the Q-V graph is drawn in Figure 3.10.

In reality, the harvester performance is more complicated. For example, because of fabrication process, the proof mass seldom positions at the middle of harvester structure, or the design of the transducers with curve or angle cantilever beams creates the comb-drive asymmetrical structure. The asymmetrical issues trigger the discrepancies of two variable harvesting capacitors. This not only changes transducer behaviors but also affects the operation, limitations, and efficiency of charge doubling circuit. Next section presents the

doubler of charge in harvesting systems with nonlinear spring stiffness.

3.2.2 Asymmetrical Harvesting Systems

Figures 2.9 and 2.8 show angled-spring and curved-spring harvesting devices which structures are made asymmetrically. It is assumed that the initial overlap x_{oa} of capacitor C_a , in the asymmetrical harvesters, is smaller than x_{ob} of capacitor C_b . Therefore, the maximum $C_{a,bmax}$ and minimum value $C_{a,bmin}$ of C_a and C_b no longer equal. Moreover, the proof mass m asymmetrically oscillate about the time axis with the maximum overlap x_m on capacitor C_a different from the maximum overlap y_m on capacitor C_b . Using the same analysis, the voltages on two capacitors at $C_a = C_{amax}$ and $C_b = C_{bmin}$ are the same as V_{bat} . Because of the displacement Δx of proof mass, the capacitor C_a decreases while C_b increases. Until the condition of $V_{Cax} = V_{Cbx} + V_{bat}$ occurs, the charge ΔQ_x starts to flow from capacitor C_a to C_b . Using the equations

$$V_{Cax} = V_{Cbx} + V_{bat} \quad (3.11)$$

or

$$\frac{C_{pa} + C_{oa}(1 + \frac{x_m}{x_{oa}})}{C_{pa} + C_{oa}(1 + \frac{x_m - \Delta x}{x_{oa}})} = \frac{C_{pb} + C_{ob}(1 + \frac{x_m}{x_{ob}})}{C_{pb} + C_{ob}(1 + \frac{x_m - \Delta x}{x_{ob}})}, \quad (3.12)$$

the quadratic function of Δx can be derive as

$$\Delta x^2 + 2(B - x_m)\Delta x - (B - x_m)(A + x_m) = 0; \quad (3.13)$$

therefore, Δx can be deduced as

$$\Delta x = \sqrt{(B - x_m)(A + B)} + x_m - B \quad (3.14)$$

where $A = \frac{C_{oa} + C_{pa}}{C_{oa}}x_{oa}$ and $B = \frac{C_{ob} + C_{pb}}{C_{ob}}x_{ob}$ are characteristic parameters of capacitors C_a and C_b respectively. To accomplishing positive charge ΔQ_x , the displacement Δx must be twice times smaller than the maximum displacement of x_m ; in other words, the condition $V_{Cax} = V_{Cbx} + V_{bat}$ must occur before the mass displacement is maximum. From this requirement, the minimum required displacement of any asymmetrical harvester is

$$x_m > x_{req} = \frac{1}{2} \left(\sqrt{(A + B)(A + 9B)} - A - 3B \right). \quad (3.15)$$

In order to calculate the amount of charge flowing from C_a to C_b when C_a reaches minimum C_{amin} and C_b reaches maximum C_{bmax} , the condition of $V_{Ca} = V_{Cb} + V_{bat}$ ends

up with the relationship (3.16) between the pumped charge and capacitors maximums and minimums or the relationship (3.17) between the charge and characteristic parameters constants A and B.

$$\Delta Q_x = V_{bat} \frac{\frac{C_{amax}}{C_{amin}} - \frac{C_{bmin}}{C_{bmax}} - 1}{\frac{1}{C_{bmax}} + \frac{1}{C_{amin}}}, \quad (3.16)$$

or

$$\Delta Q_x = V_{bat} \frac{C_o}{x_o} \left[2x_m - \frac{(A - x_m)(B + x_m)}{A + B} \right]. \quad (3.17)$$

In the next steps of doubler operation, with the same calculation in the previous section since C_a and C_b return the value of C_{amax} and C_{bmin} respectively, a charge of ΔQ_y pumped from C_b to C_a with the value is equal to ΔQ_x . The energy conservation in the charge doubler is maintained. The displacement of proof mass, when capacitor C_b starts deliver electrostatic energy to C_a , is

$$\Delta y = \frac{(A - x_m)(B + x_m)}{A + B}. \quad (3.18)$$

Of course, this displacement must satisfy the requirement that $\Delta y < 2y_m$, where y_m is the maximum amplitude of the mass displacement when the mass moves toward to C_a side. Thus, the minimum required displacement y_{req} again recalculated for this stage is

$$y_m > y_{req} = \frac{1}{2} \left(\sqrt{(A + B)(A + 9B)} - A - 3B \right) = x_{req}. \quad (3.19)$$

The mass displacement minimums of x_{req} and y_{req} are exactly equal. Figure 3.11 shows the relationship between minimum required displacements x_m or y_m and the parameters A and B of the harvesting capacitors. From this analysis, three important conclusions can be drawn out. Firstly, the required displacement x_{req} of proof mass seems to be smaller when the parameter constant A is smaller than B. In other words, when the charge doubling circuit is integrated with a transducer, the variable harvesting capacitor with smaller parameter constant (, e.g. A or B) should be put in the position of capacitor C_a near the storage capacitor or battery in Figure 3.11 whereas the larger one should be place in the position of capacitor C_b near diode D3. Secondly, the asymmetrical issue also influences the transducer design. Let consider the sum of A and B

$$A + B = \frac{C_{pa} + C_{oa}}{C_{oa}} x_{oa} + \frac{C_{pb} + C_{ob}}{C_{ob}} x_{ob} = x_{oa} + x_{ob} + \left(\frac{C_{pa}}{C_{oa}} x_{oa} + \frac{C_{pb}}{C_{ob}} x_{ob} \right), \quad (3.20)$$

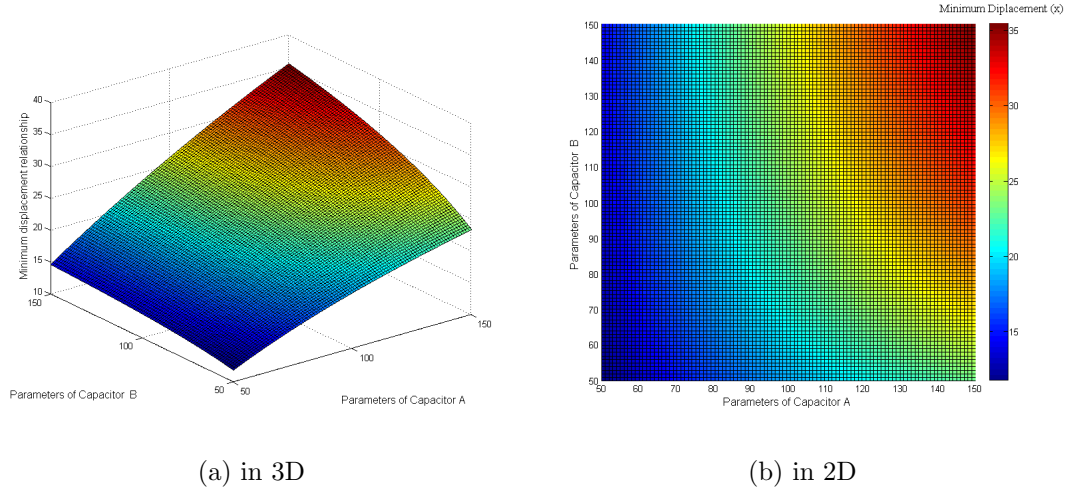


Figure 3.11: The minimum required displacement as a function of A and B.

or

$$A + B = x_{oa} + x_{ob} + \frac{C_{pa}g_o}{N\varepsilon_o t_o}. \quad (3.21)$$

with $\frac{x_{oa}}{C_{oa}} = \frac{y_{ob}}{C_{ob}} = \frac{x_o}{C_o} = \frac{g_o}{N\varepsilon_o t_o}$. Since the proof mass is moved between fixed fingers, with the constant sum of A and B or the value A and B reverse proportional and with the determination that the minimum required displacement reduces when the left capacitor has the initial overlap x_{oa} as small as possible, fabricating the proof mass at the middle of harvesting systems is not a optimal choice in terms of minimum required displacement to achieve positive power. Thirdly, in the symmetrical structures, it is easy to determine the effectiveness of the doubling circuit by using the ratio between C_{max} and C_{min} . However, in asymmetrical harvester, the doubler operation does not require both ratios $\frac{C_{amax}}{C_{amin}}$ and $\frac{C_{bmax}}{C_{bmin}}$ larger than the golden ratio. Only one of two ratios needs to be larger than golden ratio. The ratios can be determined from constant parameters A and B.

$$\frac{C_{amax}}{C_{amin}} = \frac{A + x_m}{A - x_m} \quad (3.22)$$

$$\frac{C_{bmax}}{C_{bmin}} = \frac{B + x_m}{B - x_m} \quad (3.23)$$

Another interesting suggestion is that a symmetrical harvester which the proof mass displacement is not high enough to receive the ratio $\frac{C_{max}}{C_{min}}$ in two harvesting capacitors larger than the golden ratio can be reconfigured as an asymmetrical structure to generate a positive power.

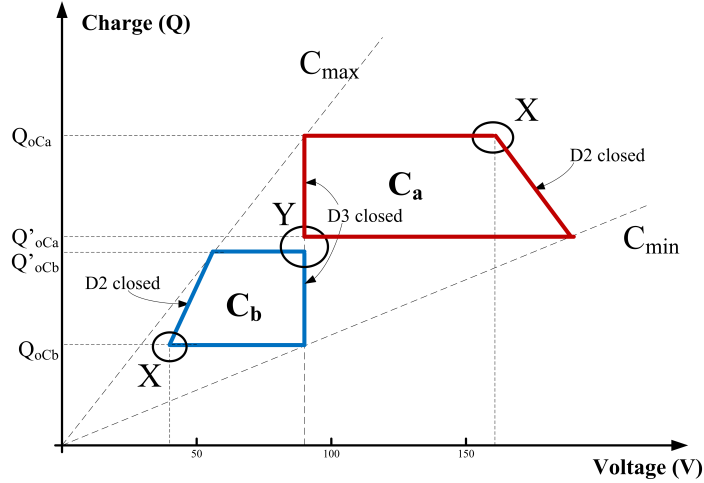


Figure 3.12: Q and V diagram of harvesting capacitors with nonlinear spring.

 Table 3.2: Capacitance value of C_a and C_b at X and Y points.

Value of C_a ; C_b	V_{Ca}
C_{ax}	$\frac{C_{oa}}{x_{oa}} \left(A + B - \sqrt{(B - x_m)(A + B)} \right)$
C_{bx}	$\frac{C_{ob}}{x_{ob}} \sqrt{(B - x_m)(A + B)}$
C_{ay}	$\frac{C_{oa}}{x_{oa}} \frac{(A - x_m)(A + 2B + x_m)}{A + B}$
C_{by}	$\frac{C_{ob}}{x_{ob}} \frac{(B + x_m)^2}{A + B}$

In harvesting systems with nonlinear spring stiffness, the displacement amplitudes x_m and y_m have different value; as a consequence, the smaller one is the limit of the capability to shift the proof mass from the middle position because when the proof mass is moved far from the middle place, the maximum displacement of proof mass is reduced.

Table 3.1 shows all computed voltage, charge and capacitance value on capacitor C_a and C_b . From this table, voltage and charge relationships on C_a and C_b in different operation steps of doubler circuit are shown in Figure 3.12.

With a battery in charge doubling circuit, the energy of doubler is all transferred into the battery. The bias voltage is kept constant V_{bat} . As the previous analysis for the in-plane overlap harvesters, the output power strongly depends on the coupling coefficient related

Table 3.3: Voltage and charge on C_a and C_b with nonlinear spring harvesters.

Value of C_a ; C_b	V_{Ca}	V_{Cb}	Q_{Ca}	Q_{Cb}
$C_{amax}; C_{bmin}$	V_{bat}	V_{bat}	$V_{bat}C_{amax}$	$V_{bat}C_{bmin}$
$C_{amax} - \Delta C_x; C_{bmin} + \Delta C_x$	$V_{bat} \frac{C_{amax}}{C_{ax}}$	$V_{bat} \frac{C_{bmin}}{C_{bx}}$	$V_{bat}C_{max}$	$V_{bat}C_{min}$
$C_{amin}; C_{bmax}$	$V_{bat} \frac{A+2B+x_m}{A+B}$	$V_{bat} \frac{B+x_m}{A+B}$	$V'_{Cao}C_{amin}$	$V'_{Cbo}C_{bmax}$
$C_{amin} + \Delta C_y; C_{bmax} - \Delta C_y$	V_{bat}	V_{bat}	$V_{bat}C_{ay}$	$V_{bat}C_{ax}$

Note: $\Delta C_x = \frac{C_a}{x_o} \Delta x$; $\Delta C_y = \frac{C_a}{x_o} \Delta y$; $V'_{Cao} = V_{bat} \frac{A+2B+x_m}{A+B}$; $V'_{Cbo} = V_{bat} \frac{B+x_m}{A+B}$

to bias voltage. Figure 3.1 shows that the output power reaches maximum at high bias voltage. However, with the battery of 5V, the harvesting system only generates very low power. In order to optimize the output power, a storage capacitor utilized in the doubling circuit replaces the battery as shown in Figure 3.8. The flow of charge builds up voltage in the storage capacitor which is also the bias source of harvesting systems. However, as shown in Figure 3.1, at certain value of bias voltage, when the V_{bias} continues increasing, the output power plummets. Therefore, a buck converter is needed to transfer a part of energy from the storage capacitor into a load or battery and sustain the voltage in storage capacitor at optimal value. Moreover, the buck converter is a step-down converter which supplies a appropriate voltage level for a normal battery which can be used as initial low-voltage source for harvester operation. The operation of the doubler of charge connected to a buck converter is discussed in the following section.

3.3 The Doubler of Charge with Buck Converter

The doubling circuit with a buck converter is shown in Figure 3.13. In the first stage, the battery initially charges the storage capacitor through diode D5. Once the voltage in storage capacitor increases, D5 is reverse-biased permanently. The above section analyzed the charge doubling systems with a battery; however, when connected with a storage capacitor

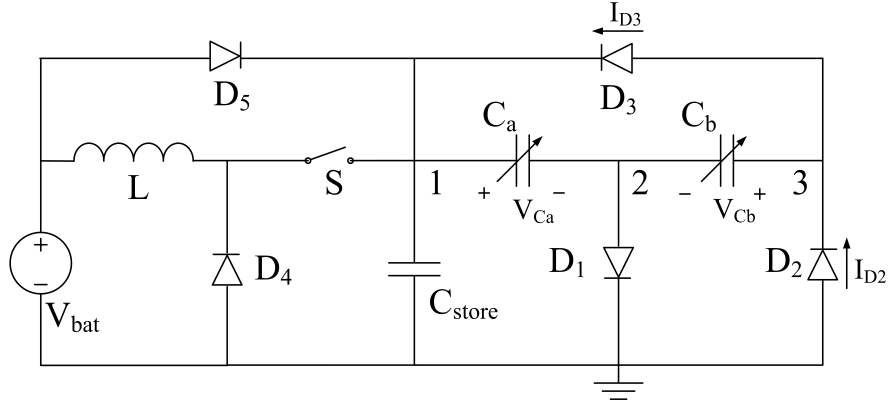


Figure 3.13: The doubler of charge with a buck converter.

C_{store} , the doubler circuit continuously charges C_{store} and therefore builds up the voltage on it. Since the voltage $V_{C_{store}}$ reaches a certain optimal value V_{opt} where the maximum displacement occurs or the harvested power is maximal, switch S in the buck converter closes. Because $V_{C_{store}}$ is much larger than V_{bat} , the charge from C_{store} flows into inductor L. In a very short time, as S is controlled to open using autonomous MEMS switch or separated power electronic circuit, diode D4 must automatically conduct to keep the current I_L continuous; the battery obtains the charge from the inductor L. The values of the current I_L , which are calculated in equation (3.25)-(3.28) when the switch is on and off, is utilized to estimate the amount of charge delivered from C_{store} to battery and maintain a constant optimal bias voltage across C_{store} .

At the moment switch S on, the equivalent circuit of the buck converter includes the storage capacitor, inductor and battery in series. The switch is on in the time of t_{on} which is much smaller than the doubler conversion period; therefore, during t_{on} , it is assumed that there is no further charge pumped into C_{store} . From the circuit, a differential equation of the inductor current $I_L(t)$ is derived as

$$\frac{1}{C} \int_0^{t_{on}} i_L(t) dt - V_{Co} + L \frac{di_L(t)}{dt} + V_{bat} = 0. \quad (3.24)$$

Using the Laplace Transform, the current and delivered charge on inductor L can be calculated as

$$i_L(t) = \frac{V_{opt} - V_{bat}}{L} \cos\left(\frac{1}{\sqrt{LC}}t\right) \quad (3.25)$$

$$q_L(t) = (V_{opt} - V_{bat}) \sqrt{\frac{C}{L}} \sin\left(\frac{1}{\sqrt{LC}}t\right) \quad (3.26)$$

With the assumption of no power loss, all of charge $Q_{C_{store}}$ from capacitor C_{store} is pumped to the inductor L; therefore,

$$Q_{C_{store}} = V_{opt}C_{store} = \int_0^{t_{on}} (V_{opt} - V_{bat}) \sqrt{\frac{C}{L}} \sin\left(\frac{1}{\sqrt{LC}}t\right) dt. \quad (3.27)$$

Then, the amount of time to turn on switch S is determined. After that, it takes the time of $t_{off} - t_{on}$ for the storage capacitor recharged to V_{opt} . In practice, because of harvesting very small power, it takes a long time to build up the voltage in the storage capacitor; therefore, t_{on} is much smaller than t_{off} during which all stored energy on inductor is rapidly transferred to the output battery. The current on inductor during charge delivery is

$$i_L(\Delta t) = \frac{1}{L} \int_{t_{on}}^{t_{on}+t_{off}} u_L(t) dt + I_{Lo} = I_{Lo} - \frac{V_{bat}}{L} \Delta t \quad (3.28)$$

where Δt is the time when charge in L is pumped to the battery. It appears that the doubler harvests highest power at $V_{C_{store}} = V_{opt}$; therefore, S is preferred to switch fast to maintain a constant voltage V_{opt} . However, all typical switches has their all rising and falling time which limit the switching speed. Because the very high voltage difference between C_{store} and battery, the charge flows into inductor L with very short time. This causes the impossibility of sustaining the bias voltage dropping to low value and therefore reduces the energy harvesting efficiency.

In next chapter, the software simulation of the doubler of charge with linear- and nonlinear-spring harvesters will be mentioned. Furthermore, the designs of controlled electronic circuits or MEMS switch and the effects of non-ideal devices such as diodes are also taken into account in details.

Chapter 4

Simulation Results

Chapters 2 and 3 have discussed mechanical energy harvesting transducers and the electrical doubler circuit individually without the consideration of mutually influences between two systems. The electronic circuit with a storage capacitor increases bias volage after each conversion cycle. This changes the performance of the mechanical transducer such as reducing mass displacement and increasing output power. Those changes in turns influence the doubler operation. In this chapter, the combination of the doubler circuit and electrostatic energy transducers will be investigated. Several comparisons in output power and required minimum displacement of the doubler circuits with a battery or a storage capacitor show the advantages of asymmetrical harvesters over those of symmetrical ones. Furthermore, the doubler is examined and compared with different effects of non-ideal diodes to find out suitable diodes for the circuit. Finally, a buck converter is simulated with a controlled electronic switch and an autonomous MEMS switch. All simulations in this chapter are processed using the LTSPICE IV software.

4.1 Symmetrical and Asymmetrical Energy Harvesters

Three types of harvesters including linear-spring harvester [6], angled-spring harvester [7], and $40\mu\text{m}$ - / $50\mu\text{m}$ -curved-spring harvesters [8] are utilized in this chapter. While angled- and curved-spring harvesters have asymmetrical transducers, the linear-spring harvester can be used as symmetrical or asymmetrical prototypes. The equivalent circuits of those

Table 4.1: Model parameters for linear-spring harvesting device [6].

Parameters	Value	Unit
Proof mass, m	30.4	mg
Spring stiffness, k_m	535	Nm ⁻¹
Damping constant, b	2.834x10 ⁻⁴	Nsm ⁻¹
Initial capacitance, C_o	3.547	pF
Initial overlap, x_o	90	μm
Parasitic capacitance, C_p	3.17	pF
Load Resistance, R_L	15	MΩ
Load capacitance, C_L	2	pF

harvesters in Figures 2.3 and 2.10 in Chapter 2 are used for simulations. Table 4.1, 4.2, 4.3 and 4.4 show the designed and fitted parameters of the harvesters. Those parameter are derived from several research in [6], [7], [8] The harvesters with angled and curved springs perform the nonlinear characteristics through stiffness coefficients from K2 to K7. Before integrated in the doubler of charge, those harvesters are simulated with frequency sweeps and different bias voltages or accelerations.

4.1.1 Linear-spring Harvester

The obtained parameters of a linear-spring harvester shown in Table 4.1 are based on Son Duy Nguyen's paper [6]. At the acceleration of 0.3 g (with the standard gravity $g = 9.81$ m/s²), Figure 4.1 shows the output voltage on resistive load and mass displacement as a function of frequency ranging from 662 Hz to 686 Hz and with different fixed bias voltages ($V_e = 10, 20$ or 30 V).

The spring-mass-damper system performs maximum power at the resonant frequency of 667.9 Hz. With low coupling coefficient, the increase in the bias voltage improves the output harvesting power; however, this lessens the proof mass displacement x_{mass} , which strongly affects the doubler harvesting efficiency. The vibration excitation can be used to accomplish a desired displacement. Figure 4.2 shows the change in the output voltage and mass displacement since the vibration acceleration changes from 0.1 g to 0.3 g .

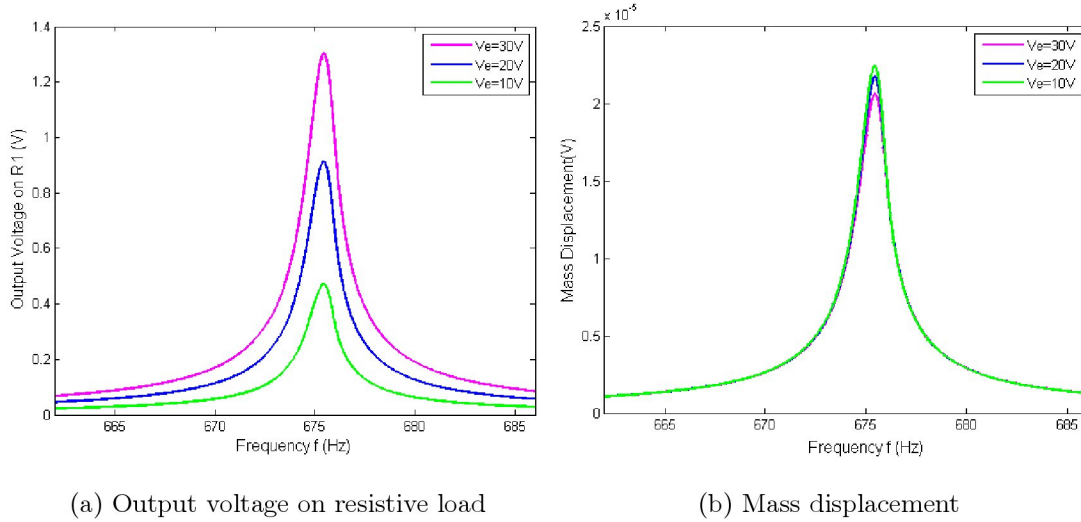


Figure 4.1: Output voltage and mass displacement of a linear-spring harvester with $0.1 g$ acceleration when $V_e = 10, 20$ and $30 V$.

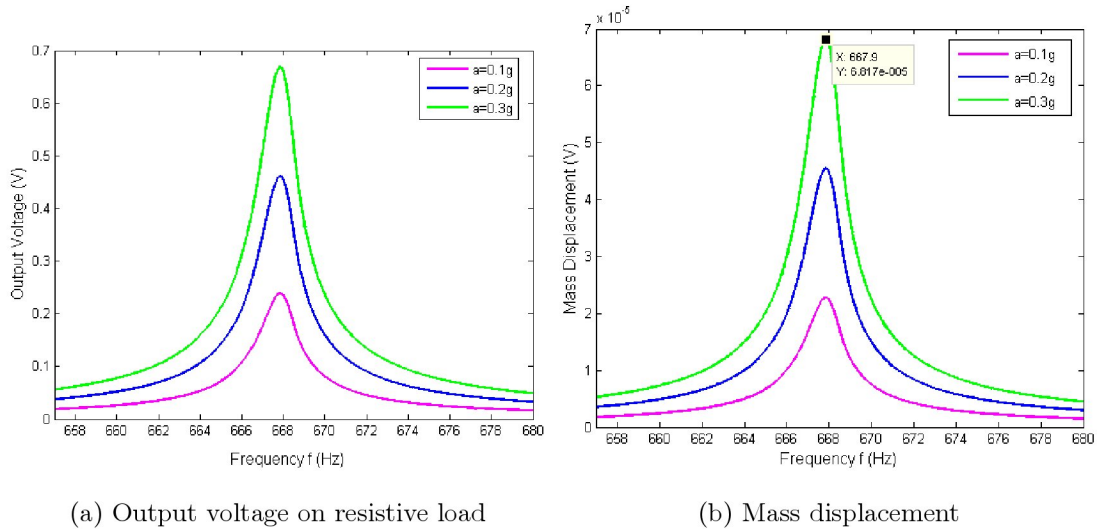


Figure 4.2: Output voltage and mass displacement of a linear-spring harvester with $V_e = 5 V$ when acceleration changes from 0.1 to $0.3 g$.

The displacement maximum is suppressed by the position of designed endstops. It is assumed that the harvester endstops limit the mass displacement at the value of $x_{max} = 90 \mu\text{m}$ equal to initial overlap x_o . With 3.17 pF parasitic and 3.547 pF initial capacitance, the required minimum mass displacement calculated using the equation (3.7) is about $40.23 \mu\text{m}$. Therefore, to operate the doubler circuit, a high excitation with the acceleration a

Table 4.2: Model parameters for angled-spring harvesting device [7].

Parameters	Value	Unit
Proof mass, m	35.25	mg
Linear spring stiffness, k_1	485	Nm ⁻¹
Coefficients of the nonlinear spring stiffness		
$k_2 = 6.128 \times 10^6 (\text{Nm}^{-2})$, $k_3 = -1.409 \times 10^{10} (\text{Nm}^{-3})$,		
$k_4 = -8.785 \times 10^{14} (\text{Nm}^{-4})$, $k_5 = -1.372 \times 10^{18} (\text{Nm}^{-5})$,		
$k_6 = 5.62 \times 10^{22} (\text{Nm}^{-6})$, $k_7 = 4.122 \times 10^{26} (\text{Nm}^{-7})$		
Damping constant, b	2.53×10^{-4}	Nsm ⁻¹
Initial capacitance of transducer 1, C_{o1}	1.98	pF
Initial capacitance of transducer 2, C_{o2}	5.15	pF
Initial overlap of transducer 1, x_{o1}	50	μm
Initial overlap of transducer 1, x_{o2}	130	μm
Parasitic capacitance of transducer 1, 2, C_{p1}, C_{p2}	3.17	pF
Load Resistance, R_L	15	M Ω
Parasitic load capacitance of transducer 1, 2, C_{pL1}, C_{pL2}	2	pF

larger than 0.18 g is needed.

4.1.2 Angled-spring Harvester

To improve harvesting bandwidth, nonlinear-spring harvesters which employ softening phenomenon are fabricated with asymmetrical structures by Son [7]. With the angled-spring harvester in Table 4.2 which parameters are designed in paper [7], the output transducer performance must be considered in both frequency up-sweep and down-sweep modes. As shown in Figure 4.3, with the vibration frequency up and down, the output voltage and displacement at acceleration of 0.11 g and 0.2 g with 30V bias voltage V_e are measured. It clearly shows that the frequency down sweep provides wider harvesting bandwidth, larger power and mass displacement with the same excitation. As a result, the frequency down-sweep simulation is only employed for the harvesters with nonlinear springs in this chapter to ensure high amplitude of displacement. An in-depth research on harvester performance with small and large vibration in different frequency ranges is out of scope of the project.

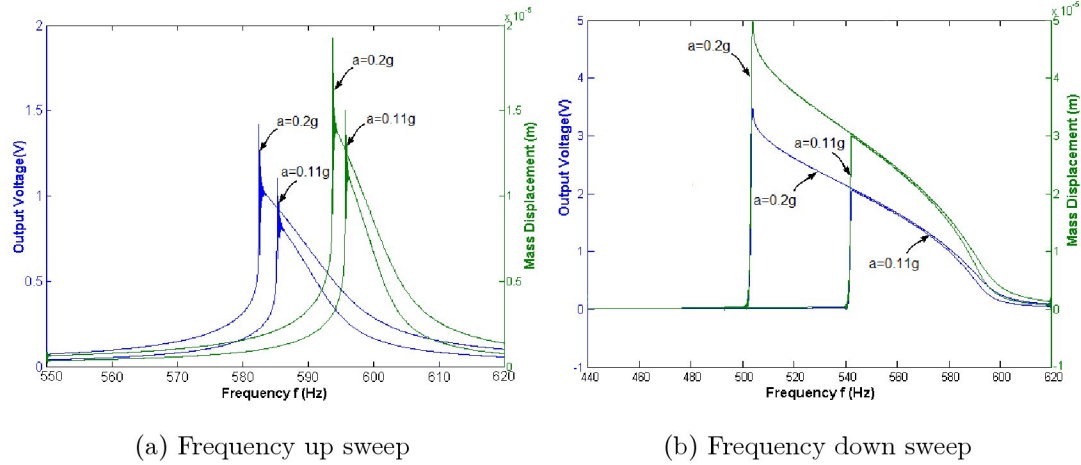


Figure 4.3: Output voltage and mass displacement of a angled-spring harvester with $V_e = 30$ V when $a = 0.11$ and 0.2 g.

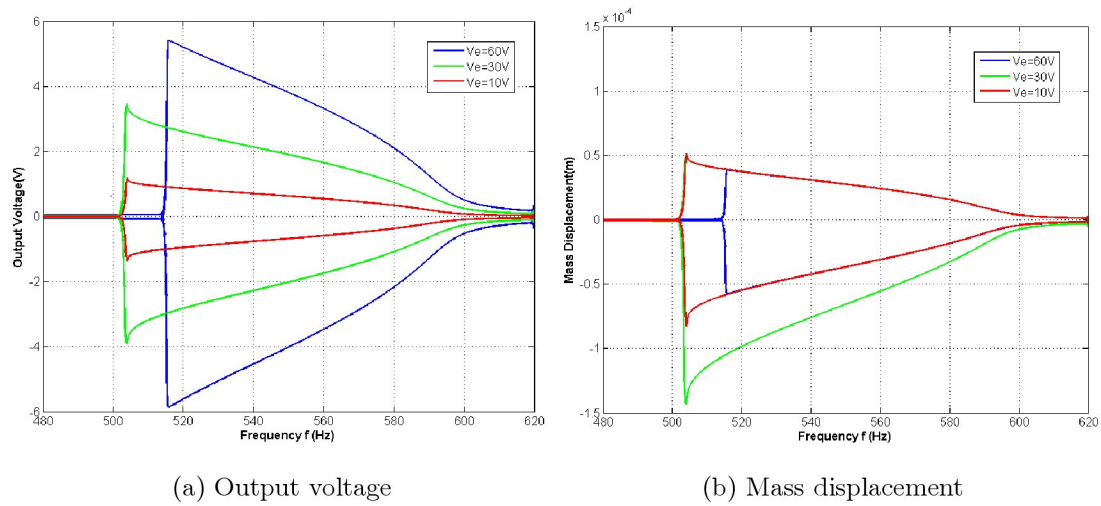


Figure 4.4: Output voltage and mass displacement of a angled-spring harvester with 0.2 g acceleration when $V_e = 10, 30$ and 60 V.

Similarly, the influences of bias voltage on harvested power and mass displacement are taken into account in Figure 4.4. The angled-spring harvester is simulated with $V_e = 10, 30$ and 60 V. The bias voltage increases leads to the improvement of harvesting output power; however, reduces the displacement of proof mass due to changing jump-down frequency points.

Table 4.3: Model parameters for 40 μ m-curved-spring harvesting device [8].

Parameters	Value	Unit
Proof mass, m	15.18	mg
Linear spring stiffness, k_1	622	Nm^{-1}
Coefficients of the nonlinear spring stiffness		
$k_2 = 2.96 \times 10^7 (Nm^{-2}), k_3 = 2.8 \times 10^{11} (Nm^{-3}),$		
$k_4 = -4 \times 10^{14} (Nm^{-4}), k_5 = 1.055 \times 10^{19} (Nm^{-5}),$		
$k_6 = 1.357 \times 10^{23} (Nm^{-6}), k_7 = 4.2005 \times 10^{26} (Nm^{-7})$		
Linear damping constant, b	2.7×10^{-5}	Nsm^{-1}
Coefficients of the nonlinear damping constant,		
b_3	0.23369	Nm^{-2}
b_5	-69.264	Nm^{-3}
b_7	8734.6	Nm^{-4}
b_9	-4.9842×10^5	Nm^{-5}
b_{11}	1.057×10^7	Nm^{-6}
Initial capacitance of transducer 1, C_{o1}	1.749	pF
Initial capacitance of transducer 2, C_{o2}	7.071	pF
Initial overlap of transducer 1, x_{o1}	93	μm
Initial overlap of transducer 2, x_{o2}	23	μm
Parasitic capacitance of transducer 1, C_{p1}	14.5	pF
Parasitic capacitance of transducer 2, C_{p2}	12.5	pF
Load Resistance, R_L	20.5	$M\Omega$
Parasitic load capacitance of transducer 1, C_{pL1}	23	pF
Parasitic load capacitance of transducer 2, C_{pL2}	8	pF

The maximum displacement x_{mass} , which proof mass m can be reached, is 50 μm while the required minimum displacement of the doubler calculated from equation (3.19) is 34.38 μm . Thus, the acceleration of 0.2 g is sufficient to make the doubler circuit work.

4.1.3 Curved-spring Harvesters

Recently, Son [1] proposed curved-spring harvesters with extremely wide bandwidth of 587 Hz at 0.208 g acceleration.

Table 4.4: Model parameters for 50 μ m-curved-spring harvesting device [8].

Parameters	Value	Unit
Proof mass, m	15.2	mg
Linear spring stiffness, k_1	861	Nm ⁻¹
Coefficients of the nonlinear spring stiffness		
$k_2 = 4.2311 \times 10^7$ (Nm ⁻²), $k_3 = 5.550 \times 10^{10}$ (Nm ⁻³),		
$k_4 = 5.6779 \times 10^{12}$ (Nm ⁻⁴), $k_5 = 8.1199 \times 10^{18}$ (Nm ⁻⁵),		
$k_6 = -2.5255 \times 10^{24}$ (Nm ⁻⁶), $k_7 = 1.7947 \times 10^{26}$ (Nm ⁻⁷)		
Damping constant, b	2.8×10^{-4}	Nsm ⁻¹
Initial capacitance of transducer 1, C_{o1}	1.11	pF
Initial capacitance of transducer 2, C_{o2}	6.69	pF
Initial overlap of transducer 1, x_{o1}	20	μ m
Initial overlap of transducer 1, x_{o2}	120	μ m
Parasitic capacitance of transducer 1, C_{p1}	8.5	pF
Parasitic capacitance of transducer 2, C_{p2}	6.5	pF
Load Resistance, R_L	11	M Ω
Parasitic load capacitance of transducer 1, 2, C_{pL1}, C_{pL2}	4	pF

The harvesters have asymmetrical structures and show bistable behaviors by fabricating curved springs with a tip displacement of y_o . The simulation is conducted with the curved-spring harvesters with $y_o = 40 \mu$ m and 50μ m tip displacement in Figures 4.5, 4.6, 4.7 and 4.8. Similar to previous simulations for the angled-spring harvester, the 40 μ m- and 50 μ m-tip-displacement harvesters are examined in frequency down-sweep mode with different accelerations ($a = 0.1$ and $0.2 g$) well as bias voltage ($V_e = 10, 20$ and 30 V).

The parameters in LTSPICE simulations for curved-spring harvesters are calibrated based on the experimental results in Cuong's thesis [8]. If it is assumed that the overall parasitic capacitance is 5 pF, the minimum required proof mass displacements are more than 23.92 μ m or 30.01 μ m with the 40 μ m- or 50 μ m-curved-spring harvesters respectively. However, the maximum displacements of proof mass of those harvester are smaller than 23 μ m. Hence, it is difficult to operate the doubler circuit using those harvesters if the parasitic capacitors are high.

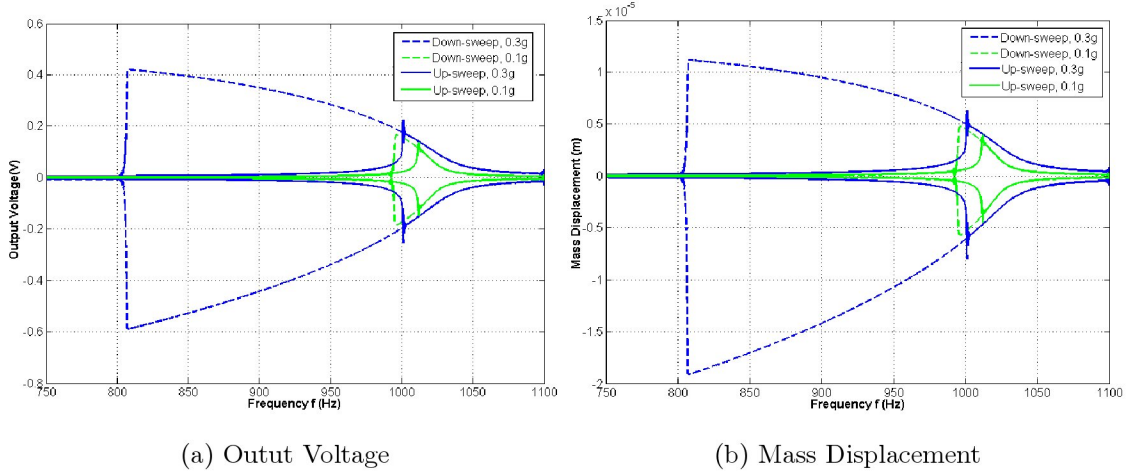


Figure 4.5: Output voltage and mass displacement of a $40\mu\text{m}$ -curved-spring harvester with $V_e = 20\text{ V}$ in frequency down sweep when $a = 0.1$ and 0.3 g .

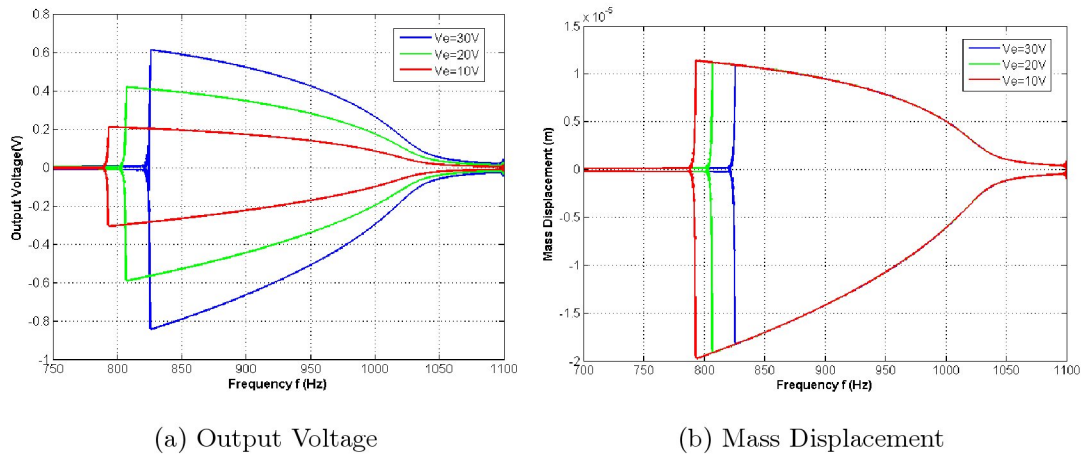


Figure 4.6: Output voltage and mass displacement of a $40\mu\text{m}$ -curved-spring harvester with 0.3 g acceleration in frequency down sweep when $V_e = 10, 20$ and 30 V .

4.2 The Doubler of Charge

Since the doubler runs with a storage capacitor C_{store} , harvested average power rises proportionally to the bias voltage V_e on C_{store} . The squared coupling coefficient κ^2 also increases, that reduces the displacement of the proof mass based on the equation (2.12). To understand this phenomenon, the storage capacitor is replaced by a battery to test the effects of V_e on power and mass displacement and compare symmetrical and asymmetrical harvesters.

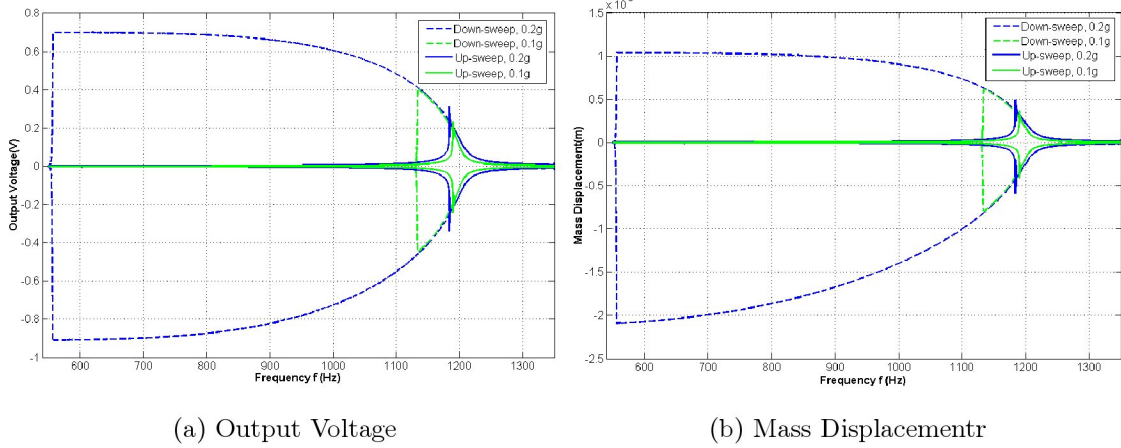


Figure 4.7: Output voltage and mass displacement of a $50\mu\text{m}$ -curved-spring harvester with $V_e = 20\text{ V}$ in frequency down sweep when $a = 0.1$ and 0.2 g .

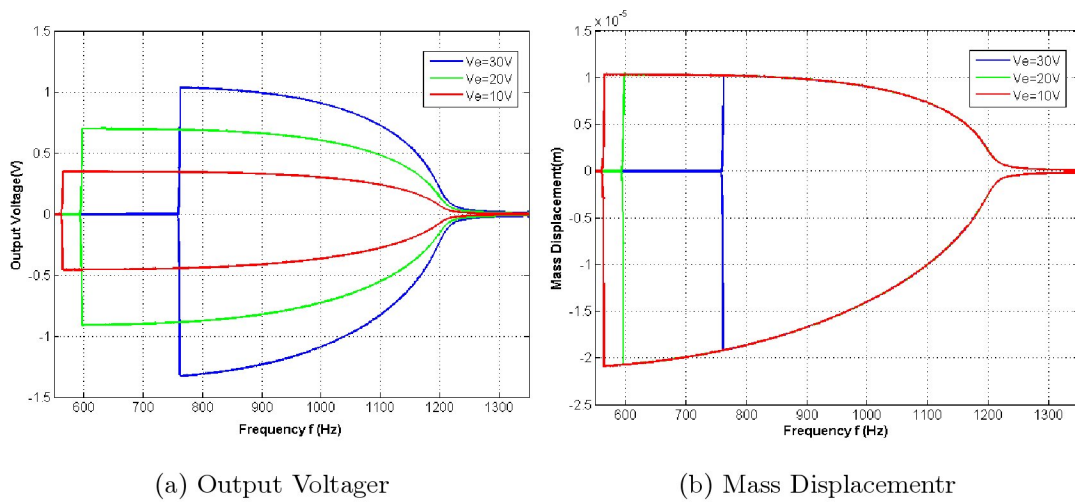


Figure 4.8: Output voltage and mass displacement of a $50\mu\text{m}$ -curved-spring harvester with 0.2 g acceleration in frequency down sweep when $V_e = 10, 20$ and 30 V .

4.2.1 The Doubler Circuit with Bias Battery

Using the linear-spring harvester, Figure 4.9 shows the output power peak or mass displacement of the doubler circuit as a function of bias voltage from 0 to 80 V. The harvester is vibrated at the resonant frequency of 667.9 Hz and fixed acceleration of 0.38 g . Initially, the mass displacement needs a few transient seconds to reach the steady state value of $80\ \mu\text{m}$. When V_e heightens, the harvesting output power rises due to the increase in elec-

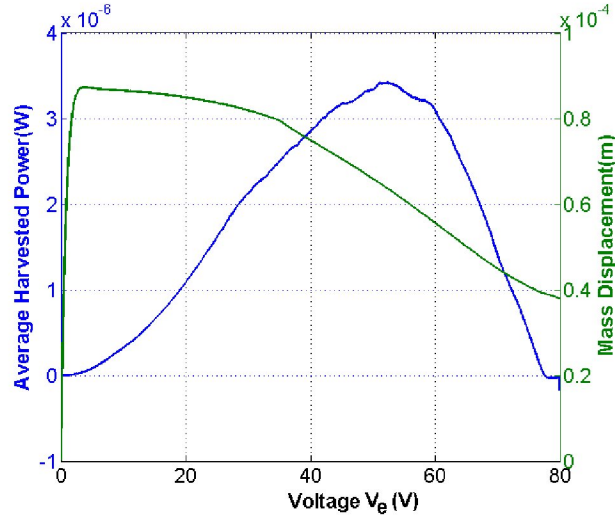


Figure 4.9: Output power and mass displacement as functions of bias voltage V_e .

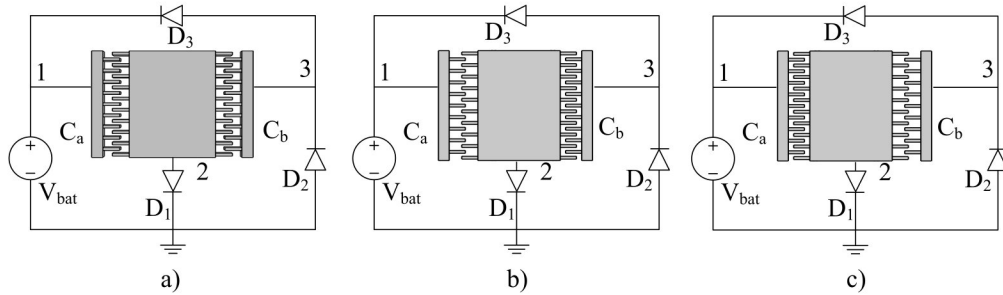


Figure 4.10: Symmetrical and asymmetrical prototypes of the doubler circuits

trical damping force while the mass displacement drops rapidly. Until mass displacement is smaller than the required minimum displacement, harvested power plummets. The optimal point for linear-spring harvester is at the bias voltage of 50-60 V and 65 μm mass displacement. The maximum harvested power is up to 3.5 μW .

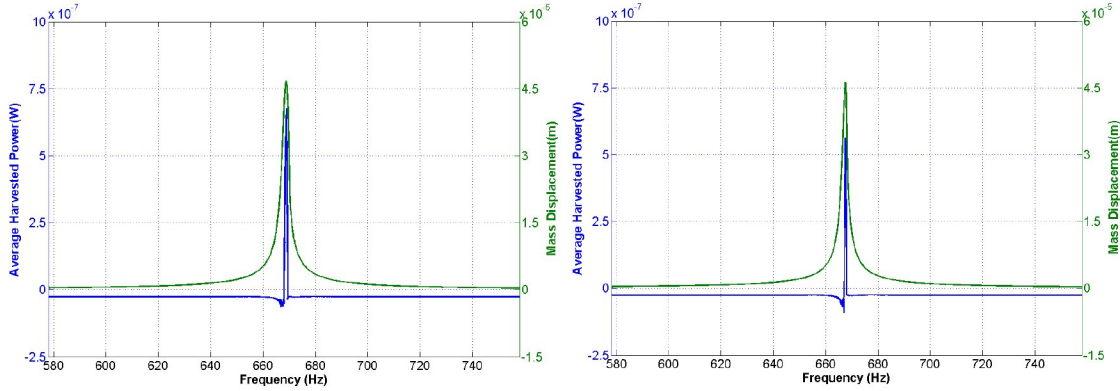
With angled-spring and curved-spring harvesters, as shown in Figures 4.4b, 4.6b and 4.8b, the increase in bias voltage not only impacts on the slope of mass displacement but also negatively changes the jump-down frequency point; as a consequence, this depletes the mass displacement.

The linear-spring harvester is also utilized to examine the influence of asymmetrical prototypes. Figure 4.10 illustrates three configurations of the linear harvesters in doubler circuits. The mass positions at the middle of the harvester in Figure 4.10 a).

Table 4.5: Harvested powers of the doubler circuit with different mass displacements and theoretical required mass displacements in three prototypes (where $A = \frac{C_{oa}+C_{pa}}{C_{oa}}x_{oa}$ and $B = \frac{C_{ob}+C_{pb}}{C_{ob}}x_{ob}$).

x_{mass}	Harvested Power (μW)		
	Prototype a)	Prototype b)	Prototype c)
	A = 170e-6 m B = 170e-6 m	A = 145e-6 m B = 195e-6 m	A = 195e-6 m B = 145e-6 m
45	0.719	1.255	0.395
44	0.573	1.0927	0.274
43	0.412	0.951	0.121
42	0.277	0.782	-0.012
41	0.106	0.627	-0.013
40	-0.012	0.480	-0.013
39	-0.013	0.321	-0.013
38	-0.013	0.153	-0.013
37	-0.013	0.023	-0.013
36	-0.013	-0.012	-0.013
x_{req}	40.234 m	36.974 m	42.172 m

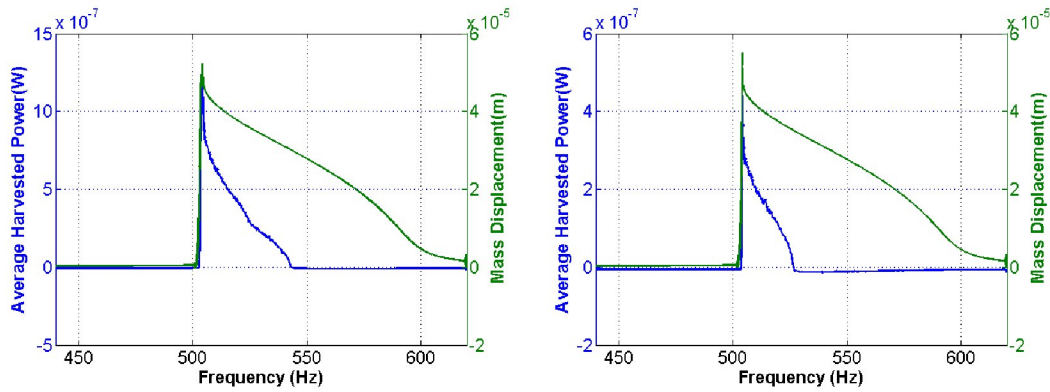
In Figure 4.10 b) and 4.10 c), the harvesters are assumed to be asymmetrically designed with their proof mass initially stabilizing at equilibrium positions displacing $25 \mu\text{m}$ from the middle. The difference between two asymmetrical structures is that the proof mass, in structure b, is initially placed farther from the battery, or the overlap of C_b is initially larger than that of C_a while, in structure c, those conditions are reverse. The output power of doubler circuits in three prototypes operating at the resonance frequency of 667.9 Hz and 50 V bias voltage are compared in Table 4.5. The mass displacement of three harvester structures is kept constant by changing the vibration acceleration. Table 4.5 shows that the doubler b) generates the largest average power with the same mass displacement and requires the lowest mass displacement about $37 \mu\text{m}$ to achieve a positive power while the doubler c) requires a larger required displacement up to $42 \mu\text{m}$. Using the analysis in Chapter 3, the theoretical required minimum displacements for each structure are calculated based on equation (3.19) and compared to simulated required displacement in Table 4.5. This proves that designing the harvester asymmetrically with $x_{C_{oa}} < x_{C_{ob}}$ is able to reduce the condition of proof mass displacement and accomplish higher output power.



(a) Prototype b) with $a=0.232\text{ g}$

(b) Prototype c) with $a=0.201\text{ g}$

Figure 4.11: A comparison in harvested power of linear-spring doubler between two different asymmetrical structures



(a) Prototype b) with $a=0.25\text{ g}$

(b) Prototype c) with $a=0.25\text{ g}$

Figure 4.12: A comparison in harvested power of angled-spring doubler between two different asymmetrical structures

The discrepancies between two linear-spring asymmetrical structures in the output power of the doubler are also drawn in Figure 4.11 with $V_e = 50\text{ V}$, and frequency ranging from 578 to 758 Hz. The mass displacements are kept the same as each other. The average power at resonant frequency in prototype b) is about $0.7\ \mu\text{W}$ while that in prototype c) is about $0.56\ \mu\text{W}$.

With the angled-spring harvester, Figure 4.12 shows the difference of output power between doubler circuits in asymmetrical configuration b and c. The down-sweep mode is

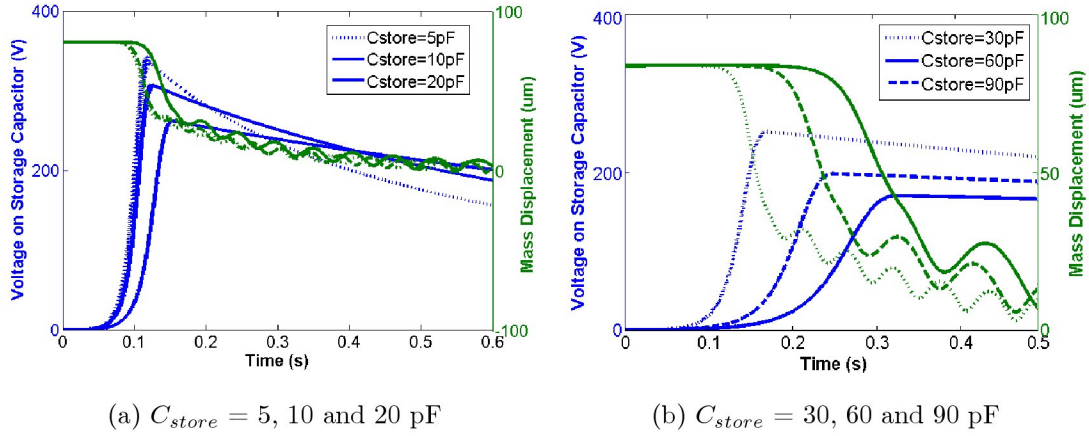


Figure 4.13: Voltage on C_{store} and mass displacement of linear-spring doubler with different values of storage capacitor C_{store}

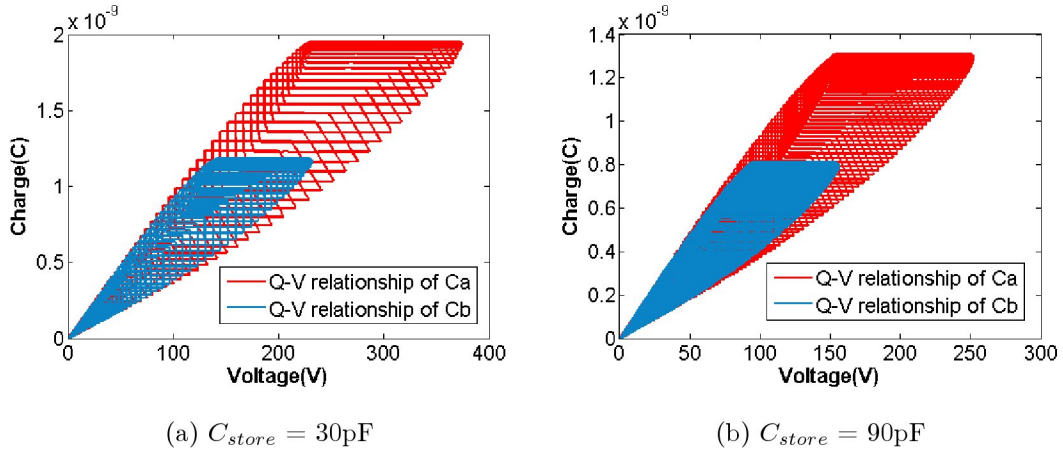


Figure 4.14: Q-V plane contours of two harvesting capacitors of linear-spring doubler

used with the vibration frequency varying from 620 to 440 Hz. The bias voltage is 30 V and the acceleration is 0.25 g . With prototype b), the power is positive since the mass displacement reaches 30 μm whereas the prototype c) needs 20

In addition to the benefits of reducing proof mass maximum required displacement of asymmetrical harvesters, the combination of doubler circuits and those nonlinear-spring harvesters offers a potential solution to broaden the harvesting bandwidth. As described in Chapter 2, the harvesting power of continuous electrostatic harvesting systems considerably depends on load resistance; therefore, the DC-DC converters of those systems are designed to track optimal resistance values at a certain resonance frequency. That the

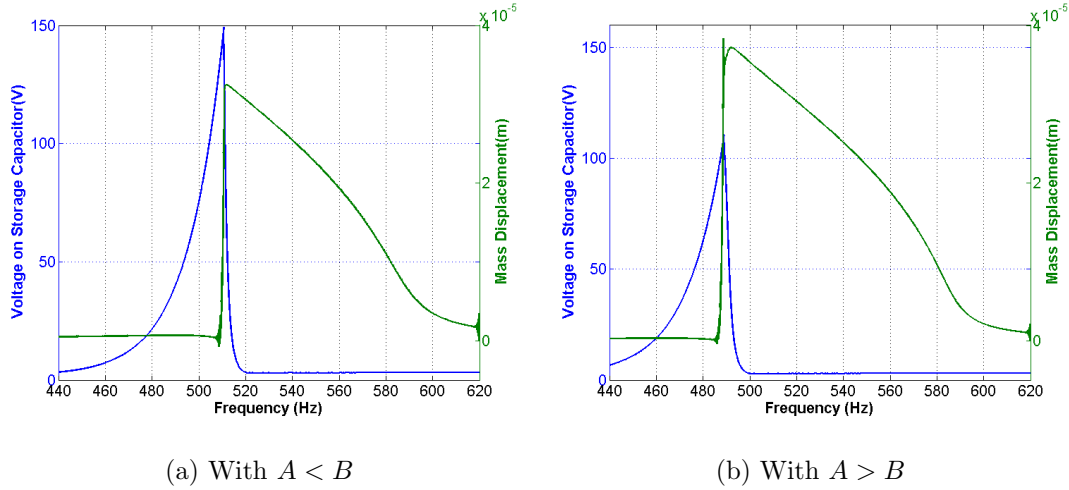
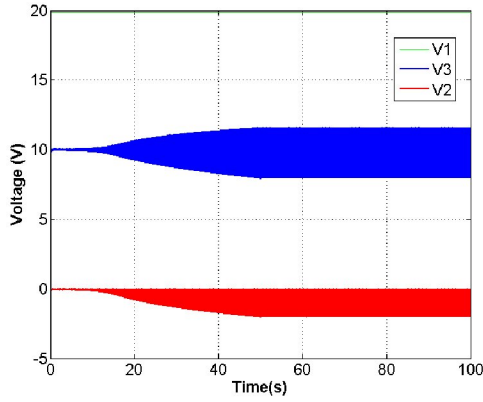


Figure 4.15: A comparison in voltage on C_{store} and mass displacement of two angled-spring prototypes with $C_{store} = 90$ pF

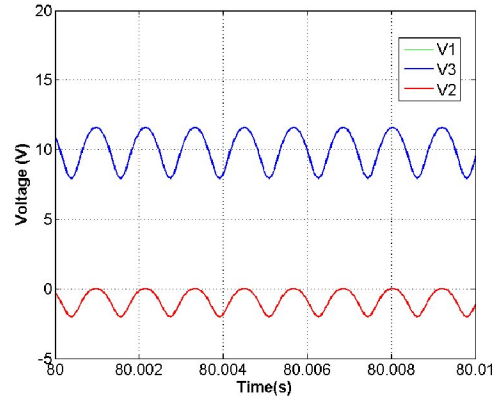
nonlinear transducers such as angled-spring or curved-spring devices harvest vibration energy in wide frequency range makes maximum power point tracking based on adjusting resistive load problematic and complicated because vibration frequency varying causes the changes in output impedance (which contains capacitance components). As a consequence, an independent-load-impedance DC-DC converter is needed for the harvesters to scavenge vibration energy in a wide bandwidth. The doubler is based on switched electrostatic harvesting technique which therefore weakly depends on output resistance. Figure 4.12 shows a broad bandwidth about 40 Hz with positive harvested power of angled-spring harvesters compared to narrow one of linear-spring harvester in Figure 4.11. However, the required mass displacement is the main reason leading to the limit in wideband harvesting of the doubler circuit.

4.2.2 The Doubler Circuit with Storage Capacitor

The doubler system with the linear-spring harvester running at the resonance frequency (667.9 Hz) using a storage capacitor C_{store} is firstly tested. Different values of the storage capacitor from 5pF to 90pF are used and the voltage across C_{store} is measured and shown in Figure 4.13. Since $V_{C_{store}} > 60V$, the mass displacement starts reducing; until mass displacement is below the minimum requirement, $V_{C_{store}}$ begins decreasing.

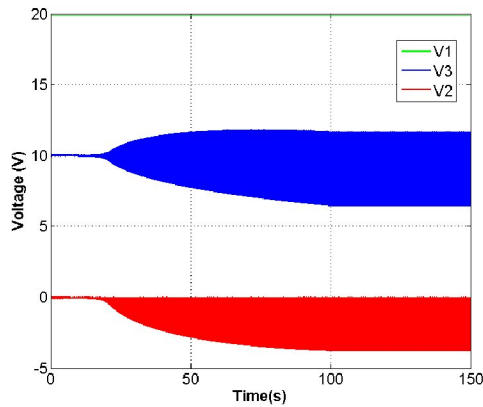


(a) During first 100 seconds

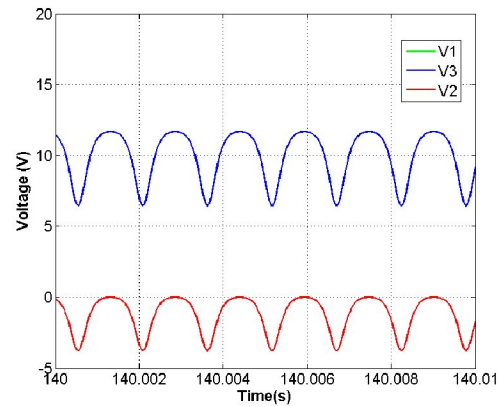


(b) During steady state

Figure 4.16: Voltage at nodes 1,2 and 3 of the doubler with 40 μm curved spring.



(a) During first 150 seconds



(b) During steady state

Figure 4.17: Voltage at nodes 1,2 and 3 of the doubler with 50 μm curved spring.

The larger storage capacitance is, the longer time the doubler needs to obtain high voltage. In paper [15], the optimal value of storage capacitor is calculated so that the voltage multiplication factor is maximal. Figure 4.14 shows the Q-V plane contours of two harvesting capacitors when $C_{store} = 30 \text{ pF}$ and 90 pF . At specific value of voltage and charge, the harvested power drops down to negative value because of power loss from reverse leakage currents or parasitic resistors as the displacement is not high enough to make doubler work. With ideal diodes, the doubler circuit can start up from any positive initial bias voltage.

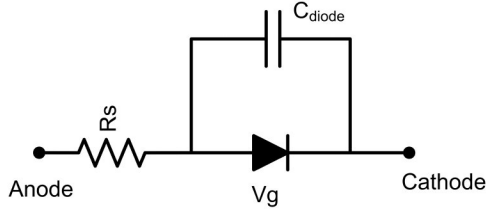


Figure 4.18: The equivalent circuit of diode for transient analysis.

Table 4.6: Harvested powers of the doubler circuit with different diode forward voltages V_f

Diode Forward Voltage (V)	Harvested Power (μW)
0	3.7661
0.6	3.6034
0.9	3.5325
1.2	3.4615
1.5	3.3705
2.0	3.2295
3	3.0121

With angled-spring harvesters, Figure 4.15 show $V_{C_{store}}$ and mass displacement when the vibration frequency changes from 620 to 440 Hz and $C_{store} = 90$ pF. Again, the asymmetric benefits are proved in the figure.

Finally, with the curve-spring harvester, high parasitic capacitors compared to initial harvesting capacitors of the harvesters lead to the difficulty to operate the doubler circuits. Thus, the voltage in the storage capacitor only oscillates around the bias voltage value. The Figures 4.16 and 4.17 show voltages at nodes 1, 2 and 3 of the doubler circuit with 20V initial bias voltage. With the $40\mu\text{m}$ -curved-spring-harvester, the acceleration is $0.3 g$ and the frequency sweeps down from 1100 Hz to 850 Hz in 50 seconds and keeps at 850 Hz in 50 seconds left while the $50\mu\text{m}$ -curved-spring-harvester vibrate at 0.2 acceleration with the frequency changing from 1350 Hz to 650 Hz during first 100 seconds and keeping at 650 Hz in 50 seconds left. Next section will focus on the influences of non-ideal diodes on the doubler operation.

Table 4.7: Harvested powers of the doubler circuit with different diode leakage currents at $V_f = 1$ V and $C_{diode} = 1$ pF

Diode Leakage Current (nA)	Harvested Power (μ W)
0.51	1.2505
1.01	1.2321
5.10	1.0689
10.20	0.8970
51.00	-0.5607

Table 4.8: Harvested powers of the doubler circuit with different junction capacitance values at $V_f = 1$ V

Diode Junction Capacitance (pF)	Harvested Power (μ W)
0	3.5147
0.1	3.3232
0.5	2.4699
1.0	1.2505
1.5	0.0203
2.0	-0.0128

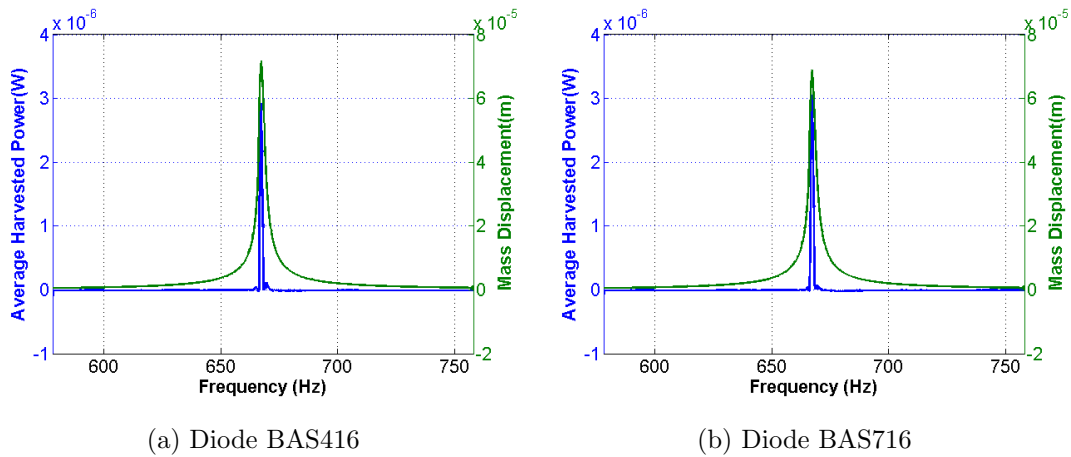
4.3 The Doubler of Charge with Non-ideal Diodes

Non-ideal effects of the doubler circuit come from diodes, opamp buffers and circuit layout. Diode nonidealities such as leakage current, forward bias voltage, parasitic capacitance lead to dilemmas related to difficulties to start the doubler with low initial bias voltage and higher power loss. The opamp buffers used in measurement process and circuit layout add a great amount of parasitic capacitance into the doubler which therefore reduces the working ability of the circuit. Those circuit design and measurement effects will be discussed in Chapter 5. This section only concentrates on the consideration of the effect of non-ideal diodes

Firstly, the linear harvester with a bias battery of 30V and 0.38 g acceleration is used to test the effects of diodes. The equivalent circuit of non-ideal diode for transient analysis is shown in Figure 4.18. The forward bias voltage V_d of diodes makes the doubler circuit unable to start up with low initial bias voltage. A larger than $2V_d$ bias voltage source is needed to charge the harvesting capacitors in doubler circuits. Furthermore, the forward bias voltage slightly causes the reduction in the flow of charge and therefore lessens the

Table 4.9: Harvested powers of the doubler circuit with different diodes.

Diode	IS	CJO	VJ	Power (μW)
N4148	2,52e-9	4e-12	0,869	0.6491
BAS416	0,80584e-15	1.9002e-12	1,2722	2.0180
PMLL4148L	3,126e-9	0,727e-12	0,7226	2.0703
BAT40	7e-9	2,9332e-12	0,3905	0.6924
BAS516	2,9891e-9	0,38341e-12	9.99	2.3973
BAS16H	6,0289e-9	0,59363e-12	0,68774	2.3197
BAS716	3,519e-15	1,817e-12	0,6508	2.4874
BAS116T	1,472e-15	1,821e-12	0,5358	2.4729

Figure 4.19: A comparison in harvested power and mass displacement of linear-spring doubler with two different diodes at $V_e = 60 \text{ V}$, $a = 0.38 \text{ g}$

output power of the harvesting systems. Table 4.6 shows the small effect of V_d on the average power of doubler circuits. At 3 V forward voltage drop, the harvested power still maintain with high value.

Secondly, diode leakage current is the main reason of power loss in the circuit. Different from forward voltage, the leakage current is taken into account since the diodes do not conduct. The leakage current is high when the inverse voltage increases. The inverse voltage V_3 on diode is much higher than the forward voltage. This causes high leakage current and the doubler must work below the diode breakdown voltage.

Moreover, with the assumption that the vibration period is much higher than the charge flowing time, the diode is off in almost all of the time.

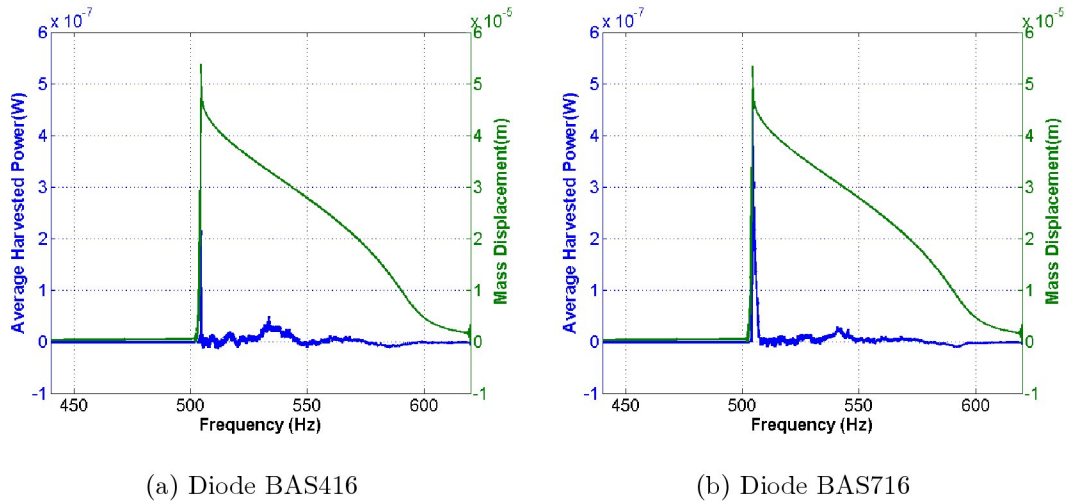


Figure 4.20: A comparison in harvested power and mass displacement of angled-spring doubler with two different diodes at $V_e = 30V$, $a = 0.25 g$

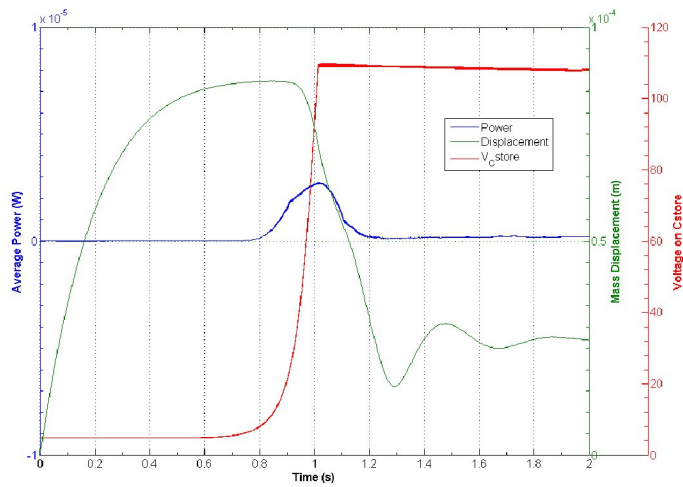
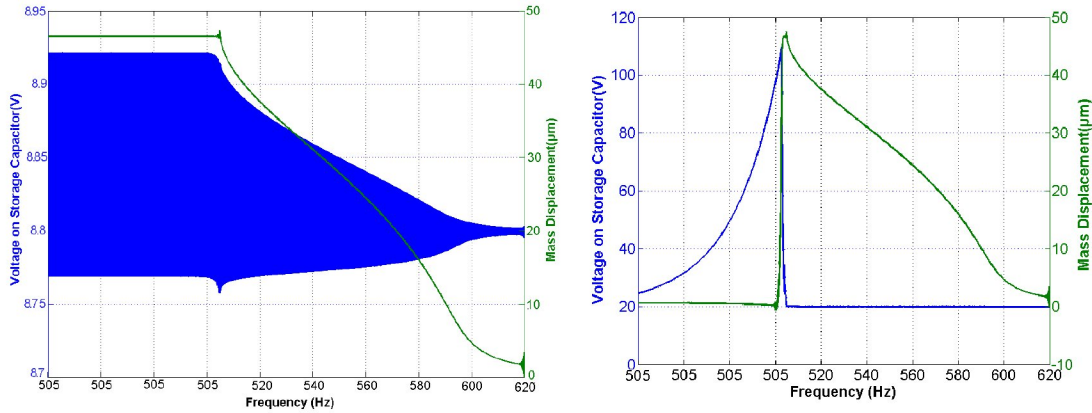


Figure 4.21: Voltage on C_{store} , output power and mass displacement of linear-spring doubler with $C_{store} = 90 pF$ and diode BAS716

As a result, the accumulation of leakage current loss is significant. Table 4.7 shows the harvested power of doubler circuit since the diode leakage current increases. There is a tradeoff between the forward voltage drop and leakage current. Based on Table 4.6 and 4.7, the diode with low leakage current is more preferable. However, reverse leakage current and forward voltage drop are not entirely uncorrelated in real diodes.



(a) With initial bias voltage $V_e = 9$ V

(b) With initial bias voltage $V_e = 25$ V

Figure 4.22: Voltage on C_{store} and mass displacement of angled-spring doubler with $C_{store} = 90$ pF and diode BAS716.

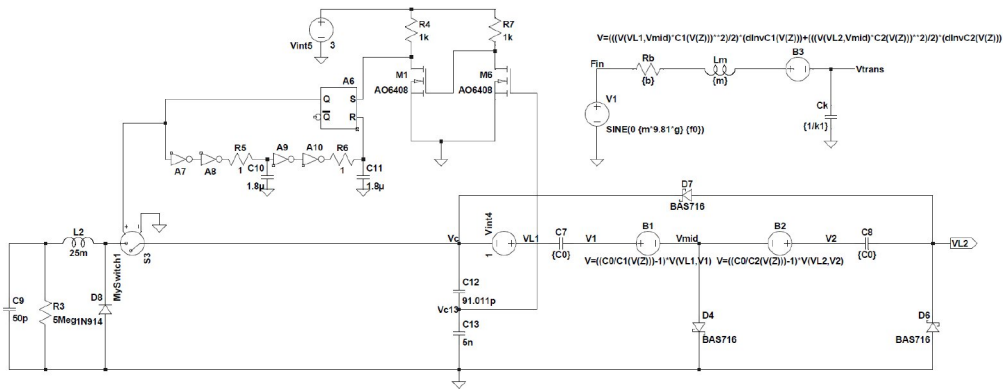


Figure 4.23: The linear-spring doubler circuit connected to a buck converter with controlled electronic switch

Some integrated techniques can produce diodes with very low leakage current and forward voltage drop. The average power is negative when the leakage current is larger than 50 nA. Finally, the doubler efficiency depends tremendously on the varying value of harvesting capacitor. Therefore, diode junction capacitance is added to parasitic capacitors. This leads to a larger required minimum displacement needed to harness the doubler circuit. Table 4.8 expresses the strong effects of diode capacitance on output power. For example, with only 2 pF diode capacitance and 1 V forward voltage drop, the power becomes below zero. Based on the above analysis in different effects of a non-ideal diode, in Table 4.9, several diode

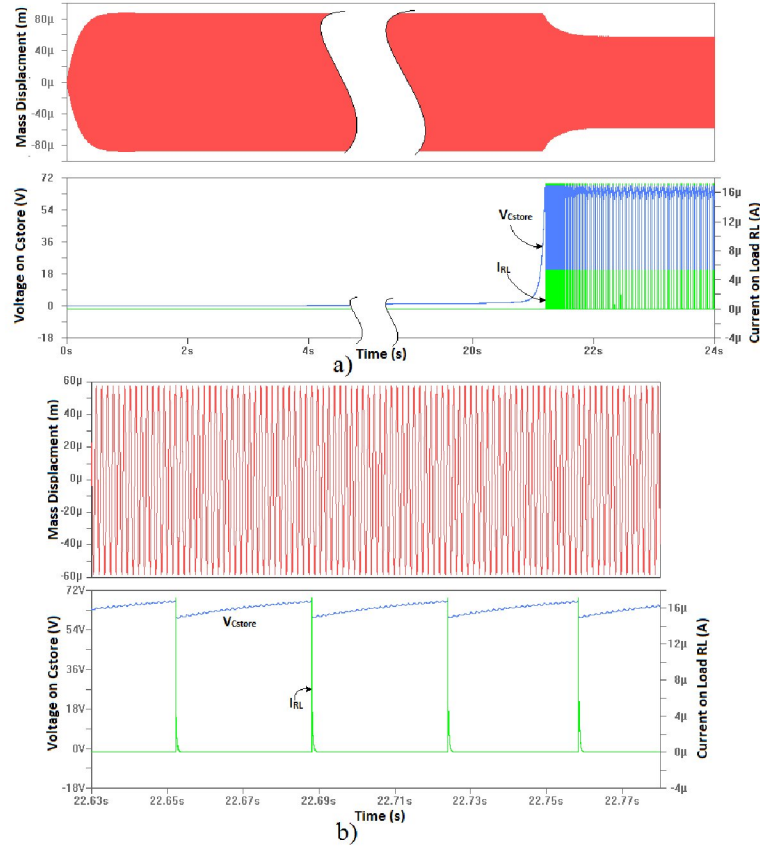


Figure 4.24: Load Current, Voltage on C_{store} and mass displacement of linear-spring doubler connected to a buck converter with controlled electronic switch, diode BAS716 and 0.25 acceleration) during transient state a) or during steady state b)..

models are selected with low leakage current and especially low diode capacitance. The average power harvested from doubler circuits using those diodes are measured and also listed in Table 4.9. Diode BAS716 with very low leakage current and parasitic capacitance is the best choice to obtain the highest average power up to $2.487 \mu\text{W}$. Some following simulations compare the output performances of the doubler circuits using diode BAS716 and BAS416. Figures 4.19 and 4.20 show the output power and mass displacement of the doubler with linear-spring and angled-spring harvesters biased by 60 V and 30 V batteries respectively. Those figures determine that diode BAS716 is better than BAS416 in term of high output power.

In the linear-spring doubler, with the storage capacitor replacing the battery in Figure 4.21, the bias voltage of doubler circuit is multiplied after each energy conversion cycle.

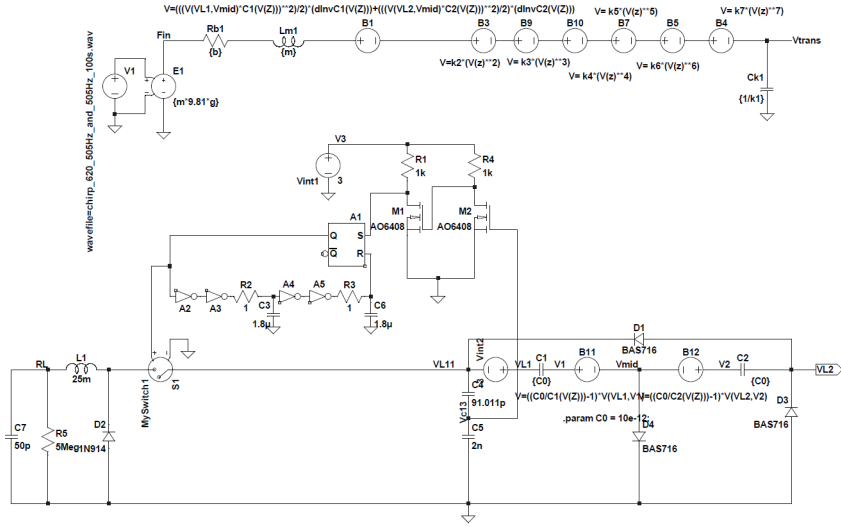


Figure 4.25: The angled-spring doubler circuit connected to a buck converter with controlled electronic switch

However, the circuit using non-ideal diode requires high initial bias voltage and larger mass displacement. For example, while the doublers with linear-spring transducers in Figure 4.21 start doubling charge on storage capacitor at 5 V, ones with angled springs (working in down-sweep mode in Figure 4.22) need larger than 25V initial bias voltage to build up harvested energy because of their lower mass displacement. One solution to solve this problem is fabricating charge permanent layers or electrets on fingers of harvesting capacitors. These layers polarize the harvester from 0.5 to 3 V which is enough to power the doubler circuit. Figure 4.22 shows that, with insufficient bias voltage, the voltage across C_{store} only oscillates around the bias voltage. Especially, since the angled-spring harvester vibrates from 620 Hz to 505 Hz and remains at 505 Hz, the mass displacement still plummets because the high bias voltage suppresses the displacement. In order to keep the doubler operating continuously at remained vibration frequency, e.g. 505 Hz, the stored energy in C_{store} should be delivered to a load using a buck converter. Next section investigates the designs in the buck converter.

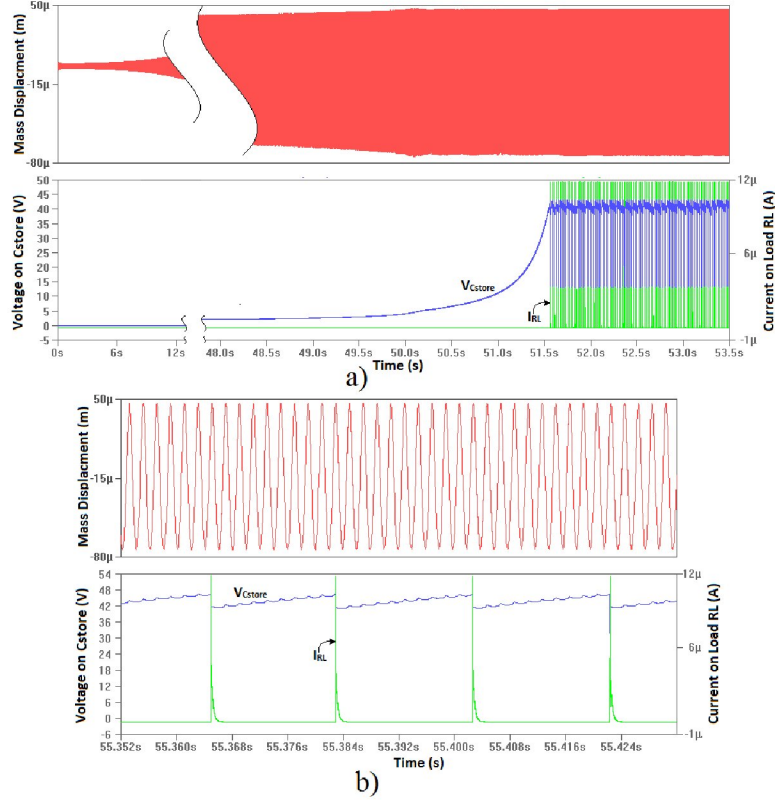


Figure 4.26: Load Current, Voltage on C_{store} and mass displacement angled-spring doubler connected to a buck converter with controlled electronic switch during transient state a) or during steady state b).

4.4 The Doubler of Charge with Buck Converter

The mass displacement, which is the most important factor in doubler design, is constrained since the bias voltage reaches high value. Therefore, the buck converter is used to maintain a constant optimal bias voltage across the storage capacitor where the output power is maximal and the mass displacement is larger than x_{req} . The whole systems are described in section 3.3. This section discusses two approaches to control the switch S of the buck converter which are using controlled electronic switch and autonomous MEMs Switch.

4.4.1 Controlled Electronic Switch

The buck circuit with controlled electronic switch connected to linear-spring doubler running with $0.38 g$ acceleration is shown in Figure 4.23. A MOSFET switch is controlled by an

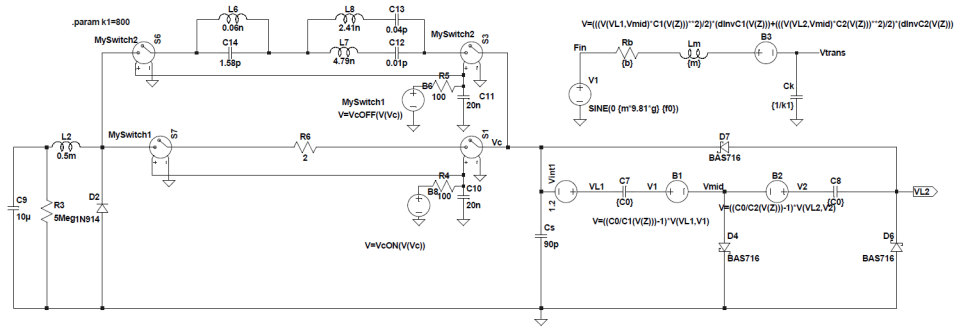


Figure 4.27: The linear-spring doubler circuit connected to a buck converter with MEMS switch

electronic circuit. A flip-flop is integrated to the circuit and works as a memory element which keeps the controlled switch on for a certain time. The duration in which the MOSFET remains on-state is determined by the time to charge and discharge capacitors in two series RC circuit. Because the voltage across C_{store} is high and unsuitable to be detected at a MOSFET gate, a voltage divider utilizing two series capacitors (i.e. $C_{12} = 91$ pF and $C_{13} = 5$ nF) is used to supply an appropriate input for the MOSFET gate of the voltage detector. For example, the electronic circuit closes the MOSFET switch when $V_{C_{store}} = 68V$ and remains on-state until $V_{C_{store}}$ drops to 60V in Figure 4.24. Due to some power loss in the MOSFET switch, it takes 20 seconds for the doubler to multiply charge in C_{store} . With the proposed bias configuration only 1 V voltage source is needed to start up the doubler of charge. Since $V_{C_{store}}$ becomes larger, the mass displacement starts dropping down and remains constant around 60 μm . Figure ?? illustrates a built-up voltage on C_{store} after each harvesting conversion cycle. The average harvested power on resistive load with ideal electronic switch is 1.19 μW . Figure 4.25 shows the doubler with the angled-spring harvester connected to a buck converter controlled by the electronic circuit. The harvester vibrates with frequency changing from 620 to 505 Hz and 0.25 g acceleration. The simulation results in Figure 4.26 shows that the doubler circuit needs a longer time up to 50 seconds to start up from a initial 3 V bias voltage. Since the buck converter is kept $V_{C_{store}}$ from 43 V to 45 V, the mass displacement is constant at 46 μm . The harvested power on resistive load is about 957.44 nW. In the simulations, a ideal switch is used to connect and disconnect the doubler to load. However, the MOSFET which can sustain high input voltage (from 40

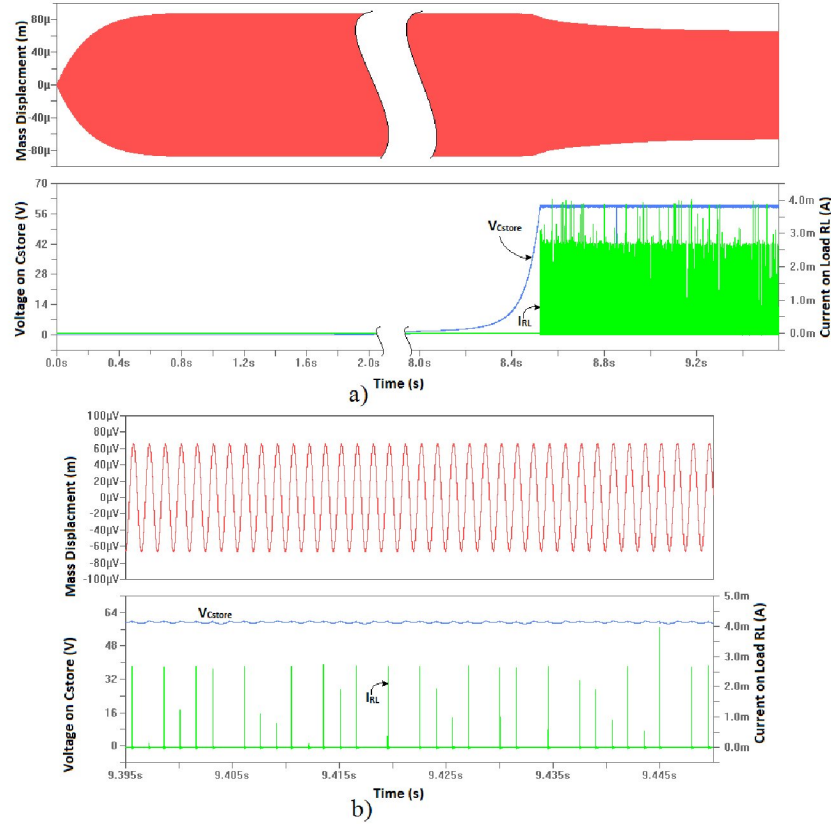


Figure 4.28: Load Current, Voltage on C_{store} and mass displacement of linear-spring doubler connected to a buck converter with MEMS switch and diode BAS716 during transient state a) or during steady state b).

to 70V) usually consume a lot of power on the storage capacitor. Therefore, the doubler system with real MOSFET cannot accumulated the power in C_{store} . Next section proposes a solution for this problem by using an autonomous MEMS switch.

4.4.2 Autonomous MEMS Switch

Different from a controlled electronic switch, a MEMS switch does not need a complex electronic circuit to control because it is able to autonomously close at a certain input voltage. An example of the MEMS switch is the MEMS switch RMSW101 produced by Company Radant MEMS. The switch closes when the input voltage reaches 90 V and opens when the input is lower than 90 V.

However, one drawback of the switch is the low switching speed which is vital to maintain

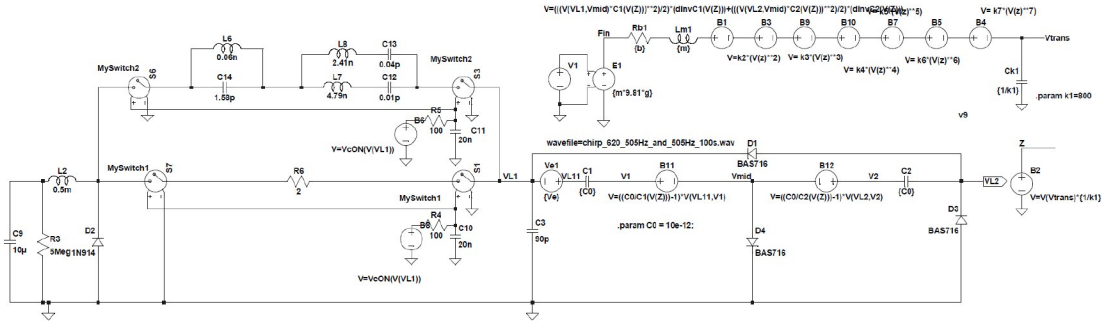


Figure 4.29: The angled-spring doubler circuit connected to a buck converter with MEMS switch

a constant voltage across C_{store} . Figure 4.27 and 4.29 shows the doubler circuits with linear and angled springs connected to a simulated equivalent circuit of autonomous MEMS switch which is proposed by Tahir and Aubert [24]. The RC circuit is also used to verify the switching time. The switch consumes more harvested power; therefore, 1.2 and 3 V bias voltage is needed to start up the doubler with linear-spring harvester and angled-spring harvester respectively. The voltage on C_{store} , currents at resistive load and mass displacement of the whole systems with linear and angled springs are shown in Figures 4.28 and 4.30. With the linear-spring harvesting system, the voltage on the storage capacitor is kept constant at 60 V. The average harvested power of the linear doubler is about 524.39 nW. With the angled-spring harvester, the MEMS switch is set to turn on at 40 V. The doubler needs more than 50 seconds to start increasing the voltage on C_{store} . The average power in steady state of this doubler system is 437.5 μ W. The MEMS switch opens and closes in a short time; therefore, $V_{C_{store}}$ is sustained around a certain bias voltage. From the calculations, compared to the doubler with buck converter using ideal electronic switch, those systems harvest about 50 The chapter has just illustrate different features of the doubler of charge in electrostatic energy harvesters through LTSPICE simulations. However, the experimental results sometimes maintain huge difference from the simulation results. To understand how the doubler operation is affected in the real designed circuit. Chapter 5 conducts several experiments of the doubler of charge using curved-spring harvesters.

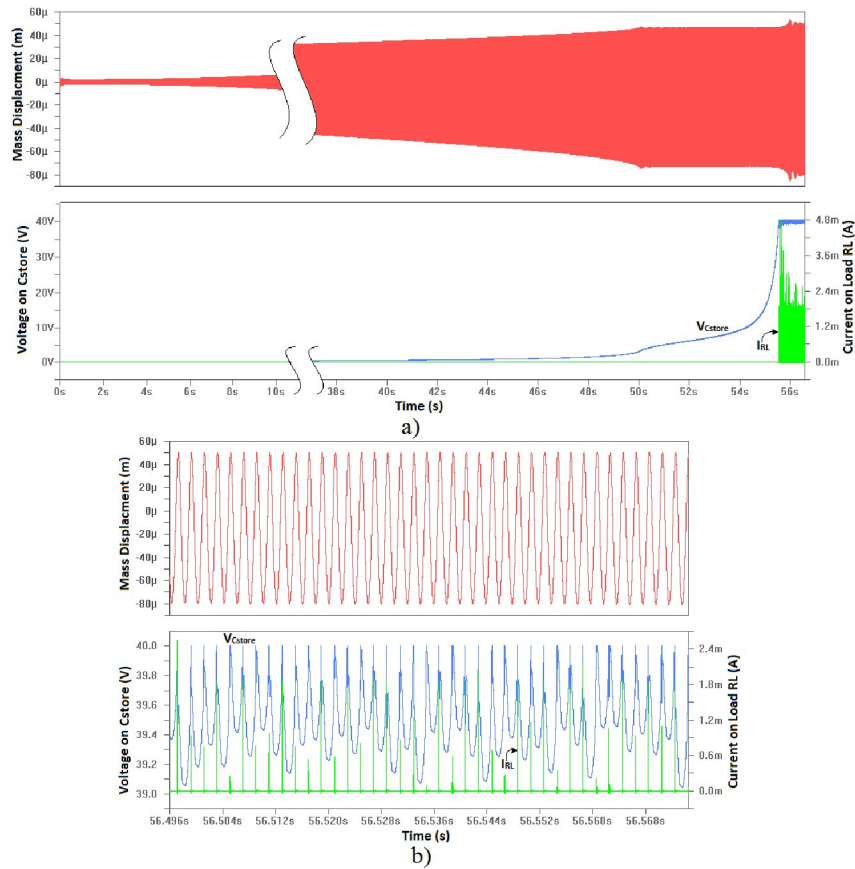


Figure 4.30: I_{load} , V_{Cstore} and x_{mass} of angled-spring doubler connected to a buck converter with MEMS switch and diode BAS716 during transient state a) or steady state b).

Chapter 5

Circuit Design and Experimental Results

While the simulation results in chapter 4 demonstrated the potential of the combination of the doubler of charge and asymmetrical harvester to harvest high energy in wide frequency range, the experiments with the doubler of charge exhibits different issues of the real circuit. Therefore, the purposes of chapter 5 is to design a real doubler circuit PCB, conduct several experiments with the circuits, and explore the vital effect which can prevent the doubler to work properly.

5.1 Curved-spring Energy Harvesters

In Figure 5.1, Curved-spring harvester with $40\mu\text{m}$ tip displacement which is fabricated by Son Duy Nguyen [1] in Berkeley Sensor & Actuator Center at University of California, Berkeley is integrated in the doubler circuits because of its availability. Figure 5.2 and 5.3 shows the harvester's springs, endstops, and fingers in two harvesting capacitors. Some measurements shows that the $40\mu\text{m}$ -curved-spring harvester obtains the overlaps of 23 and 93 μm of two capacitors while the $50\mu\text{m}$ -curved-spring harvester has the capacitor overlaps of 20 and 120 μm .

The harvesters are mounted on PCBs shown in 5.4 using nonconductive epoxy to electrically insulate the transducers' substrate from PCB copper layers. There are two epoxies

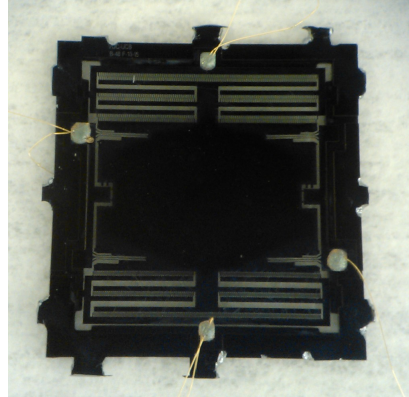


Figure 5.1: Curved-spring harvester fabricated by Son Duy Nguyen [1].

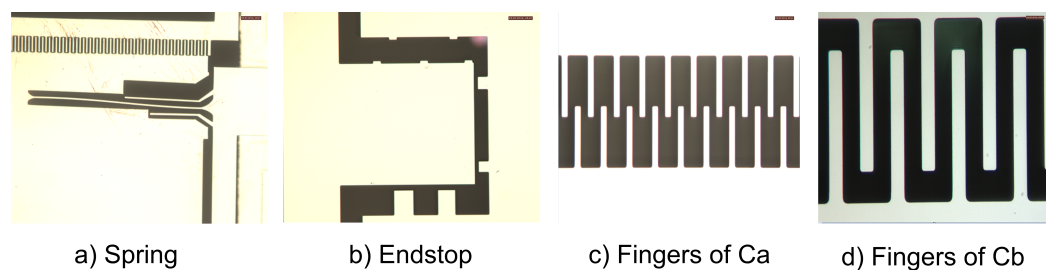


Figure 5.2: The spring, endstop, and fingers of the curved-spring harvester with $40\mu\text{m}$ tip displacement.

including EPO-TEK H70E and LOCTITE. The ceramic one may deform since hardened at 80 Celsius degree. This creates the displacement of proof mass; therefore, the first cannot be used. The second is more likely suitable for bonding harvesters on the PCB because it has no or weak effect of deformation at high temperature and it takes a reasonable time of 5 minutes to be hardened. Using an electrically conductive epoxy, the gold wires are bonded in four titanium pads of a harvester and connected to the PCB copper layers after baking at 80 Celsius degree in 90 minutes. Then, a plastic box is utilized to covers and protects the harvester from contamination.

Experiments are conducted with the new curved-spring harvesters which are needed to be firstly characterized their properties before being used for the doubler circuit. Therefore, the circuit is designed to run in two modes: characterizing mode and doubling mode. In the first mode, the harvesters are directly connected to extra resistive loads and bias voltage sources in series. The load output is connected to an op-amped-based unity gain buffer

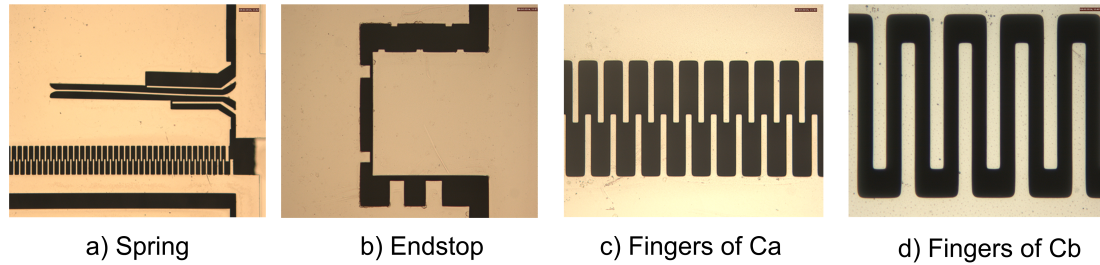


Figure 5.3: The spring, endstop, and fingers of the curved-spring harvester with $50 \mu\text{m}$ tip displacement.

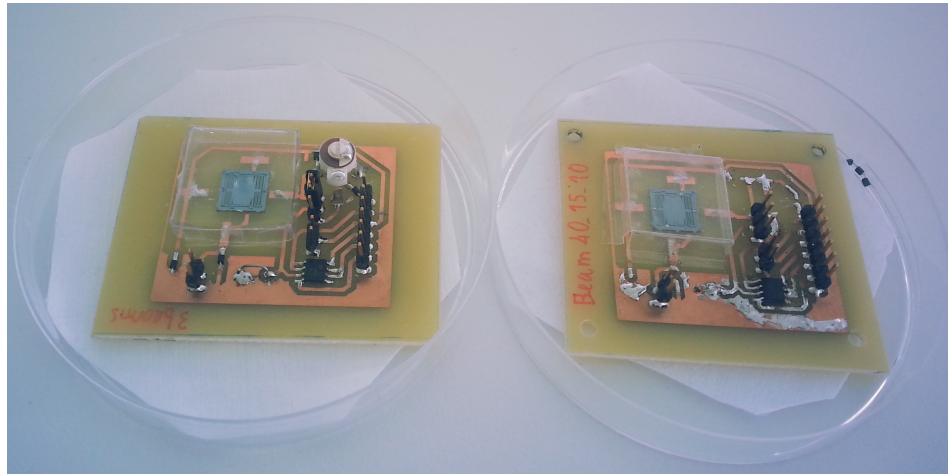


Figure 5.4: The PCBs with doubler circuits and curved-spring harvesters

amplifier before measured by a data acquisition (DAQ) device, the National Instruments USB-6211, which converts analog inputs into digital data and then transfers acquired data to a computer. The doubling mode, however, is done after making sure that the harvesters working normally. This mode allows the circuit to work as the doubler of charge with three diodes and a storage capacitor mounted on the PCB.

The measurement system is set as in Figure 5.5. The doubler PCB is placed on a $63 \times 72 \times 20$ aluminum bracket which is attached to a TIRA sacker. The piezoelectric acceleration sensor Model 352A56 SN111S53 of PCB Piezotronics is also mounted on the wall of the bracket using a thin glue layer to detect the acceleration signals and transfer them through the sensor signal conditioner Model 480E09 to the DAQ. The Labview 2013 Software collects and processes the data of output voltage and vibration from the DAQ; furthermore, Labview is also used to control the sacker to create vibration signals with

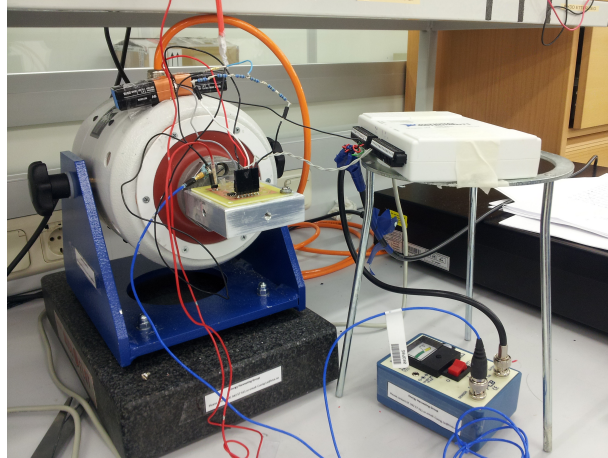


Figure 5.5: The measurement system for conducting all experiments

desired frequency and amplitude for testing. In general, the DAQ output signal is too low to run the sacker; thus, the control signals are amplified using the amplifier machine named Power Amplifier Type BAA 120.

Figures 5.6 and 5.7 show the output voltage on $15\text{M}\Omega$ resistive load of the nonlinear-spring harvesters. The tested harvesters are small with the slight mass about 15 mg; as a result, the output power is relatively low. Furthermore, the mass displacement of those harvesters is required to be larger since parasitic capacitors are too large. Therefore, the experiments with the curved-spring harvesters are conducted in frequency down sweep only to achieve the largest mass displacement and highest output power. The increase in bias voltage is beneficial in terms of higher power but not mass displacement whereas excitation improvement boosts both output voltage and mass displacement. Nevertheless, Figure 5.6 and 5.7 also show that the output voltage as well as the mass displacement are saturated at specific acceleration of 0.5 g for the $40\mu\text{m}$ -curved-spring harvester and 0.95 for the $50\mu\text{m}$ -curved-spring one. One more problem related to noise must be confronted during testing the harvesters. The impact of noise can reduce by creating a large ground plane in circuit layout or shortening and twisting the signal wires. Unfortunately, the ground plane results in large parasitic capacitance in the doubler circuit.

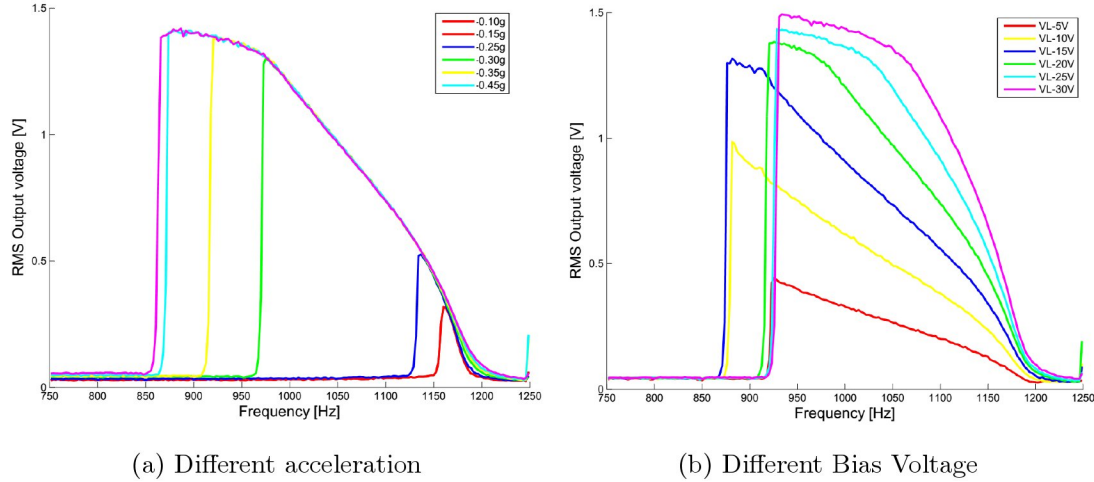


Figure 5.6: The output voltage of $40\mu\text{m}$ curved-spring harvesters with different accelerations a) and bias voltages Ve b).

5.2 Circuit Design and Experimental Results

After measuring the curved-spring harvesters in the characterizing mode, the PCB board in Figure 5.4 is added with three diodes BAS416 and a storage capacitor, i.e. the 9328 Ceramic Trimmer Capacitor produced by Johanson Manufacturing. Diode BAS416 with high sustained reverse voltage up to 85 V, maximum leakage current of 80 nA and 2 pF diode capacitance is used for the doubler circuit. The variable trimmer capacitor in Figure 5.8 is used as the storage capacitor of the doubler circuit. The capacitor can sustain the high voltage up to 250V and change from 12pF to 100pF. The capacitor is easy to adjust the value, but it is sensitive to the 50Hz noise. It is overlooked if the effect of the op-amp buffer is ignored. The op-amp OPA2137U working as a unit-gain amplifier is used in the output of the circuit. The FET input of OPA2137 with high impedance (larger than 100 G Ω) isolate the doubler circuit from low resistive input measurement devices. Therefore, it avoids power loss from the doubler. However, the op-amp adds a 2 pF parasitic capacitor to the doubler circuit.

The experiments with the doubler of charge are operated in down-sweep mode with the frequency reducing from 1300 to 450 Hz for the 50 μm harvester and from 1300 to 400 Hz for the 40 μm harvester during first 40 seconds. Then, the vibration frequency is kept

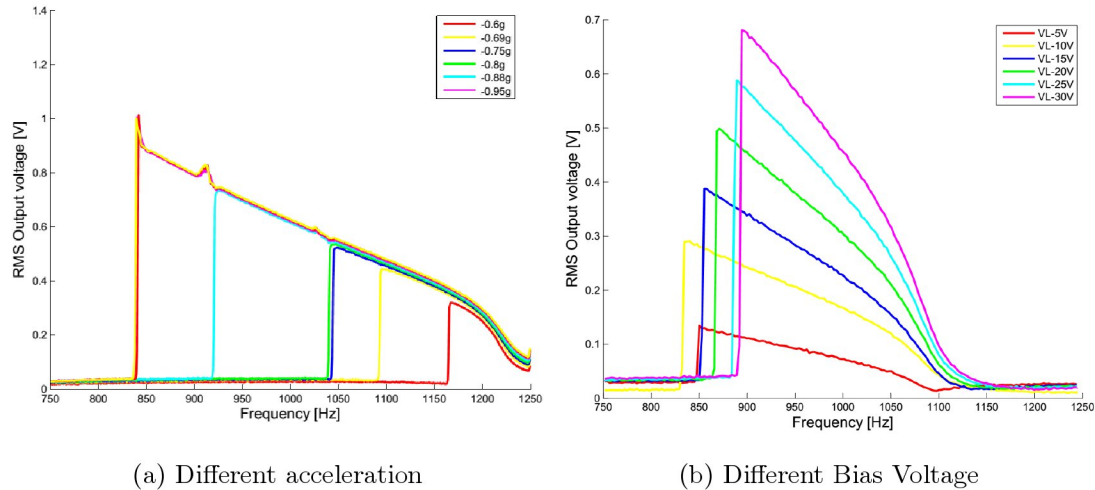


Figure 5.7: The output voltage of $40\mu\text{m}$ curved-spring harvesters with different accelerations a) and bias voltages Ve b).



Figure 5.8: The 9328 Ceramic Trimmer Capacitor produced by Johanson Manufacturing.

constant in last 10 seconds. The reason is that the harvesters only keep high power and displacement of sweep-down state at specific frequency without jumping down to sweep-up state only if the harvesters start vibrating from high to low frequency. Frequency sweep can be controlled by Labview software or manual adjustment. The output voltage of those harvesters in characterizing mode are shown in Figure 5.9. At 5 V the jump-down points move toward to very low frequency. With this down-sweep setup, the doubler circuits run in doubling mode and their voltage at nodes 1, 2 and 3 are measured in Figure 5.10. The Figure shows that the voltage on storage capacitor does not double. The mass displacement is not enough to generate a large vibration of voltage at three nodes which enables the flow of charge in doubler circuits. The doubler circuit layout is designed to reduce noise as much as possible. Nevertheless, the tradeoff of noise reduction is increasing parasitic capacitance

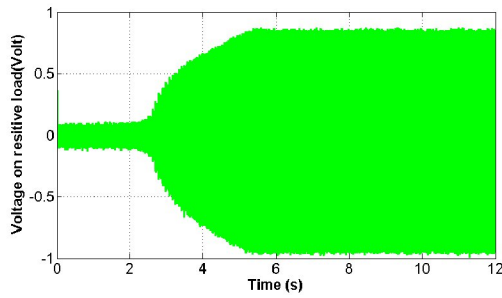
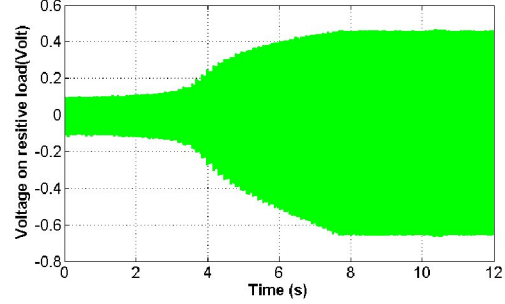
(a) $40\mu\text{m}$ -curved-spring harvester(b) $50\mu\text{m}$ -curved-spring harvester

Figure 5.9: The output voltage of the $40\mu\text{m}$ - and $50\mu\text{m}$ -curved-spring harvesters with vibration frequency sweep.

in the circuit which is also combined with the capacitors from diode and the op-amp buffer. The large parasitic capacitance in circuit is needed to experimentally measure and evaluate using a capacitance measurement circuit.

5.3 Parasitic Capacitance Measurement

Capacitance measurement requires special instruments, e.g. network analyzers or capacitance meters. Suitable measurement machines for measuring impedance in low frequency range are not available in labs or expensive to rent; thus, a simple PCB is designed to measure parasitic capacitance of the doubler circuit using the auto-balancing bridge method [25] as indicated in Figure 5.11a. The method can be employed in measuring impedance in low frequency systems. The designed circuit is an I-V converter using an operational amplifier. An external voltage source V_x is used to supply AC power for the measurement circuit. Two test cables connect the device under test (DUT) or the doubler circuit to the measuring instrument. In order to remove stray capacitance effects of the long test cables, one guarding layer is utilized to cover two cables and wired to the source or ground of the circuit as shown in Figure 5.11b. The SMD resistor R_r is used with the value of $1\text{ M}\Omega$. The most advantageous feature of the I-V converter circuit using Op-amp is very low input parasitic capacitance and high input impedance which reduce the measurement inaccuracy. With the current $I_x = I_r$, the input V_x and output V_r of the circuit are measured with

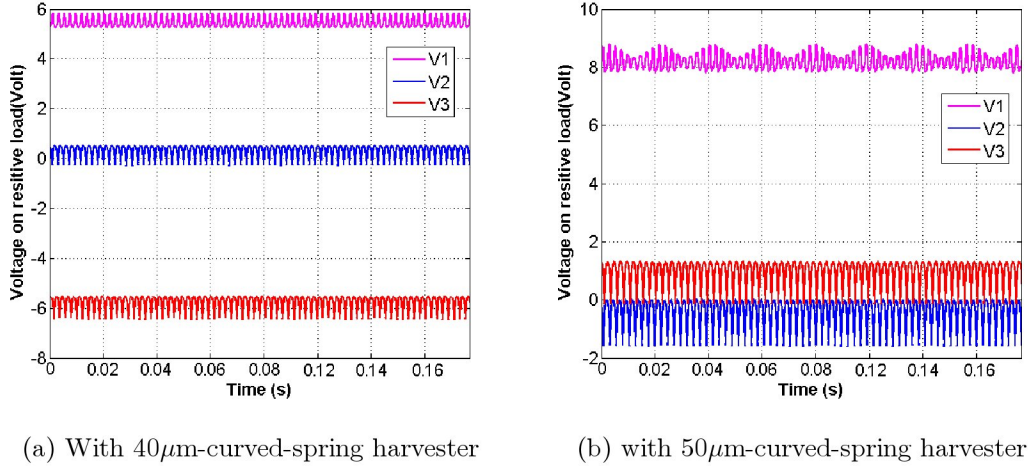


Figure 5.10: The voltage at nodes 1, 2 and 3 of the doubler circuit with 40µm- and 50µm-curved-spring harvester.

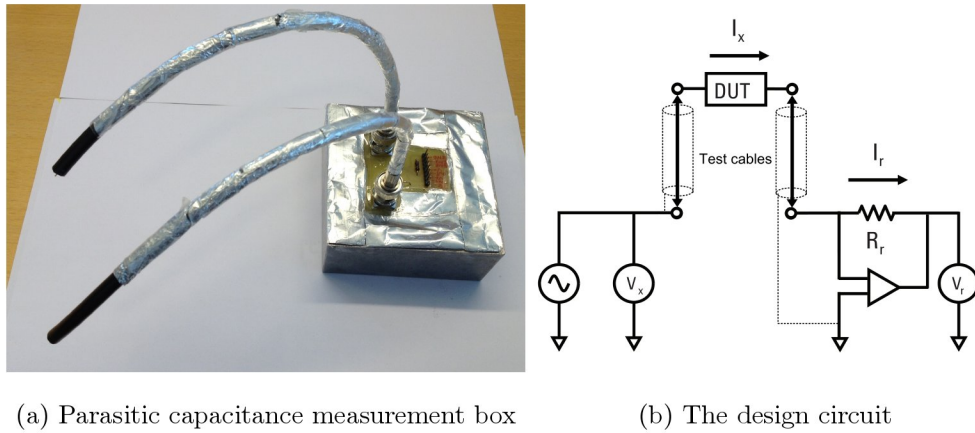


Figure 5.11: Parasitic capacitance measuring instrument and its designed circuit.

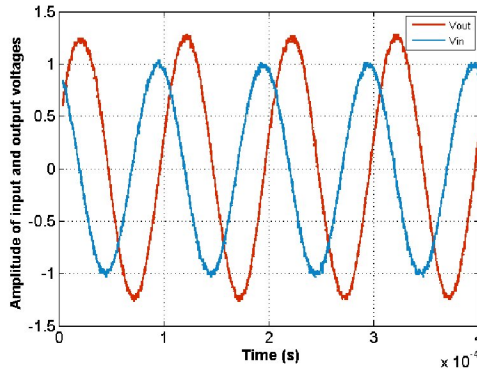
voltmeters or oscilloscopes and the impedance of the doubler circuit is calculated as

$$Z_{DUT} = R_r \frac{V_x}{V_r}. \quad (5.1)$$

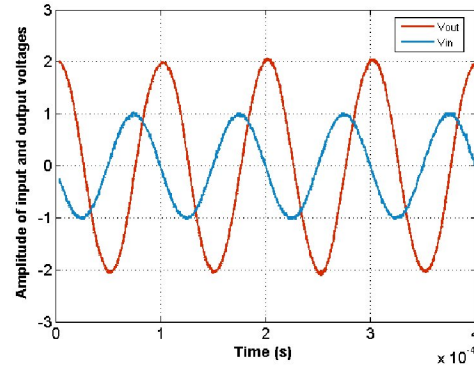
The PCB is covered with a steal box and to reduce 50Hz noise and its ground is connected to the box cover. The Table 5.1 shows several measuring results of the measuring instrument in some fixed ceramic capacitors. The measurement capacitance is evaluated by subtracting 2 pF capacitance (which is from the op-amp) from the achieved results. The measuring error is less than 10

Table 5.1: Testing results of the capacitance measuring instrument with different fixed capacitors

Capacitors	Achieved results pF	Results after cabliration pF	Error
$2.4pF$	4.293	2.293	-4.46%
$3.3pF$	5.247	3.247	-1.61%
$4.7pF$	6.996	4.996	6.30%
$10pF$	12.732	10.732	7.32%
$15pF$	16.854	14.854	-0.973%



(a) On harvesting capacitor Ca



(b) On harvesting capacitor Cb

Figure 5.12: Output and input voltage of the measurement circuit when measuring the $50\mu\text{m}$ -curved-spring doublers.

Using the designed instrument, parasitic capacitance of the doubler circuits with $40\mu\text{m}$ - and $50\mu\text{m}$ -curved-spring harvesters are evaluated by subtracting the initial harvesting capacitance and 2 pF capacitance of the op-amp input of the measuring instrument from the measured values. The measured results are displayed in Figures 5.12 and refFig513 in which $V_x = V_{in}$ and $V_r = V_{out}$. Equation refeq51 is applied to compute the values of two harvesting capacitors. With the $40\mu\text{m}$ -curved-spring harvester, a 1V - 10000Hz voltage source V_{in} is used. From the output V_{out} , the calculated values of two harvesting capacitors are 16.08 and 23.01 pF . Similarly, a 20000Hz voltage source with 1 V peak-to-peak amplitude powers the circuit to measure the parasitic capacitance of the $50\mu\text{m}$ -curved-spring device. The parasitic capacitors of the second harvester are 9.86 and 29.37 pF . In those experiments, the effects of circuit inductance and resistance are assumed to be much smaller than that

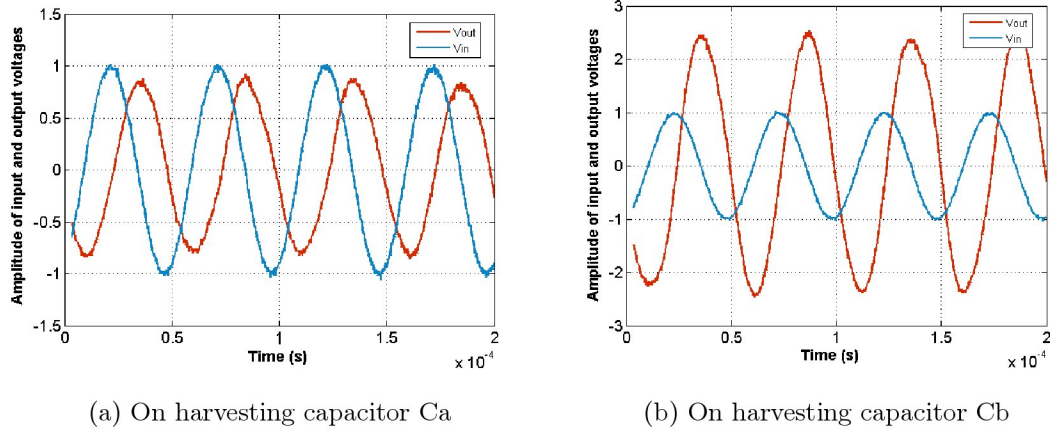


Figure 5.13: Output and input voltage of the measurement circuit when measuring the $50\mu\text{m}$ -curved-spring doubler.

of circuit capacitance and therefore ignored in measurement.

The measured parasitic capacitance of the doubler circuits are very high; as a result, a very large mass displacement is needed to run the doubler of charge. The fabricated structures of curved-spring harvesters limit the maximum mass displacement smaller than $25\ \mu\text{m}$. This demonstrates why the designed doubler cannot double the voltage on C_{store} . Previous simulations in Figures 4.16 and 4.17 also show that those curved-spring doublers cannot multiply the charge in the storage capacitors if high parasitic capacitance larger than $5\ \text{pF}$ exists in the circuit.

Chapter 6

Conclusions and Future Work

6.1 Conclusions

The thesis has researched the doubler of charge in electrostatic energy harvesting systems. The research project has explored three main areas in turns presented in each chapter. Firstly, the electromechanical performance of linear electrostatic energy harvester which is connected in series to a bias voltage source and two resistive loads has been discussed in Chapter 2. The researches of harvested power indicates a strong dependency of the output on load resistance, bias voltage and vibration frequency which then used to optimize the power on loads. The analyses in this chapter prove that the output power of linear-spring harvesters with optimal load resistance reaches maximum at resonant and antiresonant frequencies. With a very small damping factor, while the resonant frequency value is weakly dependent on the bias voltage V_e , the antiresonant can be adjusted by changing V_e . Mass displacement is also considered to be reduced since the bias voltage V_e increases. Chapter 2 has also presented several advantages of the harvesters with angled and curved springs.

Secondly, the design of power conversion circuitry for electrostatic energy harvesters is introduced in chapter 3. A review of conventional circuits exhibits the comparison in benefits and drawbacks of continuous and switched harvesting systems. Most importantly, a new kind of power converter named the doubler of charge has been investigated when it is utilized with symmetrical and asymmetrical electrostatic energy transducers. The calculations demonstrate the advantageous features of the combination between the doubler

circuit and asymmetrical harvesting transducers in terms of required mass displacement and high harvested power.

The simulations using the LTSPICE software in chapter 4 have been carried out with a linear-spring harvester, a angled-spring harvester and two curved-spring harvesters. The linear-spring harvester with a heavy mass of 30.4 mg, small 3.14 pF parasitic capacitors and potential mass displacement up to 90 μm is used with the doubler circuit to investigate three issues. The first problem is the reduction of mass displacement since the voltage across the storage capacitor of the doubler is multiplied. The optimal bias voltage around 50 to 60 V with maximum power is recognized. Moreover, different symmetrical and asymmetrical harvesting structures are compared. With the proof mass asymmetrically reconfigured 25 μm from the middle, The prototype, which has initial characteristic parameters of capacitor C_a smaller than that of C_b , generates the largest power with the same mass displacement and reduce minimum required mass displacement up to 10

Finally, the experiment results of the doubler circuit conducted with the curved-spring harvesters with 40 and 50 μm tip displacement confirm the strong impact of the large parasitic capacitor on the operation of the doubler of charge. The voltage on C_{store} cannot be doubled as the mass displacement is not enough to create a large variable capacitance compared to the parasitic one.

6.2 Future Work

The experiment results show the necessary of designing a suitable harvester with large variable capacitors and mass displacement. That parasitic capacitance exists in a harvesting system is unavoidable; therefore, the design with large structures or more fingers could increase initial harvesting capacitors which by far outweigh the parasitic ones. In parallel, the harvesters should be designed with as large mass displacement as possible. Furthermore, the asymmetrical and nonlinear-spring harvesters using the doubler circuit could be preferable to scavenge vibration energy in broad frequency range. It is important to consider the optimal position of the proof mass so that output power is maximal. Several endstops could be designed to prevent the harvester fingers from contacting each other.

The PCB for the doubler circuit is needed to carefully design with low parasitic capacitance and low power loss. In the experiments, diode BAS416 is used in the doubler circuit. The simulation results show that the better diode to achieve higher power is BAS716. Therefore, BAS716 could be used to reduce power loss of the circuit. In addition, the design of circuit layout should be employed several techniques in parasitic capacitance reduction such as designing smaller and shorter copper nets and increasing the spacing between two nets. The measurement instrument with low input capacitance could be used to measure the doubler circuits with low effects on their operation.

Finally, an ASIC design could maintain many promises to be entirely integrated in the harvesting systems. The diodes in doubler could be replaced by controlled switches. Peak detectors could be used to control the switched since the harvesting capacitor reaches maximum or minimum. The switch in buck converter could be controlled by low-power electronic circuits using the same working principle of the proposed electronic circuit.

Bibliography

- [1] Son Duy Nguyen. *Wideband MEMS energy harvesters utilizing nonlinear springs*. PhD thesis, University of Oslo, Norway, 2013.
- [2] G. Despesse S. Boisseau and B. Ahmed Seddik. Electrostatic conversion for vibration energy harvesting, small-scale energy harvesting. *Small-Scale Energy Harvesting, Intech*, 2012.
- [3] D. Guyomar, A. Badel, E. Lefeuvre, and C. Richard. Toward energy harvesting using active materials and conversion improvement by nonlinear processing. *Ultrasonics, Ferroelectrics and Frequency Control, IEEE Transactions on*, 52(4):584–595, April 2005.
- [4] Junrui Liang and Wei-Hsin Liao. Improved design and analysis of self-powered synchronized switch interface circuit for piezoelectric energy harvesting systems. *Industrial Electronics, IEEE Transactions on*, 59(4):1950–1960, April 2012.
- [5] B.C. Yen and Jeffrey H. Lang. A variable-capacitance vibration-to-electric energy harvester. *Circuits and Systems I: Regular Papers, IEEE Transactions on*, 53(2):288–295, Feb 2006.
- [6] Son Duy Nguyen, E. Halvorsen, and G.U. Jensen. Wideband mems energy harvester driven by colored noise. *Microelectromechanical Systems, Journal of*, 22(4):892–900, Aug 2013.
- [7] D S Nguyen, E Halvorsen, G U Jensen, and A Vogl. Fabrication and characterization of a wideband mems energy harvester utilizing nonlinear springs. *Journal of Micromechanics and Microengineering*, 20(12):125009, 2010.

- [8] Cuong Hung Nguyen. Modeling and characteristic of nonlinear energy harvester. Master's thesis, BUSKERUD AND VESTFOLD UNIVERSITY COLLEGE.
- [9] JamesM. Gilbert and Farooq Balouchi. Comparison of energy harvesting systems for wireless sensor networks. *International Journal of Automation and Computing*, 5(4):334–347, 2008.
- [10] Shad Roundy, Paul K Wright, and Kristofer SJ Pister. Micro-electrostatic vibration-to-electricity converters. In *ASME 2002 International Mechanical Engineering Congress and Exposition*, pages 487–496. American Society of Mechanical Engineers, 2002.
- [11] Cuong Phu Le and E. Halvorsen. Evaluation of parameters for electrostatic energy harvesters. In *Design, Test, Integration Packaging of MEMS/MOEMS, 2009. MEMS/MOEMS '09. Symposium on*, pages 286–291, April 2009.
- [12] S Boisseau, G Despesse, and A Sylvestre. Optimization of an electret-based energy harvester. *Smart Materials and Structures*, 19(7):075015, 2010.
- [13] PD Mitcheson, Tom Sterken, C He, M Kiziroglou, EM Yeatman, and R Puers. Electrostatic microgenerators. *MEASUREMENT & CONTROL*, 41(4):114–119, 2008.
- [14] Domingues M. De Queiroz, A. C M. Electrostatic vibrational energy harvesting using a variation of benet's doubler. In *Circuits and Systems (MWSCAS), 2010 53rd IEEE International Midwest Symposium on*, pages 404–407, Aug 2010.
- [15] A.C.M. de Queiroz and M. Domingues. Electrostatic energy harvesting using doublers of electricity. In *Circuits and Systems (MWSCAS), 2011 IEEE 54th International Midwest Symposium on*, pages 1–4, Aug 2011.
- [16] M. Domingues and A.C.M. de Queiroz. Ultra-low-power control systems for electrostatic energy harvesters. In *Circuits and Systems (ISCAS), 2013 IEEE International Symposium on*, pages 2960–2963, May 2013.
- [17] C.B. Williams and R. B. Yates. Analysis of a micro-electric generator for microsystems. In *Solid-State Sensors and Actuators, 1995 and Eurosensors IX.. Transducers '95. The 8th International Conference on*, volume 1, pages 369–372, Jun 1995.

- [18] Jamil M. Renno, Mohammed F. Daqaq, and Daniel J. Inman. On the optimal energy harvesting from a vibration source. *Journal of Sound and Vibration*, 320(1–2):386 – 405, 2009.
- [19] E. Lefeuvre, D. Audigier, C. Richard, and D. Guyomar. Buck-boost converter for sensorless power optimization of piezoelectric energy harvester. *Power Electronics, IEEE Transactions on*, 22(5):2018–2025, Sept 2007.
- [20] R. D’hulst and J. Driesen. Power processing circuits for vibration-based energy harvesters. In *Power Electronics Specialists Conference, 2008. PESC 2008. IEEE*, pages 2556–2562, June 2008.
- [21] Y C Shu and I C Lien. Analysis of power output for piezoelectric energy harvesting systems. *Smart Materials and Structures*, 15(6):1499, 2006.
- [22] E. Lefeuvre, A. Badel, C. Richard, L. Petit, and D. Guyomar. A comparison between several vibration-powered piezoelectric generators for standalone systems. *Sensors and Actuators A: Physical*, 126(2):405 – 416, 2006.
- [23] J. O. Mur-Miranda. *MEMS-Enabled Electrostatic Vibration-to-Electric Energy Conversion*. PhD thesis, Massachusetts Institute of Technology, 2003.
- [24] F.A. Tahir and H. Aubert. Equivalent electrical circuit model for design and optimization of mems-controlled reflectarray phase shifter cells. In *Antennas and Propagation (EUCAP), Proceedings of the 5th European Conference on*, pages 240–243, April 2011.
- [25] Agilent. Agilent impedance measurement handbook.